

Non-invasive cardiac magnetic resonance imaging techniques for assessment of myocardial
fibrosis

by

Joseph Pagano

A thesis submitted in partial fulfillment of the requirements for the degree of

Doctor of Philosophy

in

Biomedical Sciences

Department of Biomedical Engineering
University of Alberta

© Joseph Pagano, 2020

Abstract

While there may be numerous underlying origins, myocardial fibrosis is a common, unifying finding in various forms of heart disease. Unfortunately, its presence goes beyond simply being a herald of myocardial injury. The alterations in the extracellular space lead to abnormalities in both systolic and diastolic heart function and have been associated with adverse outcomes such as hospitalizations, heart failure, arrhythmias, and death. The gold standard assessment for myocardial fibrosis involves histopathological assessment of tissue acquired either at autopsy or via invasive endomyocardial biopsy, which is not without associated risks of complications.

Cardiac magnetic resonance imaging (MRI) provides clinicians and researchers a powerful and versatile imaging system to help in their endeavours to better understand and characterize how the heart develops and adapts to numerous stresses and insults. This is particularly true with recent developments in the non-invasive assessment of myocardial fibrosis using MRI based T_1 -mapping techniques. The goal of the thesis was to explore the impact of physiological and pathological stresses on the heart, through the use of MRI T_1 -mapping.

In particular, the effects of aging, sex, and risk factors for the development of heart failure were studied. It was determined that there were no significant alterations in T_1 -mapping markers of myocardial fibrosis associated with the aging process. Importantly, however, there do appear to be sex differences in the response to risk factors for heart failure. Next, different distinct phenotypes of heart failure were studied to gain insight into differences in remodeling that may contribute to the observed functional and clinical heterogeneity.

While much of the focus is on the heart's left ventricle, it cannot be forgotten that the right ventricle may be involved additionally, or even as the primary site of pathology. In patients with Anderson-Fabry disease, characterized by interstitial deposition of glycosphingolipids, the development of right ventricular thickening is driven by the same infiltrative process that occurs in the left ventricle. This contrasts with hypertrophy and myocardial fibrosis that is occurring in response to increased right ventricular afterload, as seen in pulmonary hypertension.

Finally, a novel approach to T_1 -mapping was developed to overcome some limitations in current T_1 -mapping techniques, allowing for increased spatial resolution and imaging at end-systole, at which point in time there are more pixels across the ventricular wall. This new technique, based on a lookup table approach using image ratios, was validated by means of numerical simulations, phantom experiments, and in vivo.

Cardiac MRI provides insight into myocardial form and function that may otherwise require multiple, possibly invasive, approaches. It has been instrumental in developing our understanding of the normal and diseased heart. Further studies, expanding on work presented here, will be important in providing new knowledge and techniques critical to moving the field forward.

Preface

Some of the research included in this thesis was part of a provincial research collaboration, The Alberta Heart Failure Etiology and Analysis Research Team (HEART). The overarching study (ClinicalTrials.gov NCT02052804) aim was to better understand and describe those with heart failure and preserved ejection fraction, through the study and development of novel diagnostic, therapeutic, and prognostic approaches. A multi-site prospective observational cohort study involving the University of Alberta and University of Calgary, Alberta HEART enrolled healthy participants, along with patients afflicted by, or at risk for, heart failure, who underwent testing over a 12 month period followed by outcome follow up via administrative databases.

A version of chapter 2 of this thesis has been submitted for review: Pagano JJ, Yim D, Lam CZ, Yoo SJ, Seed M, Grosse-Wortmann L. Normative Data for Myocardial Native T₁ and Extracellular Volume Fraction in Children. *Radiology: Cardiothoracic Imaging*. Submitted March 14, 2020. I was responsible for a portion of the data acquisition, study design, and all of the data analysis and manuscript composition. Deane Yim, Chris Lam, Shi-Joon Yoo, Mike Seed, and Lars Grosse-Wortmann were involved in portions of the data acquisition. Lars Grosse-Wortmann also was involved in the study design and was the supervisory author. All authors read and approved of the manuscript. The study was approved by The Hospital for Sick Children's research ethics board.

A version of chapter 3 of this thesis has been previously published: Pagano JJ, Chow K, Paterson DI, Mikami Y, Schmidt A, Howarth A, White J, Friedrich M, Oudit G, Ezekowitz J, Dyck J, Thompson RB. Effects of Age, Gender and Risk-Factors for Heart Failure on Native Myocardial T₁ and Extracellular Volume Fraction. *J Magn Reson Imaging*. 2018 Nov;48(5):1307-1317. I was involved in data collection, analysis, and manuscript composition. KC assisted in data collection and manuscript revisions. DIP was involved in data analysis and manuscript revisions. RBT was the senior author and was involved in study design and manuscript revisions. The in vivo studies received ethics approval from the University of Alberta Health Research Ethics Office and University of Calgary Conjoint Health Research Ethics Board.

A portion of chapter 4 of this thesis has been previously presented: Pagano JJ, Chow K, Paterson DI, Mikami Y, Friedrich MG, Haykowsky M, Anderson T, White J, Oudit GY, Ezekowitz J, Dyck J, Thompson RB. Sex Influence on Native T₁ and Extracellular Volume Fraction in Heart Failure. Presented at the SCMR 22nd Annual Scientific Sessions (Feb 7-9, 2019). I was involved in data collection, and completed the analysis and manuscript composition. RBT was the senior author and was involved in study design and manuscript revisions. The in vivo studies received ethics approval from the University of Alberta Health Research Ethics Office and University of Calgary Conjoint Health Research Ethics Board.

A version of chapter 5 of this thesis has been previously published: Pagano JJ, Chow K, Khan A, Michelakis E, Paterson I, Oudit GY, Thompson RB. Reduced Right Ventricular Native Myocardial T₁ in Anderson-Fabry Disease: Comparison to Pulmonary Hypertension and Healthy Controls. PLoS One. 2016 Jun 15;11(6):e0157565. I was involved in data collection, analysis, and manuscript composition. KC assisted in data collection and manuscript revisions. AK and EM were involved in patient selection and manuscript revisions. IP was involved in patient selection, data analysis, and manuscript revisions. GYO was a senior author involved in study design, patient selection, and manuscript revisions. RBT was the supervisory author and was involved in study design and manuscript revisions. The in vivo studies received ethics approval from the University of Alberta Health Research Ethics Office and University of Calgary Conjoint Health Research Ethics Board.

A portion of chapter 6 of this thesis has been previously published: Pagano JJ, Chow K, Paterson I, Thompson RB. Imaging Contrast Agent Concentration and Extracellular Volume Fraction in the Right Ventricle. *J Cardiovasc Magn Reson*. 2012; **14**(Suppl 1):O109. I was involved in the design of the pulse sequence, MATLAB programming for simulation analysis, production of the phantoms for testing, in vitro and in vivo data collection, all simulation and image analysis, statistical analysis, and manuscript composition. KC assisted in data collection and manuscript revisions. DIP was involved in data analysis and manuscript revisions. RBT was the senior author and was involved in study design and manuscript revisions. The in vivo studies received ethics approval from the University of Alberta Health Research Ethics Office.

Acknowledgments

I struggle with the knowledge that I will not be able to adequately convey the gratitude and appreciation I have for all those who have helped me not only over the course of my program, but through the many years that led me to its initiation. I have been fortunate to have wonderful mentors, colleagues, mentees, friends, and family who have all helped shape the work of this thesis, as well as shaping me along the way.

I would like to recognize the many funding agencies who provided me with financial support at times through my degree, including the Clinician Investigator Program, the Women and Children's Health Research Institute (WCHRI), and Alberta Innovates – Health Solutions (AIHS). Operation funding had also been provided by organizations such as AIHS and the University Hospital Foundation.

Balancing my clinical and research domains has been challenging. Thankfully, through the support of many individuals, I've continued to grow as a clinician. Particular thanks are needed for my cardiac MRI colleagues here in Edmonton who welcomed me into their practice, including Drs. Edythe Tham and Michelle Noga. I certainly would not be able to go without acknowledging all the clinical MRI education and mentoring I received at the Hospital for Sick Children in Toronto from Drs. Lars Grosse-Wortmann, Mike Seed, and Shi-Joon Yoo. Additionally, amongst the many others I came to consider friends and colleagues, I must thank Drs. Chris Lam, Regina De La Mora Cervantes, Deane Yim, and Davide Marini. The occasional texts asking about MRI physics from technologists Joti Gil and Vivian Tassos provide little burst of affirmation of my training.

The Department of Biomedical Engineering has always been very supportive throughout my program. Thanks must be given to our department administrators, Maisie and Catherine; certainly, I would not have gotten through as much as I did without Maisie's enduring support. Through the years I had the pleasure of learning and working along side many other graduate students and research associates, whom I consider colleagues and good friends, including Dr. June Cheng Baron, Dr. Corey Baron, Kory Mathewson, Sarah Thiesson, and Justin Grenier. In particular, Dr. Kelvin Chow was an exceptional source of all things important to my program; physics discussions, pulse sequence programming, MATLAB code and tutorials, scanner operating instruction, abstract/manuscript feedback, and coffee breaks.

Many places could have been considered a second home for me, and the scanner at the Peter S. Allen MRI Centre undoubtedly meets that definition. I am thankful to the collegiality and efforts of the Centre's staff, including Karim, Peter, and Carol, along with the many research technologists and nurses who helped keep things running. Though not intimately related to the Centre, I would be remiss if I did not give mention to Marleen, Edie, and Margo, study coordinators bringing a seemingly endless stream of subjects to the Centre.

Many thanks go to my Supervisory Committee, providing guidance and support as I ventured into unfamiliar territory. Drs. Mark Haykowsky, Ian Paterson, and Alan Wilman have always been extremely supportive through the years and provide invaluable advice and counsel.

Though I owe many thanks to many people, this thesis would never have even started if it were not for Dr. Jeffrey Smallhorn. I do not believe I really understood what a mentor was prior to meeting Jeff during my Pediatric Cardiology Residency. Not only a clinical role model, his energy and enthusiasm for research is unparalleled and infectious. A significant proportion of who I am today as a clinician, researcher, and person is as a result of his mentorship and advice.

A heartfelt thank you is of course required for my supervisor, Dr. Richard Thompson. You have been inspiring in your intelligence, dedication, curiosity, and humility. You have always been supportive and treated me as a colleague. I am certain that I learned the most through my program during our discussions on those many occasions when things were not working, including having to go back to first principles and reconsider our approach and assumptions. I look forward to where collaborating may take us in the future.

I can say with absolute confidence that none of my accomplishments would have been possible without the strength and support from my family. My mother and father have always provided unwavering support and guidance every step of the way. My mother-in-law and father-in-law have unconditionally accepted me as part of their family. Through this journey I was able to reconnect with my sister and her wonderful family, and I miss our dinners and time together in Toronto. My children, Sophia, Ethan, and Liliana, whom I've been lucky to watch grow and develop over the years of this program, have provided me with an endless stream of love and laughter, making the stress melt away when we are together. Finally, I cannot adequately convey how much love and support that my wonderful wife Catherine has provided me. You inspire me, support me and our family unconditionally, and make me so proud and happy every day. You have been there with me through it all, and I certainly could not have done it without you.

Table of Contents

1	Introduction	1
1.1	Overview	1
1.2	Heart Failure	2
1.2.1	Types of Heart Failure	2
1.3	Myocardial Fibrosis	3
1.3.1	Overview of Myocardial Architecture	3
1.3.2	Types of Myocardial Fibrosis	3
1.4	Sequelae of Myocardial Fibrosis	4
1.4.1	Functional Impact	4
1.4.2	Clinical Impact.....	5
1.5	Cardiac MRI Assessment of Myocardial Fibrosis	5
1.5.1	Basics of Cardiac MRI.....	5
1.5.2	T ₁ and T ₂ in Tissues	10
1.5.3	T ₁ , T ₂ , and Gadolinium Contrast Agents	12
1.5.4	Late Gadolinium Enhancement.....	12
1.5.5	T ₁ Quantification.....	14
1.5.6	ECV Estimation	17
1.6	Scope of Thesis	19
2	Normative Data for Myocardial Native T₁ and Extracellular Volume Fraction in Children	20
2.1	Introduction.....	20
2.2	Materials and Methods.....	20
2.2.1	Study Population.....	20
2.2.2	Cardiac Magnetic Resonance.....	21
2.2.3	Image analysis.....	22
2.2.4	Statistical Analysis.....	24
2.3	Results.....	24
2.4	Discussion	33
2.4.1	Limitations	36

2.5	Conclusion	37
3	Effects of Age, Sex and Risk-Factors for Heart Failure on Native T₁ and Extracellular Volume Fraction	39
3.1	Introduction.....	39
3.2	Materials and Methods.....	40
3.2.1	Study Subjects.....	40
3.2.2	Cardiac MR Imaging Protocol.....	40
3.2.3	Cardiac MR Image Analysis.....	41
3.2.4	Statistical Analysis.....	42
3.3	Results.....	43
3.4	Discussion.....	54
3.4.1	Limitations.....	56
3.5	Conclusion.....	57
4	Sex Differences in Native T₁ and Extracellular Volume Fraction in Heart Failure	58
4.1	Introduction.....	58
4.2	Methods.....	59
4.2.1	Study Subjects.....	59
4.2.2	Cardiac MRI Protocol.....	59
4.2.3	Image analysis.....	60
4.2.4	Outcome Data Collection.....	61
4.2.5	Statistics.....	61
4.3	Results.....	62
4.3.1	Native T ₁	62
4.3.2	ECV.....	66
4.3.3	Outcomes.....	67
4.4	Discussion.....	77
4.4.1	Limitations.....	79
4.5	Conclusions.....	79

5	Reduced Right Ventricular Native Myocardial T₁ in Anderson-Fabry Disease: Comparison to Pulmonary Hypertension and Healthy Controls	81
5.1	Introduction.....	81
5.2	Methods.....	82
5.2.1	Subjects	82
5.2.2	CMR Imaging	83
5.2.3	Data Analysis	84
5.2.4	Statistical Analysis.....	86
5.3	Results.....	87
5.4	Discussion	90
5.4.1	Limitations	92
5.5	Conclusion	93
6	End-Systolic Imaging of Myocardial Extracellular Volume Fraction with Contrast Level Assessment using Intensity Ratios (CLAIR)	94
6.1	Introduction.....	94
6.2	Methods.....	95
6.2.1	Theory	95
6.2.2	Pulse Sequence.....	97
6.2.3	Bloch Equations Simulations and Lookup Table Generation.....	99
6.2.4	Numerical Simulations.....	101
6.2.5	Phantom Experiments	101
6.2.6	In Vivo Experiments	102
6.2.7	In Vivo Image Analysis	103
6.2.8	Statistics	106
6.3	Results.....	106
6.3.1	Simulations	106
6.3.2	Phantom Experiments	107
6.3.3	In Vivo	109
6.4	Discussion	113

6.4.1	Limitations	115
6.5	Conclusion	116
7	Discussion and Conclusions	117
7.1	Summary	117
7.2	Limitations	118
7.2.1	Image Acquisition Strategies	118
7.2.2	Normative Data	119
7.2.3	Histological Correlation.....	120
7.3	Future Directions	120
7.3.1	Longitudinal Data	121
7.3.2	Prognostic and Outcome Data	121
7.3.3	Technical Advancements	121
7.4	Conclusions.....	124
	References	126

List of Tables

Introduction	1
Table 1.1: T ₁ and T ₂ Relaxation Constants for Several Tissues	11
Normative Data for Myocardial Native T₁ and Extracellular Volume Fraction in Children	20
Table 2.1: MOLLI sequence parameters	22
Table 2.2: Demographics, CMR mass and volumes	26
Table 2.3: Native T ₁ Data for the Healthy Pediatric Cohort	27
Table 2.4: Extracellular Volume Fraction Data for the Healthy Pediatric Cohort.....	28
Table 2.5: Univariate and multivariate regression between T ₁ indices and physiologic parameters.....	32
Table 2.6: Interobserver and intraobserver variability	33
Effects of Age, Sex and Risk-Factors for Heart Failure on Native T₁ and Extracellular Volume Fraction	39
Table 3.1: Study group characteristics	44
Table 3.2: Comparison of cardiac magnetic resonance values between groups	48
Table 3.3: Relationship between native myocardial T ₁ and native blood T ₁ or hematocrit.....	50
Table 3.4: Comparison of native T ₁ and ECV based on the presence or absence of late gadolinium enhancement	50
Table 3.5: Relationship between age and T ₁ measures	53
Sex Differences in Native T₁ and Extracellular Volume Fraction in Heart Failure	58
Table 4.1: Participant characteristics and CMR data	63
Table 4.2: Comparison of cardiac magnetic resonance values between groups	64
Table 4.3: Outcome occurrence, by subject group and sex	69
Table 4.4: Univariate and multivariate Cox regression analysis, considering T ₁ and ECV as continuous variable	75
Table 4.5: Univariate and multivariate Cox regression analysis, considering T ₁ and ECV as binary variable	76
Reduced Right Ventricular Native Myocardial T₁ in Anderson-Fabry Disease: Comparison to Pulmonary Hypertension and Healthy Controls.....	81
Table 5.1: Subject characteristics	87

Table 5.2: CMR variables.....	88
End-Systolic Imaging of Myocardial Extracellular Volume Fraction with Contrast Level Assessment using Intensity Ratios (CLAIR).....	94
Table 6.1: T ₁ , T ₂ , and Calculated [Gd] values for the agarose phantoms	108
Table 6.2: Subject characteristics	110
Table 6.3: CMR values	110

List of Figures

Introduction	1
Figure 1.1: Example image of k-space data and the corresponding cardiac image	7
Figure 1.2: Simplified schematic representation of "single-shot" imaging	8
Figure 1.3: Simplified schematic representation of "segmented" imaging.....	8
Figure 1.4: Sample non-contrast enhanced axial images	9
Figure 1.5: Longitudinal magnetization (M_z) recovery	10
Figure 1.6: Transverse magnetization (M_{xy}) decay.....	10
Figure 1.7: Late gadolinium enhancement.....	13
Figure 1.8: Sample T_1 maps in a healthy individual	16
Figure 1.9: Extracellular volume fraction (ECV) map	18
Normative Data for Myocardial Native T_1 and Extracellular Volume Fraction in Children	20
Figure 2.1: Sample native T_1 image from a healthy pediatric patient.....	23
Figure 2.2: Age distribution of study cohort.....	25
Figure 2.3: Native T_1 and ECV in the interventricular septum as a function of heart rate and age.....	29
Figure 2.4: Interobserver Bland-Altman plots for T_1 measures.....	30
Figure 2.5: Intraobserver Bland-Altman plots for T_1 measures.....	31
Effects of Age, Sex and Risk-Factors for Heart Failure on Native T_1 and Extracellular Volume Fraction.....	39
Figure 3.1: Example SASHA image set from a healthy male participant	42
Figure 3.2: Distribution of age by sex and risk group	45
Figure 3.3: Native T_1 and ECV between sex and risk factor groups	49
Figure 3.4: Correlation between age and native T_1 values	51
Figure 3.5: Correlation between age and ECV values	52
Sex Differences in Native T_1 and Extracellular Volume Fraction in Heart Failure	58
Figure 4.1: Mean \pm standard deviation plots shown for septal regions for native T_1 and ECV by sex .	65
Figure 4.2: Mean \pm standard deviation plots shown for septal regions for native T_1 and ECV by sex when septal regions with LGE are excluded.....	66
Figure 4.3: Kaplan-Meier survival analysis plots	71

**Reduced Right Ventricular Native Myocardial T₁ in Anderson-Fabry Disease:
Comparison to Pulmonary Hypertension and Healthy Controls.....81**

Figure 5.1: Example of bSSFP cine images in diastole used for wall thickness measurements..... 85
Figure 5.2: Example SASHA T₁-mapping case..... 86
Figure 5.3: Myocardial T₁ values by ventricle and condition..... 89

**End-Systolic Imaging of Myocardial Extracellular Volume Fraction with
Contrast Level Assessment using Intensity Ratios (CLAIR).....94**

Figure 6.1: Schematic representation of the CLAIR pulse sequence..... 98
Figure 6.2: Schematic representation with example in vivo images..... 99
Figure 6.3: Sample lookup table 100
Figure 6.4: Example pre- and post-contrast CLAIR images..... 103
Figure 6.5: Example SASHA and CLAIR images..... 105
Figure 6.6: Simulation derived errors in estimated [Gd] as a function of errors in assumptions used 107
Figure 6.7: Simulation experiments showing an increase in error in contrast agent estimation as a
function of radiofrequency (RF) pulse number 107
Figure 6.8: The error in average contrast agent estimation (CLAIR vs. SASHA) for phantom
experiments as a function of the RF pulse number..... 109
Figure 6.9: Correlation of in vivo SASHA and CLAIR values 111
Figure 6.10: Relationship between in vivo contrast agent estimation errors vs. native T₁ 112
Figure 6.11: Error in in vivo average contrast agent estimation as a function of the RF pulse number
..... 113

List of Abbreviations

ACE-I	Angiotensin converting enzyme inhibitor
AFD	Anderson-Fabry disease
ANGIE	Accelerated and navigator-gated look-locker imaging for cardiac T ₁ estimation
ANOVA	Analysis of Variance
ARB	Angiotensin receptor blocker
BMI	Body mass index
bpm	Beats per minute
BSA	Body surface area
bSSFP	Balanced steady-state free precession
CAD	Coronary artery disease
CCB	Calcium channel blocker
CI	Confidence interval
CLAIR	contrast level assessment using intensity ratios
CMR	Cardiac magnetic resonance
CoV	Coefficient of variation
CV	Cardiovascular
ECG	Electrocardiogram
ECV	Extracellular volume
FA	Flip angle
FOVphase	Field of view in phase encoding direction
FOVread	Field of view in read encoding direction
Gd	Gadolinium
Gd-DTPA	Gadolinium-diethylenetriaminepentaacetic acid
GFR	Glomerular filtration rate

GRAPPA	Generalized autocalibrating partially parallel acquisitions
HASTE	HAIf fourier Single- shot Turbo spin-Echo
HC	Healthy control
Hct	Hematocrit
HEART	Heart Failure Etiology and Analysis Research Team
HF	Heart failure
HFmEF	HF with mid-range ejection fraction
HFpEF	HF with preserved ejection fraction
HFrEF	HF with reduced ejection fraction
HR	Heart rate
Hz	Hertz
IVS	Interventricular septum
kg	Kilogram
LGE	Late gadolinium enhancement
LV	Left ventricle
LVEDVi	Indexed left ventricular end-diastolic volume
LVEF	Left ventricular ejection fraction
LVESVi	Indexed left ventricular end-systolic volume
LVI	Inferior left ventricular wall
LVMi	Indexed left ventricular mass
LVSVi	Indexed left ventricular stroke volume
MCLE	Multicontrast late enhancement
MHz	Megahertz
MI	Myocardial infarction
mm	Millimeters

mM	Millimolar
MOLLI	Modified Look-Locker inversion recovery
MRI	Magnetic resonance imaging
ms	Milliseconds
nHB	Number of heart beats
NMR	Nuclear magnetic resonance
PH	Pulmonary hypertension
RF	Radiofrequency
ROI	Region of interest
RV	Right ventricle
RVEDVi	Indexed right ventricular end-diastolic volume
RVEF	Right ventricular ejection fraction
RVESVi	Indexed right ventricular end-systolic volume
RVI	Inferior right ventricular wall
RVSVi	Indexed right ventricular stroke volume
s	Second
SASHA	Saturation-recovery single-shot acquisition
SD	Standard deviation
ShMOLLI	Shortened modified Look-Locker inversion recovery
T ₁ MES	T ₁ mapping and ECV standardisation in CMR
TE	Echo time
TI	Inversion time
TR	Repetition time
TS	Saturation time

List of Symbols

[Gd]	Concentration of gadolinium contrast agent
°	Degree
^1H	Hydrogen proton
B_0	Static magnetic field
B_1^+	Radiofrequency field
E_z	Energy difference between anti-parallel and parallel energy states
G_x, G_y, G_z	Gradient fields
\hbar	Planck's constant
I	Signal intensity
J	Joules
k	Scaling constant
k	Boltzmann constant
K	Kelvin
M_0	Net magnetization
M_{xy}	transverse magnetization
M_z	Longitudinal magnetization
$n_{\text{anti-parallel}}$	Number of spins in anti-parallel energy state
NiCl ₂	Nickel chloride
n_{parallel}	Number of spins in parallel energy state
r_1	Proton relaxivity constant for spin-lattice relaxation
R_1	Spin-lattice relaxation rate
r_2	Proton relaxivity constant for spin-spin relaxation
R_2	Spin-spin relaxation rate
t	Time
T	Temperature

T	Tesla
T_1	Spin-lattice relaxation time
T_1^*	Apparent spin-lattice relaxation time
T_2	Spin-spin relaxation time
T_2^*	Apparent spin-spin relaxation time
γ	Gyromagnetic ratio
η	Saturation pulse efficiency
λ	Blood-tissue partition coefficient

Chapter 1

Introduction

1.1 Overview

The field of medical imaging is driven by the principle to obtain the most accurate and reliable information, with an important focus on developing alternative methods to obtain information that may otherwise require more invasive approaches. Within cardiology, this is exemplified in the evolution of the use of invasive cardiac catheterization and angiography. Assessment of myocardial function, anatomy, and perfusion are now readily assessed using alternative techniques such as echocardiography, radionuclide imaging, cardiac computerized tomography, and cardiac magnetic resonance imaging (MRI).

While many aspects of cardiac catheterization have non-invasive alternatives, there is significant interest in developing methods to supplant perhaps its most invasive diagnostic use – endomyocardial biopsy. While there are many factors that affect the safety and risks associated with biopsy, there can be complications related to the venous access or the biopsy procedure itself, with an overall complication rate of approximately 6%, including death.(1) These risks are balanced with the breadth of information available from examination of the acquired tissue, including histology, molecular analysis, immunologic assessment, and/or detection of viral genetic materials.(1)

Non-invasive imaging of the heart, and in particular the myocardium, can be performed with numerous modalities. The most familiar to many may be cardiac ultrasonography, typically referred to as echocardiography. Due to its portability, relative reduced expense, and safety, an echocardiogram may be a patient's first non-invasive imaging study. While it was once stated that echocardiography may be “the single most useful diagnostic test in the evaluation of patients with heart failure”, as stated in the 2001 ACC/AHA guidelines for the evaluation and management of chronic heart failure,(2) the strength of this statement is less evident in the updated guidelines from 2013.(3) Echocardiography typically will focus on ventricular structure and function, such as estimates of ventricular sizes and ejection fraction, and provides excellent evaluation of the cardiac valves. However, though overt structural changes of the myocardium may be present in severe

cases, there is limited clinical use of echocardiography for assessment of the myocardium itself. While there had been interest in techniques such as integrated backscatter,(4) routine use in the clinical sphere is not present. Cardiac computerized tomography is able to provide complimentary information on structure, and to a lesser extent function; however, it provides excellent non-invasive assessment of the epicardial coronary arteries. Similar to echocardiography, myocardial assessment is limited with computerized tomography, particular in clinical use; however, non-invasive assessment of the extracellular space has been shown.(5) Unfortunately, as its use is associated with ionizing radiation, alternative strategies are continually sought after.

Recently, there has been a significant amount of effort in the non-invasive assessment of myocardial fibrosis, particularly in the field of cardiac MRI. Tissue characterization, of which the assessment of fibrosis falls under, is a principal strength of cardiac MRI and is relatively unique to the modality. As the field matures, the application of existing techniques in health and illness is crucial to aid in comprehending not only the effects diseases have on the heart, but also the strengths and limitations of these techniques, providing valuable information to influence technical development.

1.2 Heart Failure

Many individuals worldwide are affected by heart failure (HF), with an estimated 600,000 Canadians(6) and 6.5 million Americans(7) affected. The heart is often considered as a simple pump, and its inability to maintain effective contractile function would be expected to be associated with typical symptoms of “heart failure”. However, the reality is much more complex and requires synthesis of numerous clinical, imaging, and biochemical aspects.

1.2.1 Types of Heart Failure

Individuals may be asymptomatic even in the presence of reduced left ventricular (LV) systolic function, though they are at high risk for progression to overt HF.(8) Alternatively, individuals may demonstrate HF symptoms in the presence of preserved ejection fraction, the gold standard measure of heart pump function, equivalent to the fraction of blood pumped from the full ventricular chamber in each heartbeat. Recent Canadian guidelines on the management of heart failure utilize three main terminologies when discussing heart failure phenotypes(9): HF with preserved ejection fraction (HFpEF): LV ejection fraction (LVEF) $\geq 50\%$; HF with a mid-range ejection fraction (HFmEF): LVEF 41%-49%; HF with reduced ejection fraction (HFrEF): LVEF

≤ 40%. There is also further consideration to individuals who may display a “recovered EF” phenotype,(9) where an individual who was previously classified as HFrEF has recovery of their systolic function and may be considered as a HFmEF or HFpEF. Importantly, while these classifications of heart failure help to provide a sense of commonality in cohorts of patients, there may be numerous divergent, underlying diagnoses and risk factors that have led to the development of HF which may carry additional prognostic information not accounted for by simple categorization. Given the varying underlying pathophysiology of myocardial dysfunction in heart failure, varying patterns of myocardial remodeling can be expected. Much of this remodeling is related to myocardial fibrosis, which may occur in distinct patterns.

1.3 Myocardial Fibrosis

1.3.1 Overview of Myocardial Architecture

To best understand the disease state, it is important to appreciate the healthy state. In the normal heart, cardiac myocytes represent roughly 2/3 – 4/5 of the heart tissue volume, despite representing only 1/4 - 1/3 of the number of cells.(10, 11) Of the remaining non-myocyte space, roughly 14% is represented by blood vessels, and 2% by connective tissue cells, based on animal studies.(12) Finally, the extracellular space (~20% of the heart muscle volume) primarily consists of a gel-like substance containing glycosaminoglycans, glycoproteins, and collagen fibres.(11, 12)

Changes to the extracellular space, particularly alterations in the distribution and types of collagen fibres, are the hallmark of myocardial fibrosis. The extracellular matrix, and in particular collagen fibres, plays a key role in the structure and function of the heart, including providing support and connections between myocardial cells and blood vessels, impacting myocardial stiffness over the cardiac cycle, altering the shape and relative wall thickness.(11)

1.3.2 Types of Myocardial Fibrosis

While myocardial fibrosis is a common finding in many conditions affecting the cardiovascular system, the extent and distribution will vary depending on the disease severity and etiology. It is then helpful to think of, and describe, myocardial fibrosis based on the pattern of changes to both the cellular and extracellular components of the myocardium. Overall, three main patterns of myocardial fibrosis are typically described(13):

Reactive Interstitial Fibrosis

Characterized by a typically progressive, diffuse distribution of increased collagen throughout the extracellular space from increased production by myofibroblasts, this form of interstitial fibrosis is seen in a variety of conditions, including diabetes, dilated cardiomyopathy, and pressure-overloaded conditions such as hypertension or aortic stenosis.(13) It is not typically associated with myocyte cell loss, the key feature of replacement fibrosis,(11) described further below. Importantly, it is felt to be a potentially therapeutic target, with the goal of reversing the changes.(14-19)

Replacement Fibrosis

Following myocyte loss, such as that associated with myocardial infarction or myocarditis, there is significant remodeling that occurs within the myocardium including the formation of overt scar tissue.(20, 21) The scar tissue acts together with other remodeling processes to distribute wall stress and minimize dilation.(20) Since myocyte replacement of those lost to necrosis or apoptosis does not typically occur, this form of fibrosis is felt to be irreversible.

Infiltrative Interstitial Fibrosis

Lastly, there is an additional form of fibrosis, which can be considered a variation of interstitial fibrosis. However, it is associated more so with abnormal infiltrative processes explicit to the specific disease, rather than the abnormalities in collagen synthesis and remodeling seen in reactive or replacement fibrosis. Examples of this include the non-caseating granulomas in sarcoidosis,(22) cardiac amyloid deposition in amyloidosis,(23) or as is the case in Anderson-Fabry disease, a deficiency in the α -galactosidase A enzyme causes progressive multiorgan accumulation of intracellular sphingolipids, including within the heart. However, though data is limited, coexisting myocardial fibrosis can be seen on biopsy.(24, 25)

1.4 Sequelae of Myocardial Fibrosis

1.4.1 Functional Impact

The increased production of collagen and other extracellular matrix proteins will ultimately impact the performance of the myocardium. Typically, myocardial stiffness is increased, affecting ventricular filling and diastolic function.(14, 26, 27) This stiffness may be mediated by the amount of collagen present,(28) alterations in the ratio of collagen types,(29) and/or the degree of collagen cross-linking,(30) independent of the presence of ventricular hypertrophy (increased wall

thickness and mass).(28) The presence of myocardial fibrosis is also associated with systolic dysfunction,(31, 32) and the degree of dysfunction has been correlated with the fibrosis burden.(32, 33)

1.4.2 Clinical Impact

In addition to structural and functional changes the heart, the presence of fibrosis can also have considerable clinical impact. Alterations in collagen synthesis and fibrosis have been shown to alter the electrical propagation in the heart, creating a substrate for arrhythmias.(34-39) Presumed to be related to this increased risk of arrhythmias, there is extensive evidence that myocardial fibrosis is associated with increased mortality risk.(40-46) Much of our understanding of the association of myocardial fibrosis and clinical outcomes is due to advances in non-invasive imaging, particularly cardiac MRI.

1.5 Cardiac MRI Assessment of Myocardial Fibrosis

1.5.1 Basics of Cardiac MRI

Since the first MRI image of thin water-filled glass capillaries almost 50 years ago,(47) there have been incredible advances in the field of MRI. While the versatility of MRI allows it to be used for nearly limitless applications, those with experience in MRI understand there are balances required in the acquisition of MRI images affecting various aspects of the final image quality, including the overall signal intensity, spatial resolution, temporal resolution, and total acquisition time. This is likely no better exemplified than in the field of cardiac MRI, where additional challenges are presented with both respiratory and cardiac motion. A comprehensive resource on MRI physics and techniques can be found in a textbook by Brown et al.(48)

The ability to obtain an image, be it from a water-filled capillary or a living person, stems from the fact that certain arrangements of the constituent nuclei within atoms are able to create a magnetic, or “dipole”, moment. While not all atoms, or their associated isotopes, are able to have a magnetic moment, it is fortunate that the hydrogen nucleus, consisting of a single proton, is not only able to produce such a moment, but is also the most abundant nucleus in the body. Water, and other complex molecules such as fats, exist in nearly all body tissues. Therefore, the hydrogen nucleus, henceforth referred to simply as a “proton”, is an ideal source of magnetic resonance signal.

The production of an image with MRI requires, in a simplistic description, three main steps. Initially, all the protons within the body's tissues are "prepared" when exposed to the strong, static magnetic field (B_0) within the MRI scanner. The strong magnetic field causes the protons to find an equilibrium between high and low energy states, though this process is not instantaneous, as will be discussed below. Importantly, there are not equal amounts of protons existing in the two energy states, described as being either parallel or anti-parallel to the external magnetic field, and this inequality is necessary in providing a net magnetization state. The ratio of the number of anti-parallel to parallel protons can be estimated using the Boltzmann distribution:

$$\frac{n_{anti-parallel}}{n_{parallel}} = e^{\frac{-E_z}{kT}}$$

where n is the number of protons in a given state, E_z is the difference in energy between the two states, k is the Boltzmann constant (equal to 1.38×10^{-23} J/K), and T is the temperature in Kelvin.

The difference in energy between states is related to the gyromagnetic ration (γ), which are constant values for a given nucleus, Planck's constant ($\hbar = 6.63 \times 10^{-34}$ J s), and the strength of the external magnetic field (B_0), by the following:

$$E_z = \gamma \hbar B_0$$

To put this into perspective, for protons ($\gamma = 42.58$ MHz/T) in the body (37°C , 310 K) at 1.5T (B_0) field strength, this equates to about 10 more protons in the parallel state for every 1,000,000 protons in the anti-parallel state. Given one millilitre of water has approximately 6.7×10^{22} protons, this would translate to roughly 3.3×10^{17} more parallel spins.

As stated above, the inequality of parallel to anti-parallel protons leads to net magnetization, noted as M_0 , along the main magnetic field (conventionally assigned the Z-axis). The net magnetization (M_0) can, using non-quantum descriptions, can be considered as a vector with components that project onto the longitudinal (Z-axis) or transverse (XY-axis) planes. In the unperturbed state, following exposure to a strong external magnetic field (B_0) and reaching equilibrium, all of the net magnetization (M_0) exists as longitudinal magnetization (M_z) along the Z-axis, with no net transverse magnetization (M_{xy})

However, hydrogen protons in the tissues can be "excited" to rotate the net magnetization towards the transverse plane following an applied, time-varying magnetic field (B_1^+). Following excitation, the excited protons produce a signal that is received using radiofrequency antennae

(“coils”). In conjunction with subtle changes to the static magnetic field, referred to as gradients (G_x , G_y , and G_z), the excited transverse magnetization is encoded with characteristic frequencies (or phases) that are related to the position of the precessing magnetization (^1H nucleus) within the MRI system. As such, this frequency and phase information can be used for spatial localization, paramount to creation of a 2- or 3-dimensional image.

Typically, these repeated excitations are collected one “line” at a time in a grid-like fashion, referred to as k-space, from which an image can be generated using a Fourier transformation of the acquired frequency information.

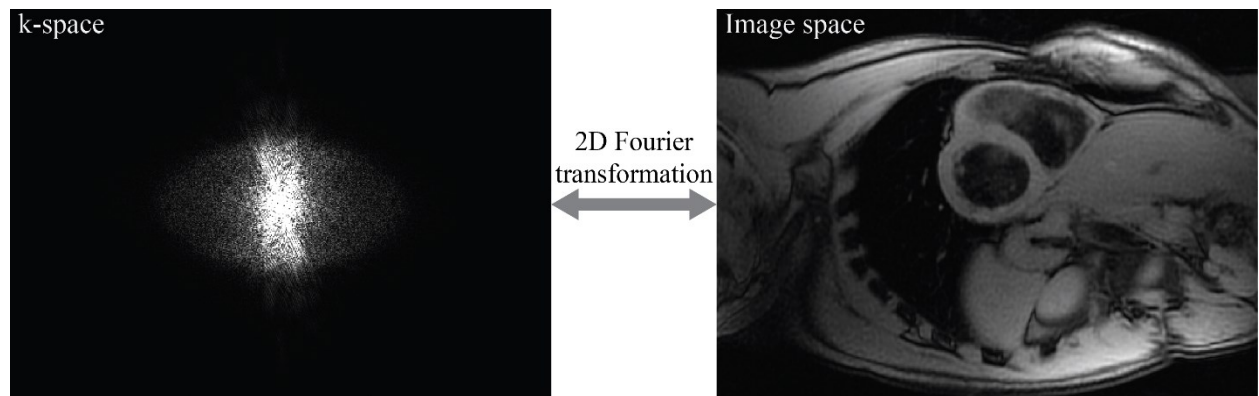


Figure 1.1: Example image of k-space data and the corresponding cardiac image that results from a two-dimensional Fourier transformation

While there are many approaches to this process of acquiring magnetic resonance imaging data, there are two general strategies that are commonly used for cardiovascular MRI, in particular. Specifically, these methods have different approaches to address the primary technical challenge of cardiac MRI, the constant and rapid motion of the beating heart.

First, all k-space data can be acquired as quickly as possible, for example within one heartbeat. Advantages to this “single-shot” technique include less sensitivity to irregular cardiac rhythm or diaphragmatic movement. However, it typically comes at the expense of limitations in spatial and temporal resolution, as the overall number of lines of k-space need to be minimized to be collected all within a period where the heart is as still as possible, such as the diastasis filling phase that occurs shortly after the rapid early filling phase prior to the atrial contraction.

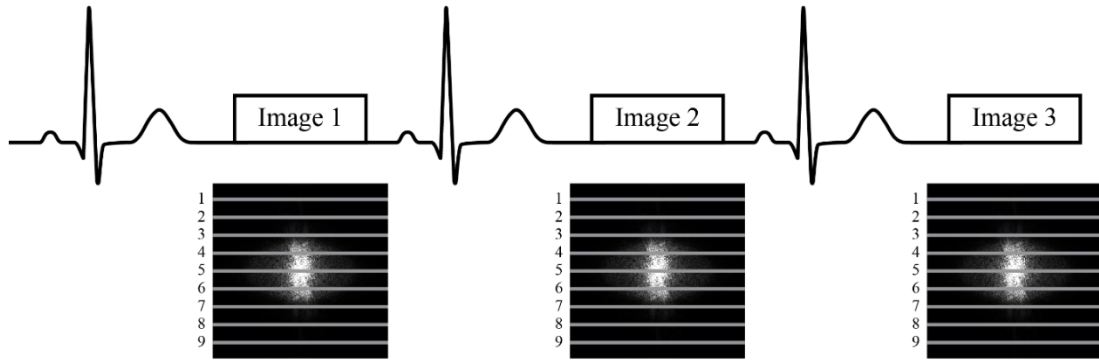


Figure 1.2: Simplified schematic representation of "single-shot" imaging, where all necessary k-space data for a given image (ex: Image 1) is collected within one heartbeat, with subsequent images collected in subsequent heartbeats

Alternatively, portions of k-space can be acquired over a series of heartbeats, referred to as “segmented” imaging. Through the use of a physiologic trigger, such as the electrocardiographic impulses, the segments of k-space can be acquired at a consistent part of the cardiac cycle. This typically allows more total k-space lines to be acquired for a given image (i.e. an increased imaging matrix size), leading to an increase in spatial resolution. Though the time required to obtain an image may be longer using the segmented approach, as complete k-space data is acquired over multiple heartbeats, each segment occurs over a small temporal footprint. Thus, there is less motion over that shorter period, which if present can lead to image blurring or artifacts.

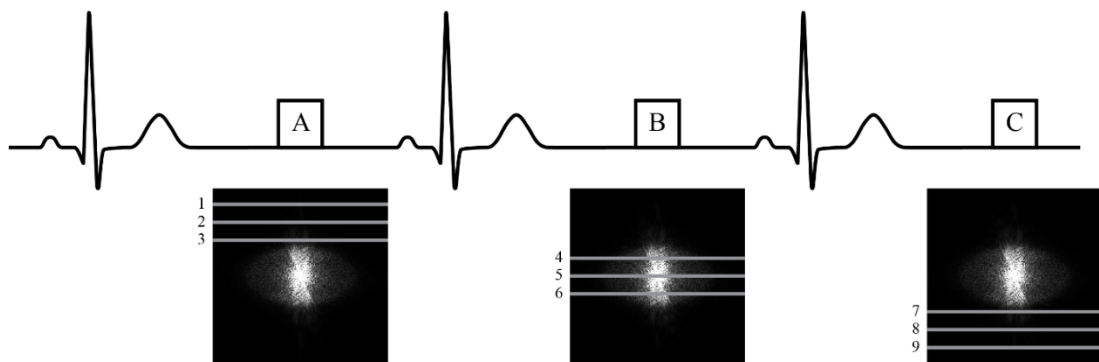


Figure 1.3: Simplified schematic representation of "segmented" imaging, where a defined portion of k-space data (ex: portion A, B, and C) is collected at separate instances, such as sequential heartbeats

One of the strengths of MRI imaging is its ability to obtain images with excellent and highly programmable contrast between different tissues and structures in the body. There are numerous factors that determine the appearance (relative signal intensities) of the attained MRI images. This tissue response is primarily affected by its relaxation properties, which govern how groups of protons behave following excitation and in their return to their pre-excited, or “equilibrium” state. Importantly, protons will have differing relaxation properties, depending on the tissue as well as the pathological state.

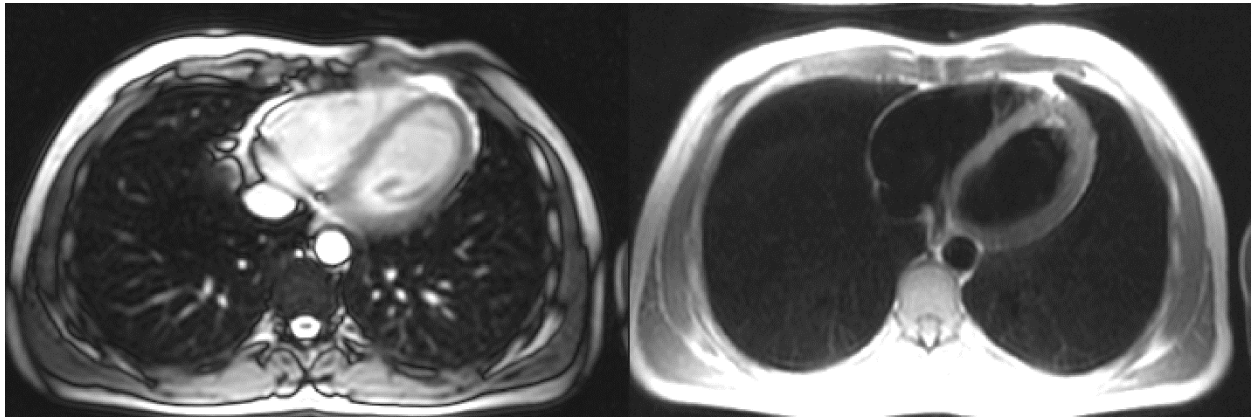


Figure 1.4: Sample non-contrast enhanced axial images through the chest at similar slice locations in the same individual, highlighting the different appearances of the same structures depending on the imaging sequences used, such as a balanced steady-state free precession (bSSFP) image on the left and a Half Fourier Single-shot Turbo spin-Echo (HASTE) image on the right

T₁ – Longitudinal Relaxation Time

As alluded to above, protons exposed to a strong, static magnetic field will seek a state of equilibrium between energy states. This occurs both when the subject is initially placed in the MRI system, and following the perturbation of this equilibrium during excitation in image acquisition. Through this process, protons exchange energy through interactions with other molecules in the environment, or so-called “lattice”. Thus, the time that characterizes this recovery to equilibrium is referred to as the longitudinal relaxation time (T_1), or spin-lattice relaxation, with a T_1 value specifically identifying the time it takes to recover 63% of the equilibrium value when starting from zero longitudinal magnetization.

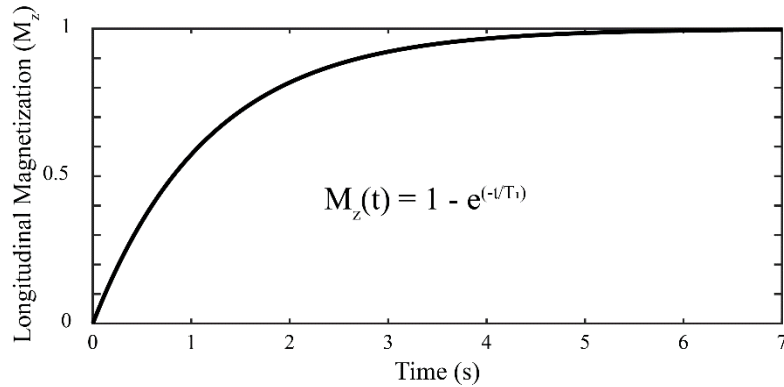


Figure 1.5: Longitudinal magnetization (M_z) recovery, or spin-lattice relaxation, as a function of time (t) following a saturation pulse ($M_z = 0$)

T_2 – Transverse Relaxation Time

Following excitation, the precessing magnetization decays in amplitude due to a number of mechanisms including a loss of coherence of phase due to interactions between neighbouring molecules. The rate at which the coherence disappears is referred to as the transverse relaxation time (T_2), or spin-spin relaxation, characterized by the time it takes to lose ~63% of the maximum signal. Additional causes of loss of phase coherence can occur that have the potential to be recovered or refocused, such as inhomogeneities in the static magnetic field. When all sources of signal loss of transverse magnetization are considered, the notation T_2^* is used.

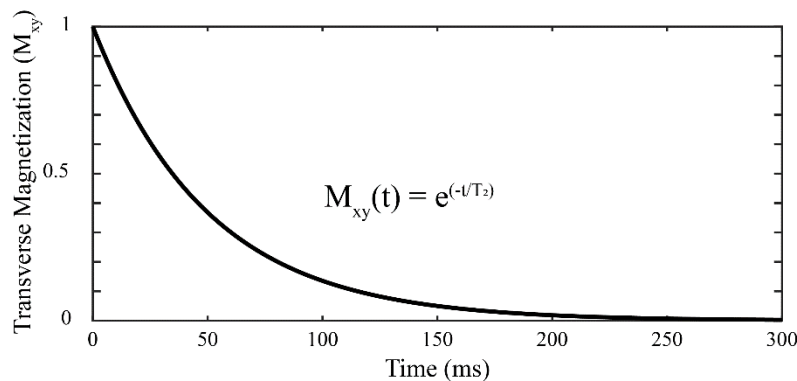


Figure 1.6: Transverse magnetization (M_{xy}) decay, or spin-spin relaxation, as a function of time (t) following an ideal 90-degree excitation pulse ($M_{xy} = 1$)

1.5.2 T_1 and T_2 in Tissues

As stated above, tissues can have differing proton relaxation times due to inherent differences in molecular environment, such as inherent differences between organ composition, such as between the brain and skeletal muscle. Importantly, relaxation times are also field strength dependent. Typical values for various biological tissues are provided in Table 1.1, with examples of differences for two field strengths.(49) Myocardial T_1 values range between 965 to 1170 ms at 1.5T and 1315 to 1523 ms at 3T, depending on the measurement method.(50-52). Myocardial T_2 values are typically 53 ms at 1.5T and 44 at 3T.(53)

Table 1.1: T_1 and T_2 Relaxation Constants for Several Tissues. Table from Bushberg et al. The Essential Physics of Medical Imaging. (2011)

Tissue	T_1 (0.5T) (ms)	T_1 (1.5T) (ms)	T_2 (1.5T) (ms)
Fat	210	260	80
Liver	350	500	40
Muscle	550	870	45
White matter	500	780	90
Gray matter	650	900	100
Cerebrospinal fluid	1800	2400	160

However, it is also important to note that relaxation time can also change as a result of pathological tissue changes that can occur as a result of a disease process. For example, subjects with acute myocarditis, characterized by myocardial inflammation and edema, demonstrate increased T_1 and T_2 relaxation times compared to control subjects, with increases in average T_1 from 965 ms to 1048 ms and average T_2 from 52.6 ms to 62.2 ms.(54) Decreased relaxation times can also be seen, with perhaps the best example in those with iron overload, including reduced T_1 values(55) and T_2^* values.(56)

1.5.3 T₁, T₂, and Gadolinium Contrast Agents

As discussed above, the T₁ and T₂ of a tissue are important factors that affect the acquired MRI signal. These values are strongly affected by the surrounding molecular environment and thus they may be altered in the disease state. Importantly, however, they can also be purposely manipulated through the use of contrast agents, including the highly paramagnetic gadolinium-based agents typically delivered via an intravenous injection as part of the cardiac MRI study protocol.

Gadolinium-based contrast agents lead to changes in both T₁ and T₂ in a predictable pattern, based on the agent's proton relaxivity, which can be thought of as the magnitude to which the agent can shorten the proton's T₁ and/or T₂ times for a given concentration. The mechanism of relaxation enhancement is result of a direct dipole interaction between the water molecules and the unpaired electron spins in the gadolinium itself. Ultimately the agents' effects can be described following the relaxivity equations:

$$R_{1Gd} = R_1 + r_1[Gd]$$

$$R_{2Gd} = R_2 + r_2[Gd]$$

where R₁ represents 1/T₁, R₂ represents 1/T₂, r₁ and r₂ represent the agent's proton relaxivity (mM⁻¹s⁻¹) for T₁ and T₂, respectively, and [Gd] represents the concentration of contrast agent. Thus, any tissue that contains a higher concentration of the contrast agent will have a proportionally shorter relaxation time.

1.5.4 Late Gadolinium Enhancement

Perhaps the most widely recognized and utilized cardiac MRI sequence for assessing the presence or absence of myocardial fibrosis, called "late gadolinium enhancement" (LGE), exploits the behaviour of gadolinium contrast agents. Typical gadolinium agents used clinically remain extracellular, residing in the vascular and interstitial space. However, water molecules move between tissue spaces, from the cells to the other pools, and thus the contrast agents affect the whole tissue water pool, but with an effective dilution effect as a function of the relative size of the extracellular volumes. Therefore, changes in the myocardial architecture associated with fibrosis, resulting in a relative increase in the extracellular space, will accrue more contrast agent and have proportionally shorter relaxation times than other non-fibrotic areas.

The LGE technique uses T_1 -weighted imaging (increased signal intensity with reduced T_1 values) to highlight these areas with shorter T_1 times due to the high concentration of gadolinium contrast, like those seen with replacement fibrosis following myocardial infarction.(57) The image acquisition for the LGE technique occurs following a preparatory inversion pulse, resulting in protons returning to equilibrium based on their respective T_1 times. The timing of the imaging portion of the pulse sequence, following a prescribed “inversion time”, is such that normal, healthy myocardium will provide no signal, leaving signal only to be obtained from tissue where there is additional T_1 shortening due to a relative increase in contrast agent concentration.

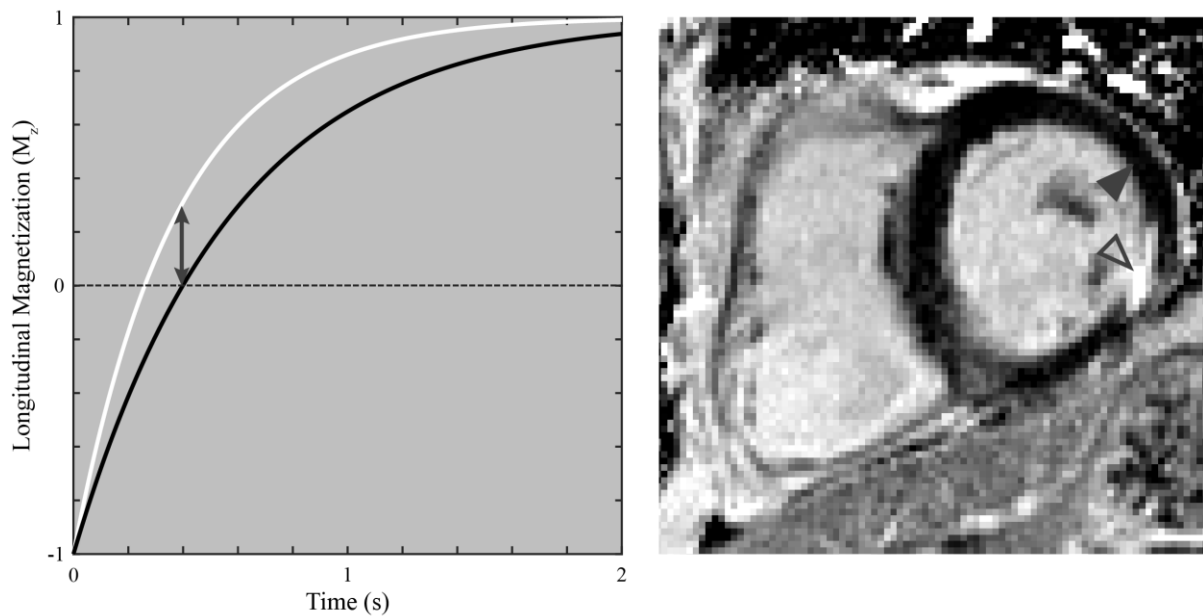


Figure 1.7: Late gadolinium enhancement. Left: An illustrative example of two different longitudinal magnetization (M_z) recovery curves following a preparatory inversion pulse. The white curve represents an area of tissue with fibrosis and relative increased gadolinium concentration, and thus a relatively reduced recovery time of M_z compared to the black curve, which would represent healthy myocardial tissue. The double arrow head line highlights the principle of late gadolinium enhancement (LGE) imaging, wherein image contrast is created by imaging at a time where there is separation in the M_z recovery curves and healthy tissue (black curve) would provide little signal as the longitudinal magnetization is at a null point ($M_z = 0$). Right: An in vivo illustration of "positive" late gadolinium enhancement imaging in a 52 year old male, depicting a moderate sized subendocardial infarction (replacement fibrosis) involving the inferolateral wall (open arrowhead), compared to healthy myocardium (solid arrowhead)

The development of LGE imaging meant that the relationship between functional and clinical abnormalities and fibrosis could be explored without the need for invasive biopsy or post-mortem histopathology.

1.5.4.1 Critical Limitations of LGE Imaging

The image contrast illustrated in Figure 1.7 that is used to detect myocardial scar is dependent on the relative signal intensity difference between the scar and surrounding, assumedly healthy, tissue. No information is provided regarding the potential presence of scar, notably the more diffuse interstitial fibrotic scar. Additionally, LGE is used most commonly as a binary test, to identify pixels that are positive for scar, but provides no information regarding the severity of the scar. Thus, LGE imaging is of no utility in the case where there are no focal areas of fibrosis and cannot be used to more acutely classify the nature of the scar, by the severity of changes in the tissue environment.

1.5.5 T₁ Quantification

As described previously, the relaxation times of a tissue are related to the tissue's composition, which can be altered in the disease state. Thus, if the relaxation times can be measured directly, they may provide a more objective and quantifiable biomarker. Indeed, T₁ measurements found some early clinical use in the assessment of myocardial fibrosis or perfusion, however scan time was often long or required multiple breath-holds.(58-62)

More recent technical advances have led to the development of robust, reproducible and patient-friendly measurements of T₁ in the heart, referred to as T₁-mapping. Messroghli et al. developed a T₁-mapping method of the heart that was feasible within a breath-hold.(63) This modified Look-Locker inversion recovery (MOLLI) sequence, and its variants, are the most widely used approach for cardiac T₁-mapping today. They all share a common approach, where a series of T₁-weighted images are obtained following an inversion preparation pulse. The signal intensities within the images, obtained at varying inversion times (TI) can be used to solve for T₁, following the equation for T₁ recovery following an inversion pulse:

$$Signal(TI) = A - Be^{-TI/T_1^*}$$

$$T_1 = \left(\frac{B}{A} - 1\right) T_1^*$$

where T_1^* is the “apparent” T_1 , affected by the Look-Locker imaging sets altering the relaxation course, that may be accounted for with the use of the “Look-Locker correction factor” $(B/A-1)$. While the MOLLI family of sequences have been extensively used, there is extensive evidence illustrating systematic errors in the T_1 values on several pulse sequence and physiologic parameters, such as inversion pulse efficiency, flip angle, off resonance, T_2 values, magnetization transfer, and heart rate.(50, 64) Many of these dependencies stem from the need to acquire multiple images in each Look-Locker set (i.e. with each inversion pulse). It may take 8-10 seconds for full recovery of longitudinal magnetization following an inversion pulse, which is important in combining Look-Locker sets. Thus, to acquire more than 2-3 images within an achievable breath-hold, multiple images are obtained following each inversion pulse.

T_1 -mapping can also be performed using a saturation preparation pulse, instead of an inversion pulse, as is performed in the SATuration-recovery single-SHOT Acquisition (SASHA method).(51) The principal advantage to the saturation approach is that an image can be acquired following each preparatory pulse without needing to wait for full recovery of longitudinal magnetization, thus minimizing many of the sources of dependencies seen with the inversion approach.(50) Similar to the inversion recovery approach, the signal intensities within the series of images, each acquired a variable saturation time (TS) following their own saturation pulse, can be used to solve for T_1 , following the equation for T_1 recovery following a saturation pulse:

$$Signal(TS) = k \left(1 - \eta e^{-TS/T_1} \right)$$

where k is a scaling constant and η is the saturation pulse efficiency. Note there is no T_1^* term, as the signal recovery is not altered by the readout effects as is seen in the Look-Locker approach. The main disadvantage to the saturation method is a reduced range of image contrast, which adds some loss of precision to the fitting.(50, 51)

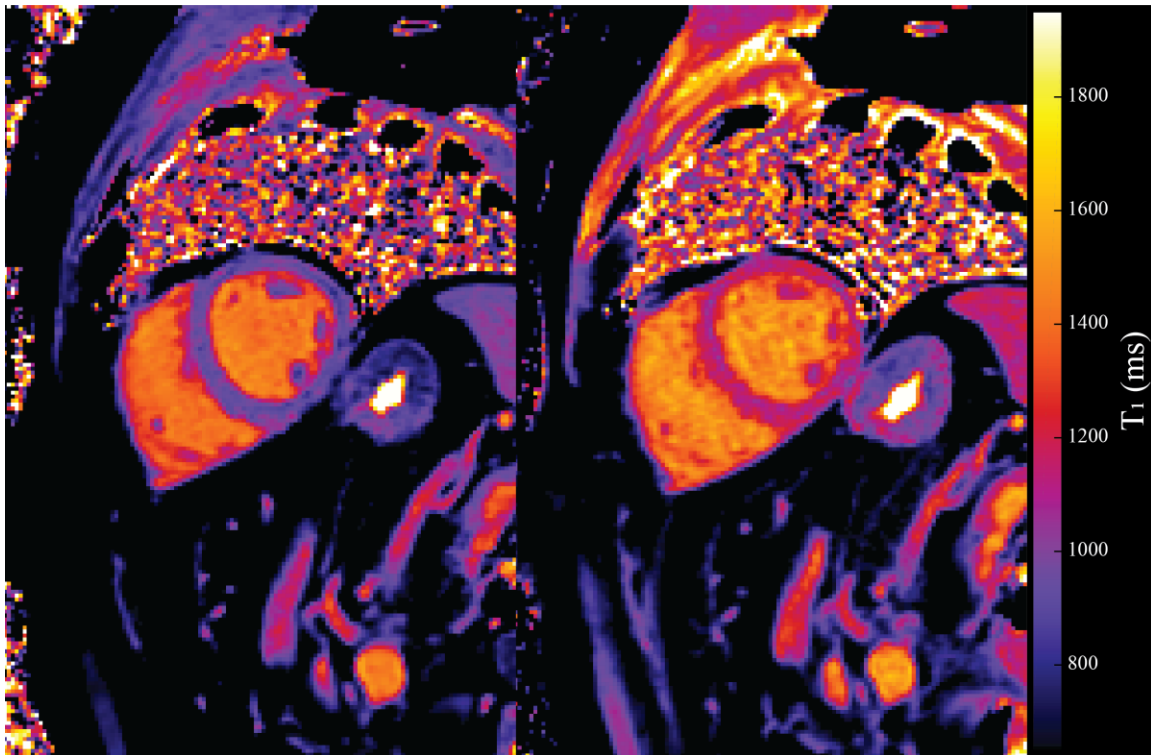


Figure 1.8: Sample T_1 maps in a healthy individual, including MOLLI (left) and SASHA (right), where pixel-wise T_1 values are calculated to generate an image where the signal intensity in a given pixel corresponds to a particular T_1 time

Myocardial non-contrast T_1 times, or “native T_1 ”, have been used to study a variety of physiological and pathological conditions, such as aging, hypertension, heart failure, dilated cardiomyopathy, hypertrophic cardiomyopathy, myocarditis, myocardial infarction,(65-71) where interstitial, diffuse fibrosis may be expected in addition to possible areas of replacement fibrosis. Native T_1 evaluation has also been performed in conditions associated with infiltrative interstitial fibrosis, such as amyloidosis, Anderson-Fabry disease, and iron-overload.(55, 69, 72-75)

Performing T_1 -mapping following the administration of a gadolinium-based contrast agent can take advantage of the same principle used for LGE imaging; the relationship between shortened T_1 times and contrast agent concentration. Indeed, this has been correlated with endomyocardial biopsies showing a strong relationship between the post-gadolinium myocardial T_1 time and histological measures of diffuse fibrosis.(76-78) However, the post-gadolinium T_1 time is dependent on a variety of factors including the contrast agent’s relaxivity, dose, time between injection and imaging, and an individual’s hematocrit and renal clearance.(13) This limits

the ability to perform comparisons between different sites, or even within the same site, as any of these factors may lead to differences in T_1 values that are not related to the disease process itself.

1.5.6 ECV Estimation

Thankfully, some of these factors that affect post-gadolinium T_1 times may be mitigated by considering that the concentration of contrast agent in the tissue is dependent on the blood contrast agent concentration. This ratio is referred to as the partition coefficient, or lambda (λ).

$$\lambda = \frac{[Gd]_{tissue}}{[Gd]_{blood}}$$

However, as described previously, the gadolinium contrast agent resides only outside of cells, including red blood cells. Thus, a correction factor is also needed to normalize the estimated blood concentration of gadolinium-based on an individual's plasma volume, equal to 1-hematocrit. Thus, the extracellular volume fraction (ECV) can be estimated using lambda and the hematocrit.

$$ECV = \frac{[Gd]_{tissue}}{\left(\frac{[Gd]_{blood}}{1 - hematocrit}\right)}$$

Considering the relaxivity equation described previously, and that a contrast agent's relaxivity is typically assumed to be consistent between the blood and tissue,(79) the equation can be rewritten as:

$$ECV = (1 - hematocrit) \left(\frac{[R_{1Gd} - R_1]_{tissue}}{[R_{1Gd} - R_1]_{blood}} \right)$$

This can further be expressed in terms of T_1 values:

$$ECV = (1 - hematocrit) \left(\frac{\left[\frac{1}{T_{1Gd}} - \frac{1}{T_1} \right]_{tissue}}{\left[\frac{1}{T_{1Gd}} - \frac{1}{T_1} \right]_{blood}} \right)$$

This approach to myocardial ECV estimation has been shown to have good agreement with invasive histological measurements of fibrosis.(80-85) Alterations in ECV have been demonstrated in a variety of conditions, such as aortic stenosis, myocardial infarction, myocarditis, dilated cardiomyopathy, hypertrophic cardiomyopathy, heart failure, cardiac amyloidosis, congenital heart disease, and following heart transplantation, amongst others.(86-95) Importantly, it has also been found to have important prognostic information, showing associations with adverse outcomes such as hospitalization and death.(85, 96-103)

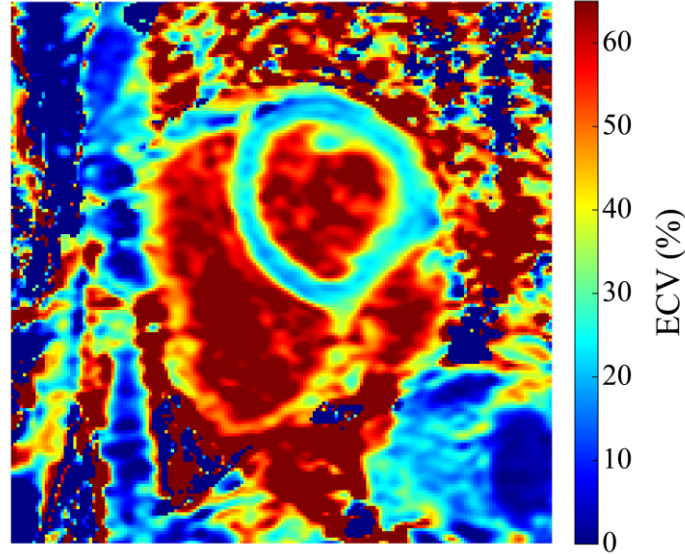


Figure 1.9: Extracellular volume fraction (ECV) map, using the SASHA sequence, in a healthy 63 year old female. Similar to the T_1 maps in Figure 1.8, pixel-wise ECV values are calculated, and the signal intensity in a pixel corresponds to a given ECV value

It is important to note, that despite evidence of correlation between T_1 -mapping and histological measures of fibrosis, they are not direct measures of collagen accumulation. Any causes of changes to the ratio of extracellular and intracellular compartments may be detected, such as edema.(104-106) While T_1 -mapping sequences have been shown to have dependencies on various physiologic and imaging parameters, as described above, it is not yet known how these may interact together when deriving ECV.

The achievement of developing cardiac T_1 -mapping within a single, comfortable breath-hold requires some concessions to image acquisition. The single-shot acquisition strategy typically used limits the spatial resolution to 1.4 to 2.3 mm.(50) This, along with a typical slice thickness of 8 mm, may lead to partial volume artifacts of structures adjacent to the myocardial tissue, such as blood or epicardial fat. Additionally, the single-shot images are acquired over 150 to 200 ms,(50) thus are typically restricted to the diastasis phase of diastole, where cardiac motion may be minimum. Significant cardiac phase or respiratory motion can lead to significant artifacts, and even subtle motion can lead to blurring within the acquired image.(50) This limits the application of T_1 -mapping in thin walled structures, such as the right ventricle. Thus, ongoing development is often focused on improvements in image acquisition strategies, including alternatives to the single-shot approach.

1.6 Scope of Thesis

Subsequent chapters in this thesis will focus on the development and application of T_1 -mapping in health and disease, along with the development of a novel approach for non-invasive ECV assessment that has improved spatial and temporal resolution. Chapters 2 and 3 uses T_1 -mapping to investigate for alterations in ECV as a function of age and sex. In Chapter 3, consideration is given to any differences that may exist in the heart's adaptation in healthy individuals compared to those with cardiovascular risk factors associated with the development of heart failure, such as hypertension and diabetes. Chapter 4 uses T_1 -mapping to characterize differences within the heart failure population, including the different phenotypes often encountered in clinical practice. This includes individuals with reduced ejection fraction, who have long been the "classical" perception of those with heart failure, and those with preserved ejection fraction, a group that is receiving increasing attention in the cardiology community. Chapter 5 examines right ventricular changes, when hypertrophy is present, in subjects with Anderson-Fabry disease and those with pulmonary hypertension. In addition to highlighting different pathophysiologic origins to the right ventricular hypertrophy, it also demonstrates limitations in the use of existing techniques in all areas of the heart. Chapter 6 explores the development of a new method for estimation of tissue contrast agent concentration and extracellular volume. With this method, the single-shot approach is abandoned for a segmented acquisition to provide an increase in spatial resolution and decreased temporal footprint, allowing imaging at end-systole when there is increased myocardial wall thickness. The technique, referred to as Contrast Level Assessment using Intensity Ratios (CLAIR), relies on pre- and post-contrast signal intensity ratios that can be converted to tissue contrast agent concentrations based on a lookup table approach. Finally, Chapter 7 speaks to some of the limitations encountered in both the application and development of cardiac T_1 -mapping techniques, with further discussion on future directions of the field.

Chapter 2

Normative Data for Myocardial Native T_1 and Extracellular Volume Fraction in Children

2.1 Introduction

Measurement of myocardial T_1 relaxation times and extracellular volume fraction (ECV) by cardiac magnetic resonance (CMR) provides non-invasive biomarkers for diffuse myocardial fibrosis, demonstrating excellent correlation with invasive histological methods.(80, 95) Myocardial fibrotic remodelling occurs in a variety of pediatric and congenital heart diseases and is associated with ventricular dysfunction and arrhythmias.(91, 107, 108) Cardiac magnetic resonance metrics of diffuse myocardial fibrosis have been shown to be increased in children following repair of tetralogy of Fallot,(109) Fontan physiology,(93) heart transplantation,(95) and muscular dystrophy.(110)

The clinical and scientific utility of measures of diffuse fibrosis in children is hampered by a lack of reference values. While it has been suggested that each centre establish their own local reference values,(111) this is challenging in the pediatric population due to limitations to research in children, especially when it involves intravenous access and administration of gadolinium.

The primary aim of this study was to establish pediatric normative myocardial native T_1 times and extracellular volume fractions using the modified Look-Locker inversion recovery (MOLLI) approach.

2.2 Materials and Methods

2.2.1 Study Population

This study was approved by the research ethics board at The Hospital for Sick Children (study number 1000053256). Due to the retrospective nature of the study, the need for informed consent was waived.

Between April 2014 and March 2017, a convenience sample of healthy pediatric subjects, between 9-18 years of age, who underwent a clinical cardiac magnetic resonance examination including T₁-mapping were identified via the institutional CMR database. Subjects were included if there was no known history of recent viral illness and the CMR was indicated for: 1) screening of an asymptomatic individual based on a family history of cardiomyopathy or sudden cardiac death, in whom all other tests, including the CMR study and genetic workup, were normal; 2) anatomic clarification based on findings from echocardiography, such as difficulty visualizing portions of the aorta, pulmonary veins, or coronary arteries, which were found to be normal on CMR; 3) a workup of syncope or chest pain if the clinical suspicion of a cardiac etiology was low and if the CMR study revealed normal proximal coronary arteries and origins and was otherwise normal; 4) a workup for inverted T waves in leads V1-V3 (which are a normal finding in children and most adolescents) or frequent monomorphic premature ventricular complexes without coupled complexes if the CMR study was normal.

2.2.2 Cardiac Magnetic Resonance

Studies were performed on a single 1.5T system ('Avanto', Siemens Medical Solutions, Erlangen, Germany. Software release VB17 and VE11B), with a phased array flexible surface coil for signal receiving and the inherent system bodycoil for radiofrequency transmission. Assessment of ventricular volumes, function, and myocardial mass was performed using balanced steady-state free precession imaging, acquired as a short-axis stack. Typical parameters included: minimal repetition (TR) and echo times (TE), flip angle (FA) 70°, in-plane spatial resolution between 1.5-2.0 mm², slice thickness 5 mm, gap adjustment to cover both ventricles with at least nine slices, temporal resolution to provide 20 true reconstructed frames per cardiac cycle.

T₁ quantification was performed at a mid-ventricular short axis level during diastasis, using a 5(nHB)3 MOLLI sequence, including inline motion correction, where nHB was 3 to 5 heart beats depending on the heart rate to allow for T₁ recovery between the two inversion experiments. Typical scan parameters are provided in Table 2.1, and include 8 mm slice thickness, FA 35°, TE 1.13-1.26 ms, TR 2.68-2.95 ms, bandwidth 1085 Hz/pixel, minimum inversion time 100-120 ms with 80 ms increment, and generalized autocalibrating partially parallel acquisitions (GRAPPA)

with an acceleration factor of two. When gadolinium was injected, T₁ quantification was repeated 15 minutes after administration of 0.2 mmol/kg gadobenate dimeglumine (‘MultiHance’, Bracco Diagnostics Inc., Montreal, QC, Canada).

Table 2.1: MOLLI sequence parameters

Weight	HR	Recovery Beats	FOVread (mm)	FOVphase (%)	Matrix	Pixel Size (mm)
20-49 kg (n=16)	<80	3	320	85.2	256x144	1.89x1.25
	80-100	4	320	85.2	256x144	1.89x1.25
	>100	5	320	85.2	256x144	1.89x1.25
>50 kg (n=33)	<80	3	360	85.2	256x144	2.13x1.41
	80-100	4	360	85.2	256x144	2.13x1.41
	>100	5	360	85.2	256x144	2.13x1.41

2.2.3 Image analysis

Ventricular volume analysis was performed in 'Qmass' (in 'MedisSuite', Version 2.1, Medis, Leiden, The Netherlands), following a standardized approach, with manual tracing of the endocardial borders of both ventricles on the short-axis images for quantification of end-diastolic and end-systolic volumes. Papillary muscles were included in the blood pool. Ejection fraction was calculated as the stroke volume (end-diastolic – end-systolic volumes), normalized to the end-diastolic volume. Left ventricular epicardial tracing was also performed to derive the myocardial mass, calculated from the myocardial muscle volume multiplied by the specific gravity of the myocardial tissue (1.05 g/mL). All volumes and masses were indexed to the individual's body surface area, with Z-scores derived based on data from Buechel et al.(112)

T₁ quantification was carried out by a single observer (JP), with 7 years experience in CMR, in 'Qmap' (in 'MedisSuite', Version 2.1, Medis). For assessment of interobserver and intraobserver reliability, analysis was repeated by a second, independent observer (CZL), blinded to any previous results. Studies with significant artifacts were excluded from analysis. Left ventricular (LV) endo- and epicardial borders were contoured on the in-line motion corrected T₁-

weighted images, including only the inner 50% of myocardium to avoid partial volume errors (Figure 2.1). Contours were manually adjusted on individual T_1 -weighted images to compensate for incomplete motion correction. A single region of interest (ROI) was placed in the blood pool of the left ventricular cavity. The LV myocardium was divided into six segments according to the American Heart Association model, which allowed for removal of segments containing visible artifact and for quantification of septal (average of T_1 in the antero- and inferoseptal segments) and LV free wall (average of T_1 in the antero- and inferolateral segments).

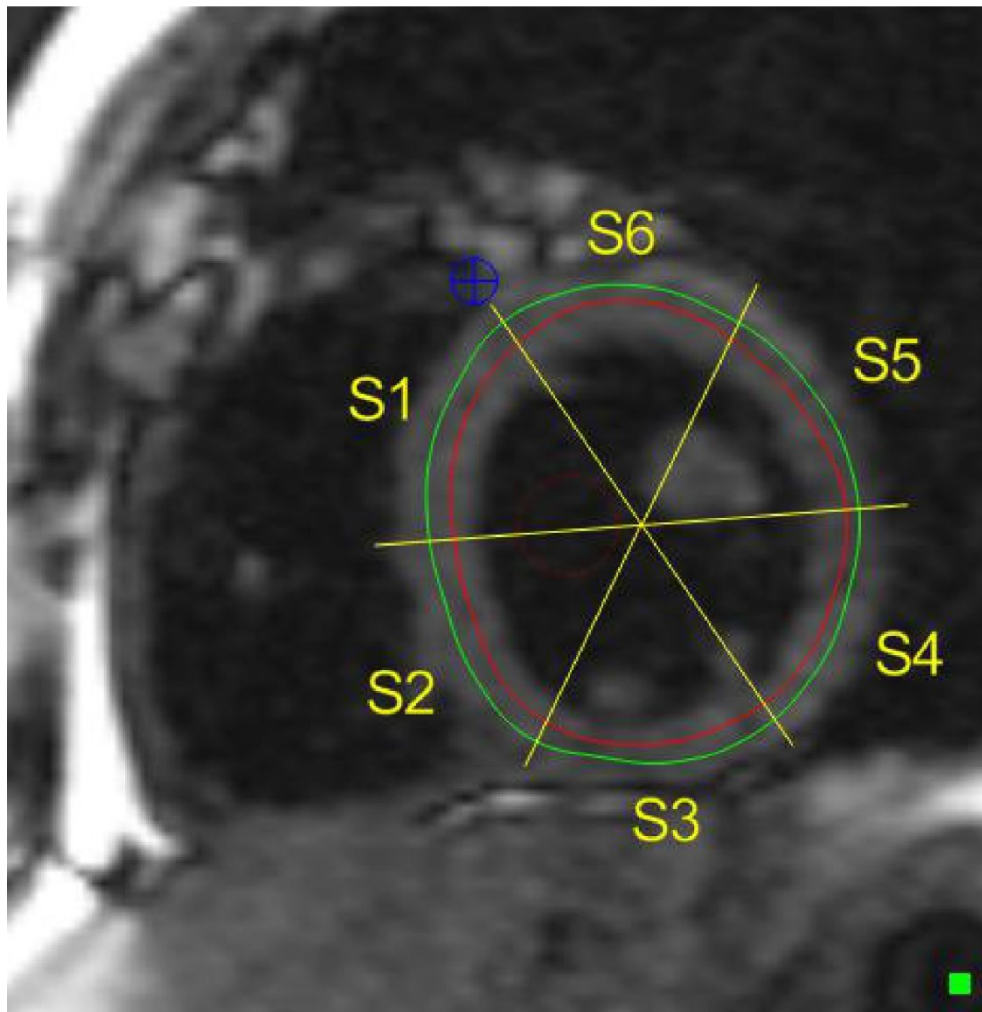


Figure 2.1: Sample native T_1 image from a healthy pediatric patient, including endocardial (red), epicardial (green), and blood pool (dashed maroon) contours. The slice is divided into six equidistant segments.

T_1 values were calculated using average ROI signal and a curve fitting algorithm. Resultant T_1 times were corrected for incomplete inversion using correction factors depending on the inversion pulse utilized; 1.0811 for a traditional hyperbolic secant pulse and 1.0365 for a tan/tanh

adiabatic pulse.(113) In those subjects receiving intravenous contrast, ECV was calculated as previously described(111) using pre- and post-contrast T₁ times and the subject's hematocrit, drawn immediately prior to the CMR and analyzed in the hospital central laboratory.

2.2.4 Statistical Analysis

Values are reported as mean ± standard deviation, or count (%), where applicable. Comparisons within the same patients were performed using paired Student's t-tests. Comparisons between groups of patients were undertaken using the unpaired Student's t-test or Mann-Whitney U test, depending on the normality of the data. Associations between myocardial native T₁ or ECV and other parameters, were assessed using univariate linear regression, with variables included in a multivariate regression model if the p-value was < 0. 1 on univariate testing. Reliability was assessed using intraclass correlation coefficient for interobserver and intraobserver reliability, with additional assessment using Bland-Altman plots and associated limits of agreement. A p-value of 0.05 was regarded as significant. Statistical analysis was performed using STATA software (Version 11.2, Stata Corporation, College Station, TX, USA).

2.3 Results

The CMR examinations of 50 subjects met the inclusion criteria and were included in the study. Two patients were excluded due to significant image artifacts precluding analysis. Patient characteristics for the 48 analyzed subjects are outlined in Table 2.2. The most common indication for cardiac MRI was for screening of asymptomatic individual based on a positive family history (19/48, 40%), followed by both anatomical clarification (12/48, 25%) or syncope/chest pain (12/48, 25%), and finally for abnormal T-waves / PVCs (5/48, 10%). The youngest subject was 8.6 years old, while the oldest was nearly 18 (Figure 2.2), and there was no significant difference in ages between boys and girls (p=0.057). There was a significant correlation with BSA and age (R² = 0.513, p<0.001).

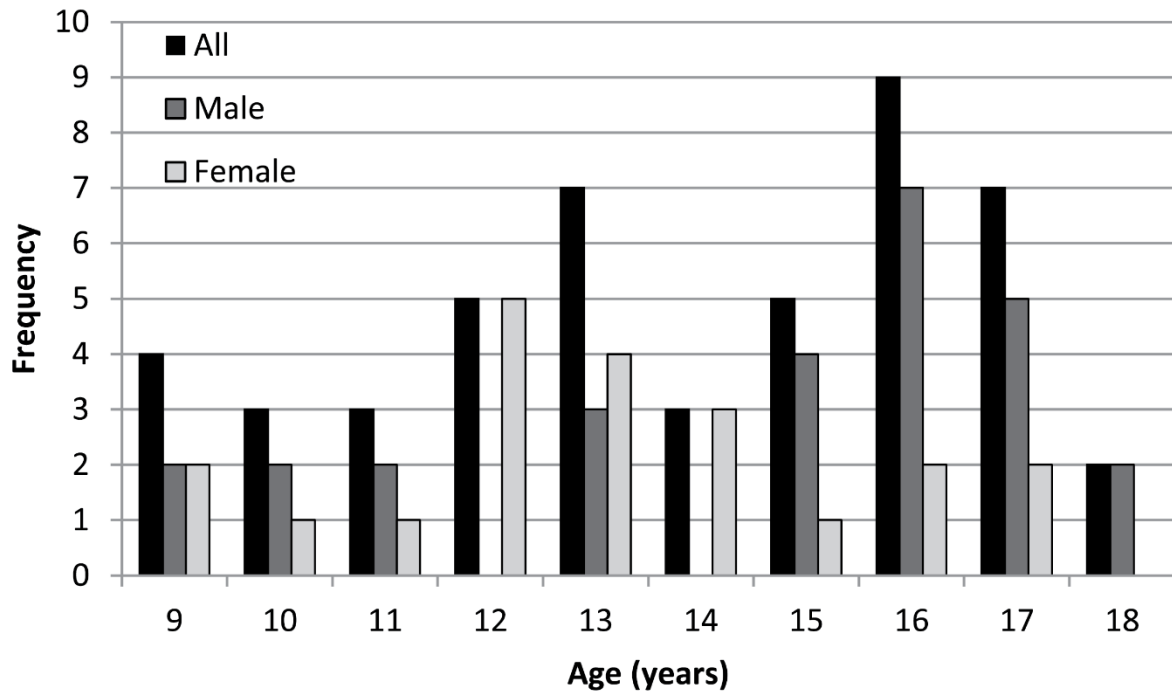


Figure 2.2: Age distribution of study cohort, rounded to the nearest year.

Cardiac magnetic resonance results from volumetry are listed in Table 2.2. While ventricular mass and volumes were different between sexes (LV mass $p=0.003$, LVEDVi $p=0.015$, LVESVi $p=0.001$), there was no difference between Z-score values for these metrics between sexes (LV mass Z-score $p=0.873$, LVEDVi Z-score $p=0.078$, LVESVi Z-score $p=0.889$). While there was no significant sex difference between LV mass-to-volume ratio ($p=0.082$), there was a slight increase in ejection fraction in females (0.047). T_1 and ECV results are presented in Table 2.3 and Table 2.4. Myocardial native T_1 was longer in girls when considering only the septal ($p=0.014$) or free wall segments ($p<0.001$), with non-significantly longer T_1 for the entire LV in females ($p=0.066$). Overall, the average native T_1 in the interventricular septum was significantly higher than in the free wall ($p<0.001$); however, this difference remained significant only in boys ($p<0.001$). The average native blood T_1 was longer in girls versus boys ($p=0.013$), likely related to lower average hematocrit in girls ($p=0.0334$).

Table 2.2: Demographics, CMR mass and volumes

	All n=48	Male n=27	Female n=21	p-value*
Age (years)	13.9±2.7	14.5±2.7	13.1±2.4	0.057
Height (cm)	162±15	167±16	156±10	0.008
Weight (kg)	62.7±23.3	69.9±25.3	53.5±16.7	0.014
BSA (m ²)	1.66±0.37	1.78±0.40	1.51±0.28	0.011
Heart rate (bpm)	73.7±14.1	71.4±14.9	76.6±12.7	0.210
LV mass (g/m ²)	55±12	60±13	49±9	0.003
LV mass Z-score	-0.6±1.9	-0.6±2.0	-0.5±1.7	0.873
LVEDVi (ml/m ²)	91±13	96±14	86±11	0.015
LVEDVi Z-score	0.3±1.6	0.0±1.6	0.8±1.4	0.078
LVESVi (ml/m ²)	38±7	41±6	35±6	0.001
LVESVi Z-score	0.8±1.2	0.8±1.2	0.8±1.2	0.889
LVSVi (ml/m ²)	53±9	55±10	52±8	0.256
LVSVi Z-score	-0.2±1.6	-0.7±1.6	0.4±1.4	0.020
LVEF (%)	58±5	57±4	60±5	0.047
LVEF Z-score	-0.8±1.1	-1.1±1.1	-0.4±1.1	0.045
LV mass/volume (g/ml)	0.60±0.10	0.62±0.11	0.57±0.09	0.082
RVEDVi (ml/m ²)	98±18	103±19	92±15	0.044
RVEDVi Z-score	-0.1±1.6	-0.5±1.7	0.3±1.5	0.093
RVESVi (ml/m ²)	47±10	50±10	42±7	0.003
RVESVi Z-score	0.4±1.2	0.2±1.3	0.5±1.0	0.386
RVSVi (ml/m ²)	52±11	53±11	50±10	0.258
RVSVi Z-score	-0.7±1.8	-1.2±1.7	0.0±1.6	0.026
RVEF (%)	52±4	51±4	54±4	0.012
RVEF Z-score	-0.8±1.0	-1.1±1.1	-0.5±0.8	0.069

BSA = body surface area, CP = chest pain, PVCs = premature ventricular complexes, LV = left ventricle, LVEDVi = indexed left ventricular end-diastolic volume, LVESVi = indexed left ventricular end-systolic volume, LVSVi = indexed left ventricular stroke volume, LVEF = left ventricular ejection fraction, RVEDVi = indexed right ventricular end-diastolic volume, RVESVi = indexed right ventricular end-systolic volume, RVSVi = indexed right ventricular stroke volume, RVEF = right ventricular ejection fraction

*p-values represent comparisons between male and female subjects

Table 2.3: Native T₁ Data for the Healthy Pediatric Cohort, presented as mean±SD and [95% Confidence Intervals]

	All n=48	Male n=27	Female n=21	p-value*
Native T ₁ (ms)				
Whole LV	1008±31 [999,1017]	1001±33 [988,1014]	1017±27 [1005,1030]	0.066
IVS	1022±32 [1013,1032]	1012±34 [999,1025]	1035±26 [1023,1047]	0.014
Free wall	1001±42 [989,1014]	981±29 [969,993]	1024±42 [1005,1044]	<0.001
Blood T ₁ (ms)	1578±74 [1557,1600]	1555±63 [1530,1580]	1608±77 [1573,1643]	0.013

LV = left ventricle, IVS = interventricular septum

*p-values represent comparisons between male and female subjects

Contrast was administered in 19/48 (40%) of cases, in 10 boys and 9 girls, and therefore permitted the calculation of ECV. Extracellular volume fraction, although higher on average in girls, was not statistically different between sexes ($p=0.123$). Average ECV in the interventricular septum was significantly higher than in the free wall ($p=0.018$); though this difference did not remain statistically significant in only boys or girls ($p=0.052$ and $p=0.209$, respectively).

Table 2.4: Extracellular Volume Fraction Data for the Healthy Pediatric Cohort, presented as Mean \pm SD and [95% Confidence Intervals]

	All n=19	Male n=10	Female n=9	p-value*
Hematocrit	0.43 \pm 0.03	0.45 \pm 0.03	0.42 \pm 0.03	0.0334
ECV (%)				
Whole LV	20.8 \pm 2.4 [19.6,21.9]	20.0 \pm 2.6 [18.1,21.8]	21.7 \pm 1.9 [20.2,23.1]	0.123
IVS	21.7 \pm 2.6 [20.5,23.0]	20.9 \pm 2.9 [18.8,22.9]	22.7 \pm 2.1 [21.1,24.3]	0.133
Free wall	20.6 \pm 2.6 [19.2,22.0]	19.7 \pm 2.4 [17.8,21.6]	21.7 \pm 2.5 [19.4,24.0]	0.128

LV = left ventricle, IVS = interventricular septum, ECV = extracellular volume fraction

*p-values represent comparisons between male and female subjects

Univariate regression demonstrated significant associations between myocardial native T_1 and nearly all parameters for the entire LV, interventricular septum, and free wall (Figure 2.3, Table 2.5). However, only LV mass Z-score remained significant for each location after multivariate analysis, while sex associations remained for the septum and free wall (Table 2.5). Univariate regression only showed a relationship for ECV with age and BSA (Figure 2.3, Table 2.5), however neither remained significant on multivariate analysis.

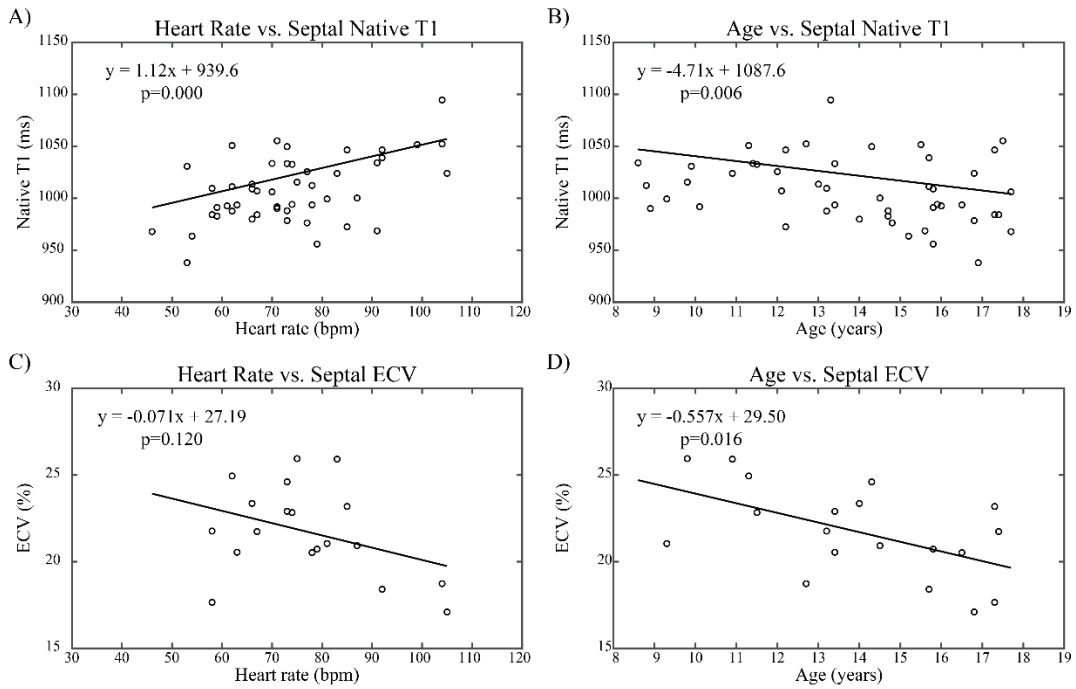


Figure 2.3: Native T₁ and ECV in the interventricular septum as a function of heart rate and age.

As assessed by intraclass correlation coefficients, interobserver and intraobserver reliability is overall excellent, with all values ≥ 0.75 and most ≥ 0.9 (Table 2.6). Bland-Altman plots are presented in Figure 2.4 and Figure 2.5.

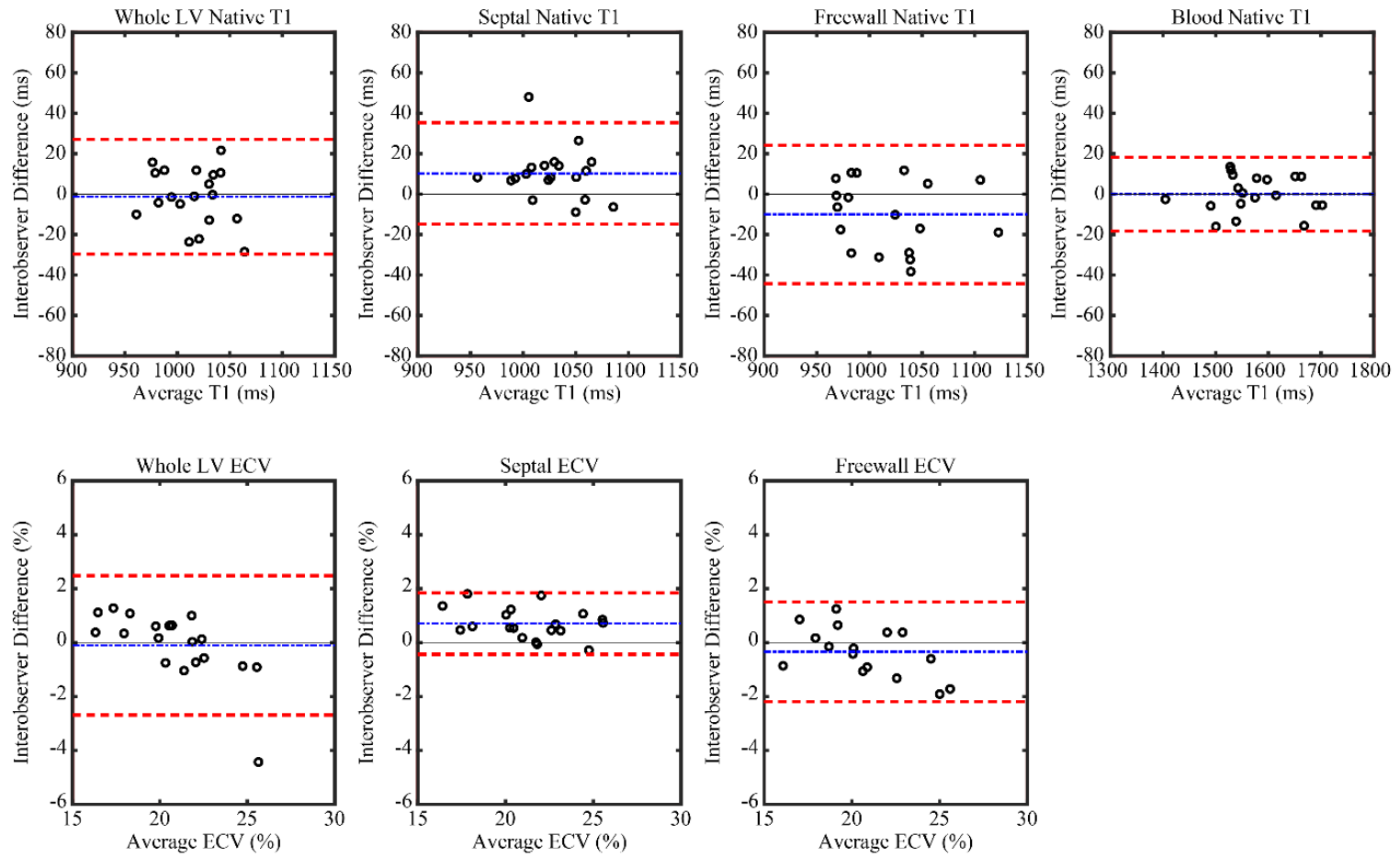


Figure 2.4: Interobserver Bland-Altman plots for T_1 measures.

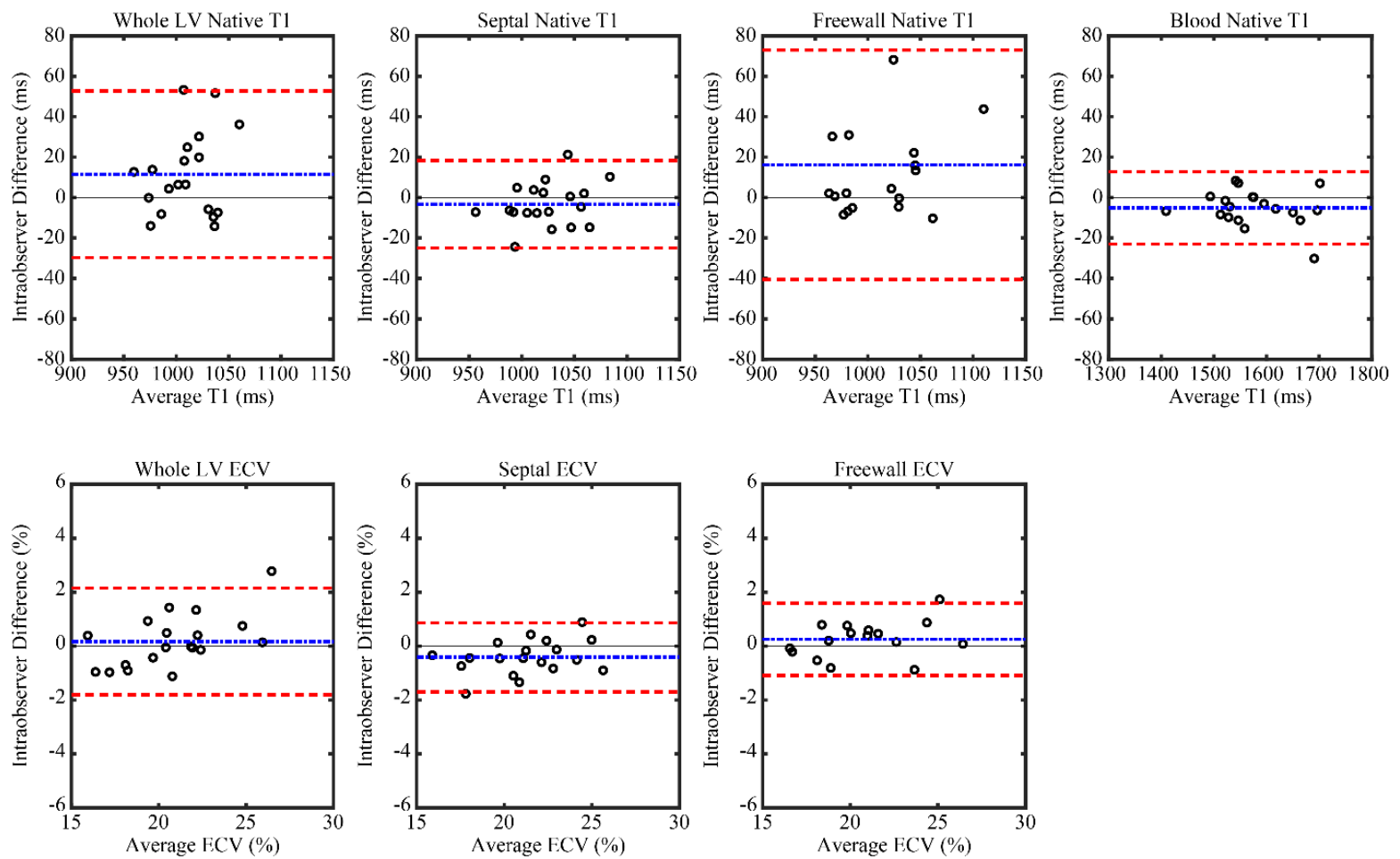


Figure 2.5: Intraobserver Bland-Altman plots for T_1 measures.

Table 2.5: Univariate and multivariate regression between T₁ indices and physiologic parameters

	Whole LV			Septum			Free Wall		
	slope	[95% CI]	p-value	slope	[95% CI]	p-value	slope	[95% CI]	p-value
<u>Univariate</u>									
Native T ₁									
Age (years)	-3.14	[-6.49,0.20]	0.065	-4.71	[-8.02,-1.41]	0.006	-5.23	[-9.64,-0.81]	0.021
Sex (Female)	-16.76	[-34.66,1.13]	0.066	-22.87	[-40.78,-4.95]	0.014	-43.77	[-65.22,-22.32]	<0.001
BSA (m ²)	-10.12	[-34.86,14.62]	0.414	-19.93	[-44.94,5.09]	0.116	-47.20	[-81.58,-12.82]	0.008
Heart Rate (bpm)	1.12	[0.55,1.69]	<0.001	1.12	[0.52,1.71]	<0.001	1.18	[0.21,2.16]	0.019
LV mass Z-score	-8.84	[-13.20,-4.48]	<0.001	-8.66	[-13.36,-3.96]	0.001	-10.73	[-17.74,-3.71]	0.004
LVEF (%)	1.24	[-0.81,3.30]	0.230	1.73	[-0.41,3.86]	0.110	3.09	[0.32,5.86]	0.030
ECV									
Age (years)	-0.46	[-0.87,-0.06]	0.026	-0.56	[-0.99,-0.12]	0.016	-0.47	[-0.95,0.00]	0.050
Sex (Female)	-1.69	[-3.88,0.50]	0.123	-1.83	[-4.28,0.62]	0.133	-2.01	[-4.67,0.65]	0.128
BSA (m ²)	-3.15	[-5.86,-0.44]	0.025	-3.20	[-6.31,-0.09]	0.044	-3.98	[-7.70,-0.27]	0.037
Heart Rate (bpm)	-0.06	[-0.14,0.03]	0.177	-0.07	[-0.16,0.02]	0.120	-0.02	[-0.13,0.10]	0.757
LV mass Z-score	-0.26	[-0.85,0.34]	0.374	-0.27	[-0.93,0.40]	0.410	-0.47	[-1.13,0.18]	0.145
LVEF (%)	0.05	[-0.18,0.27]	0.669	0.01	[-0.24,0.26]	0.917	0.14	[-0.13,0.41]	0.283
<u>Multivariate</u>									
Native T ₁									
Age (years)	-1.38	[-4.40,1.64]	0.362	-3.03	[-6.05,-0.01]	0.049	1.82	[-3.99,7.63]	0.529
Sex (Female)	-13.41	[-29.44,2.62]	0.099	-18.05	[-34.08,-2.02]	0.028	-33.59	[-54.97,-12.20]	0.003
BSA (m ²)	-	-	-	-	-	-	-43.10	[-87.81,1.61]	0.058
Heart Rate (bpm)	0.56	[-0.05,1.18]	0.072	0.55	[-0.07,1.16]	0.080	-0.12	[-1.01,0.78]	0.791
LV mass Z-score	-6.75	[-11.31,-2.18]	0.005	-6.13	[-10.69,-1.56]	0.010	-10.67	[-16.92,-4.41]	0.001
LVEF (%)	-	-	-	-	-	-	1.86	[-0.37,4.09]	0.099
ECV									
Age (years)	-0.28	[-0.80,0.23]	0.262	-0.43	[-1.00,0.15]	0.134	-0.26	[-0.87,0.35]	0.374
BSA (m ²)	-1.95	[-5.42,1.52]	0.251	-1.39	[-5.25,2.47]	0.457	-2.66	[-7.54,2.23]	0.261

LV = Left ventricle. BSA = body surface area. bpm = beats per minute. LVEF = left ventricular ejection fraction.

Table 2.6: Interobserver and intraobserver variability, represented as the intraclass correlation coefficient

	Inter		Intra	
	Native T ₁	ECV	Native T ₁	ECV
Whole LV	0.886	0.897	0.748	0.945
IVS	0.925	0.978	0.944	0.972
Free wall	0.934	0.948	0.789	0.975
Blood pool	0.993	-	0.993	-

LV = left ventricle, IVS = interventricular septum, ECV = extracellular volume

fraction

2.4 Discussion

This study provides normative pediatric data for native T₁, along with myocardial ECV from a single institution, using the 5(nHB)3 MOLLI acquisition on a 1.5T Siemens system. Myocardial T₁ and ECV are altered in a variety of conditions in adults, including myocarditis,(66) cardiomyopathies,(67) and congenital heart disease.(108) They are linked to outcomes and aid in the prediction of cardiac events.(96, 97) Reports in pediatrics are scarcer; however elevated myocardial T₁ and ECV have been demonstrated in acquired and congenital heart disease,(91, 93, 109, 114), following heart transplantation,(95, 115) and in cardiomyopathies.(110, 116-118) The use of T₁ and ECV has not yet reached a stage where it independently impacts clinical management, and it is typically used to shape an overall diagnostic impression for individuals undergoing a comprehensive CMR examination. A major barrier towards a more widespread clinical application of this technique in the care of children with heart disease is the lack of normative data. In the recently published consensus statement on parametric mapping,(111) it is suggested that while local reference ranges for T₁ and ECV should be derived and obtained, they require comparisons with published reported ranges. Whereas it may be possible for centres to establish their respective norms for myocardial native T₁ in healthy children, limitations in the administration of contrast agents will hamper the derivation of local reference values for ECV. The consensus statement(111) recommends utilization of literature values in this situation,

particularly given the reduced dependence of ECV on various system and sequence parameters. Thus, this study, which presents the largest known pediatric normative values for T_1 and ECV to date, using a widely applied T_1 relaxometry technique,(95, 110, 117-119) provides important benchmarks for these metrics for those performing CMR at 1.5T, using the 5(nHB)3 MOLLI pulse sequence as described above.

The average T_1 values reported in this study are higher than most published adult values using MOLLI, which are between 950-982 ms.(120-122) This may be due to the use of the 5(nHB)3 acquisition scheme in the current study, as most adult reports employ the traditional 3(3)3(3)5 acquisition scheme. A comprehensive review of all T_1 -mapping sequences is beyond the scope of this study, and the reader is directed to an excellent review by Kellman et al.(50) However, important differences between the “traditional” 3(3)3(3)5 and 5(nHB)3 MOLLI variants include the number of inversion pulse sets (3 inversion sets for traditional MOLLI, 2 sets for the variant in this study), the number of images in the first inversion set (3 images for the traditional MOLLI, 5 for the variant in this study), and the number of total number of images obtained (3+3+5=11 for traditional MOLLI, 5+3=8 for the variant in this study). By acquiring 5 images in the first inversion set, the 5(nHB)3 scheme increases the number of heart beats between inversion pulses, which increases the time between inversion sets to allow for fuller T_1 recovery. This decreases the heart rate sensitivity,(50) and results in increased T_1 times versus the original MOLLI scheme.(123) Therefore, usage of the 3(3)3(3)5 acquisition scheme is becoming less common. A recent study of healthy children, using a modified version of the “traditional” 3(3)3(3)5 MOLLI sequence with fixed time intervals between inversion sets [3(3s)3(3s)5] which reduces heart rate dependence, reports native T_1 values for the mid-ventricular slice of 1010 ms for the whole LV and 1017 ms for the IVS, which appear similar to those of the current study.(124) However, ECV was not reported. In a study of a large, healthy, adult Chinese cohort, average myocardial T_1 using the 5(3)3 MOLLI sequence was 1013 ± 27 ms, and yielded higher values in female vs. male subjects (1025 ± 26 ms vs. 1001 ± 23 ms),(119) similar to our findings. This study did not report ECV values. In contrast to native T_1 times, values for ECV in the current study are lower than those reported using the 3(3)3(3)5 acquisition scheme in adults which range from 25% to 27%.(121, 122) Whether this difference is reflective of a smaller relative extracellular matrix size or a result of differences in pulse sequences is unclear.

While a relationship between either T₁ or ECV and age has been shown,(65, 125) most published studies did not confirm an age related variation in healthy adults(86, 119, 121, 122, 126) or children.(124, 127) Myocardial native T₁ values from a small controls cohort of healthy children and young adults (n=21, 71.4% males, 15.7±1.5 years, with a range of 12-18) that were recently published report an average T₁ value of 965.6±30.2 ms using a similar 5(nHB)3 MOLLI acquisition.(118) Similar to the current study, they did note lower T₁ values in the lateral wall compared to the septum, but no difference in whole LV native T₁ between males and females (964.7±16.4 ms vs. 967.2±19.4 ms, respectively, p=0.40) , though the control group was smaller and predominantly boys. The exact reason for the slightly lower reported T₁ values as compared to those found in the present study is not readily clear. It is possible that it relates to the higher prevalence of boys, as well as a slightly older cohort, compared to our study. As only 4 control subjects received contrast, they did not report ECV. Olivieri and colleagues reported myocardial native T₁ and ECV for small cohorts of exclusively males 16.1±2.2 years old,(110) using a similar acquisition strategy as in the current study. Entire LV values were not provided, only reporting septal and free wall values of 990±34 ms and 978±36 ms, respectively.(110) These values are comparable to those for boys in the current study. Olivieri et al. found septal and free wall ECV values of 26.0±3.3% and 24.4±3.5%, respectively, again all in males. These ECV values are higher than those found here. Of note, these studies used a different post-contrast sampling scheme than the current study, used registration algorithms to create ECV maps, and averaged values from 4 short axis slices and a 4-chamber slice, all of which may contribute to the differences, and thus limit the comparability.

Native T₁ and ECV were increased in the septum compared to the free wall. This finding is in keeping with previous reports(118, 122) and likely relates to factors affecting the accuracy of T₁ in the free wall region, most prominently field inhomogeneity at the air-tissue interface.(50) For this reason, current guidelines suggest the use of the interventricular septum for T₁ and ECV quantification, unless the disease process is regional.(111)

The increased myocardial T₁ times in females in this study are in line with previously published results in adults,(65, 86, 119) although not consistently.(122, 125) Additionally, there is inconsistency in published pediatric literature, with studies showing no sex differences in native T₁.(124, 127) In adults, male and female hearts demonstrate different myocardial remodelling.(128) This is noted on imaging, including sex-related differences in age dependencies

on left ventricular mass, mass-to-volume ratio, and stroke volume,(126) and on histology, with preservation of both the number and size of myocytes in women over time, versus a loss of number and increased myocyte size in men.(129) This is felt to be related to different hormone environments, such as a proposed protective effect of estrogen and possible more detrimental effect of testosterone.(128) Much of this data is derived from studies involving differences in adaptation pre- and post-menopause, and thus may not be relevant in children or adolescents. In the pediatric group, the reasons for possible differences are not established. Sex differences in blood T_1 were found in this study, likely related to differences in hematocrit, which may affect myocardial T_1 via signal from the capillary compartment, or via partial volume effects with the intraventricular blood pool. Conservative ROI placement was used in this study in attempts to mitigate the latter effects, however given the differences in indexed myocardial mass between the sexes it is possible that an effect persists. Irrespective of the cause, consideration should be given to the use of different normative values for myocardial native T_1 and ECV for boys and girls.

Due to the changes in cardiac mass and chamber size during childhood, we investigated relationships with native T_1 and ECV using CMR variables less associated with age and body surface area, such as ejection fraction or the Z-score for LV mass. Univariate regression analysis revealed significant associations with myocardial native T_1 and age, sex, heart rate, and LV mass Z-score, but less consistently with BSA. The negative association with age and native T_1 or ECV may relate to differences in the extracellular or cellular components, such as a relative increase in myocyte size with age leading to a compensatory reduction in the extracellular component. Alternatively, this association may simply reflect difficulties in avoiding partial volume errors in those with smaller hearts. It should be noted that, as all our patients were > 20 kg, a slice thickness of 8 mm was used, however in smaller children a thinner slice appears preferable. Following multivariate analysis, only sex and LV mass Z-score typically remained independently associated with native T_1 . The relationship with LV mass Z-score is supportive of the hypothesis of the difficulty in eliminating partial volume errors. Interestingly, only age and BSA were significantly associated with ECV on univariate analysis; however, neither remained significant in multivariate analysis. It is possible that the smaller number of cases with ECV obscured further associations of physiologic parameters with ECV.

2.4.1 Limitations

Several important limitations exist. The modest sample size of our study population may have obscured differences, such as between boys and girls for ECV, as well as associations between fibrosis markers and other imaging biomarkers. There is a possibility that the association of sex with T_1 is confounded by sex disparities other than the differences in myocardial architecture. The cohort size may limit overall generalizability to other groups, particularly as the number of subjects with ECV measurements is not large; however, the sample size is comparable to widely used reference studies for normative pediatric ventricular volumes.(112, 130) Secondly, the cohort is a retrospective sample of convenience, derived from the ~700 clinical CMR studies per year in our institution, in which T_1 -mapping is routinely performed. While all known testing, including the CMR, was normal, we cannot rule out subclinical pathology. While no age dependence was noted with T_1 measures, our study population was skewed toward older children, and no information is available on children less than 8 years of age, as most children below that age often require a form of sedation which raises the clinical threshold to proceed with CMR and limiting the prevalence of healthy, younger children. It is important to note that native T_1 values can vary considerably with differences in field strength, sequence choice and imaging parameters(50) and it is important to ensure that these parameters are comparable between clinical practice and the reference values used. In comparison, ECV is more robust towards variations in hardware, software, and settings,(111) though can show small variations between contrast agents.(131) Thus, due to a variety of factors, T_1 and ECV may differ between sites even with what would otherwise be matching sequence parameters. Scanner operating performance can vary or drift over time and, although we suspect that any impact would be small, we cannot rule out an influence on the values obtained. Although the discrepancies are likely small literature references must be considered with care. This may become a less significant concern over time thanks to efforts to develop corrective algorithms and/or phantom calibration methods, such as the T_1 MES program.(132) However, whenever possible, site-specific normative data is established in accordance to current recommendations.(111)

2.5 Conclusion

In conclusion, normative data are presented for myocardial native T_1 and ECV using the MOLLI T_1 -mapping sequence at 1.5T. Consistent with findings in adults, there are suggestions of

increased values in females, supporting the consideration for different normal ranges for boys and girls.

Chapter 3

Effects of Age, Sex and Risk-Factors for Heart Failure on Native T_1 and Extracellular Volume Fraction

3.1 Introduction

Global changes in left ventricular dimensions,(133) mass,(133) and diastolic function(134) are associated with advanced age, as is an increased burden of interstitial collagen.(135) Additionally, several of these age-associated changes are sex-dependent, including ventricular mass and volume,(133) as well as alterations of myocyte volume fraction(129) and extracellular matrix proteins.(136) These changes are also modulated by several common cardiovascular risk factors associated with the development of heart failure, such as diabetes and hypertension, which are known to compound negative changes in cardiac structure and function,(137) and in the microstructure, including increased collagen deposition.(138, 139) The indirect assessment of these myocardial cellular and microstructural variations with magnetic resonance is a continually developing field of study.

Cine cardiac magnetic resonance (MR) imaging is used routinely to study changes in the global structure and function of the heart, and quantitative T_1 -mapping with cardiac MR is increasingly used to assess changes in the extracellular matrix environment. Both native (non-contrast) myocardial T_1 values and contrast-agent derived extracellular volume fraction (ECV) are altered in a wide array of conditions(140) and ECV has a documented correlation to fibrosis burden.(81, 82, 85, 141) However, the possibly smaller effects of sex and age on native T_1 and ECV values have not been consistent between studies. Additionally, differences in acquisition methods, including the MODified Look-Locker Inversion recovery (MOLLI) method,(63) the Shortened MODified Look-Locker Inversion recovery (ShMOLLI) method,(142) and the SATuration recovery single-SHOT Acquisition (SASHA) method,(51) among several others, give rise to relatively large systematic differences in native T_1 and ECV values, which necessitates the evaluation of method-specific normative values.

The aim of this study was to evaluate ECV and native T_1 values for the SASHA T_1 -mapping method(51) as a function of sex, aging, and risk factors for the development of heart failure, including diabetes mellitus, hypertension, obesity, and atrial fibrillation.

3.2 Materials and Methods

3.2.1 Study Subjects

All studies from which anonymized data were used had approval by either the University of Alberta Health Research Ethics Office or the University of Calgary Research Ethics Board, with all participants having provided written informed consent. Anonymized data from research subjects evaluated with cardiac MR that included native and gadolinium contrast T_1 -mapping at the University of Alberta and the University of Calgary were identified, including those from the Alberta HEART study.(143) Subjects with a history of heart failure, coronary artery disease, valvular heart disease, congenital heart disease or cardiomyopathy were excluded. Individuals were separated by sex and categorized into healthy or at-risk groups, based on the presence of at least one risk factor for the development of heart failure,(3) including diabetes mellitus, hypertension (defined as a history of hypertension or antihypertensive medication use), obesity (BMI > 35kg/m²), or atrial fibrillation. Subjects were excluded from the healthy group if there was a history of hyperlipidemia. Any subject with late gadolinium enhancement consistent with an ischemic event was excluded.

3.2.2 Cardiac MR Imaging Protocol

Cardiac magnetic resonance imaging was performed on 1.5T Siemens systems (Siemens MAGNETOM Sonata or Avanto, Siemens Healthcare, Erlangen, Germany). Gated, segmented balanced steady-state free precession (bSSFP) cine imaging was performed in short- and long-axis orientations covering the entire left ventricle. Typical scan parameters were: echo time 1.24ms, repetition time 2.48ms, flip angle 51°, slice thickness 8mm with 2mm gap, field of view 400×288mm, acquisition matrix 256×138, phase resolution 75%, 930 Hz/pixel, 14 views per segment, rate 2 parallel imaging (GRAPPA), and 30 reconstructed cardiac phases. The SASHA pulse sequence(51) was used for T_1 -mapping, performed on basal and mid-ventricular short-axis slices during diastole. Typical SASHA parameters were: echo time 1.37ms, repetition time 2.74ms, flip angle 70°, 9 images spanning 90–900ms saturation recovery times plus a non-saturated image,

slice thickness 8mm, field of view 360×270mm, acquisition matrix before interpolation 192×108, phase resolution 75%, and 1000 Hz/pixel. Interpolated in-plane spatial resolution was 0.94mm. Either rate 2 parallel imaging (GRAPPA) or 6/8 partial Fourier was used for image acceleration. Images were acquired pre-contrast for native T₁ and repeated 15-20 minutes post contrast-agent delivery. A phase-sensitive inversion recovery sequence was used for conventional late gadolinium enhancement (LGE) imaging, typically starting 7 minutes following gadolinium-based contrast injection, with coverage matching cine locations. Subjects received 0.15mmol/kg of either gadobutrol (Gadovist; Bayer HealthCare Pharmaceuticals, Montville, NJ) or gadolinium-diethylenetriaminepentaacetic acid (Gd-DTPA, Magnevist; Bayer Healthcare, Toronto, Canada).

3.2.3 Cardiac MR Image Analysis

Analysis of ventricular volumes, function, and mass were completed using standard commercial software (cvi42, Circle Cardiovascular Inc., Calgary, Canada, or Syngo Argus, Siemens Healthcare, Erlangen, Germany). In all cases, left ventricular endo- and epicardial borders were traced on the short axis bSSFP cine images, with inclusion of the papillary muscles in the blood pool. Ventricular volumes and mass were indexed to a calculated idealized body surface area, based on idealized body weight.(144) Late gadolinium enhancement images were assessed visually for the presence of areas with high signal intensity.

T₁-mapping analysis was performed using custom software written for use in MATLAB (R2015a, The MathWorks, Natick, United States).(51) Image registration was used to correct for residual in-plane motion during breath-holds.(51) For blood pool and myocardial T₁ analysis, a circular region of interest (ROI) was drawn in the left ventricular blood pool and a 2mm width ROI was drawn over the interventricular septum, respectively (Figure 3.1). The septal region was chosen to minimize heterogeneity introduced by unintentional inclusion of artifacts, which predominately affect the anterior or inferolateral segments.(51) Adjustments of ROI placement in each single-shot image were made if residual motion was present despite motion correction. To maintain ROI size consistency, ROIs drawn on the native T₁ image sets were copied onto their corresponding post-contrast image sets, and adjusted to match location as closely as possible. Averaged ROI signal intensities were fit to a 3-parameter mono-exponential recovery curve

$$Signal(TS) = k(1 - \eta e^{-TS/T_1})$$

with scaling constant k , saturation efficiency η , longitudinal relaxation time T_1 , and saturation recovery time TS .(51) Analysis was performed blind to subject grouping.

In those who had a hematocrit available, extracellular volume fraction was calculated as previously described(145):

$$ECV = (1 - \text{hematocrit}) \frac{\Delta R_1 \text{myocardium}}{\Delta R_1 \text{blood}}$$

where $\Delta R_1 = 1/T_1(\text{post-contrast}) - 1/T_1(\text{native})$.

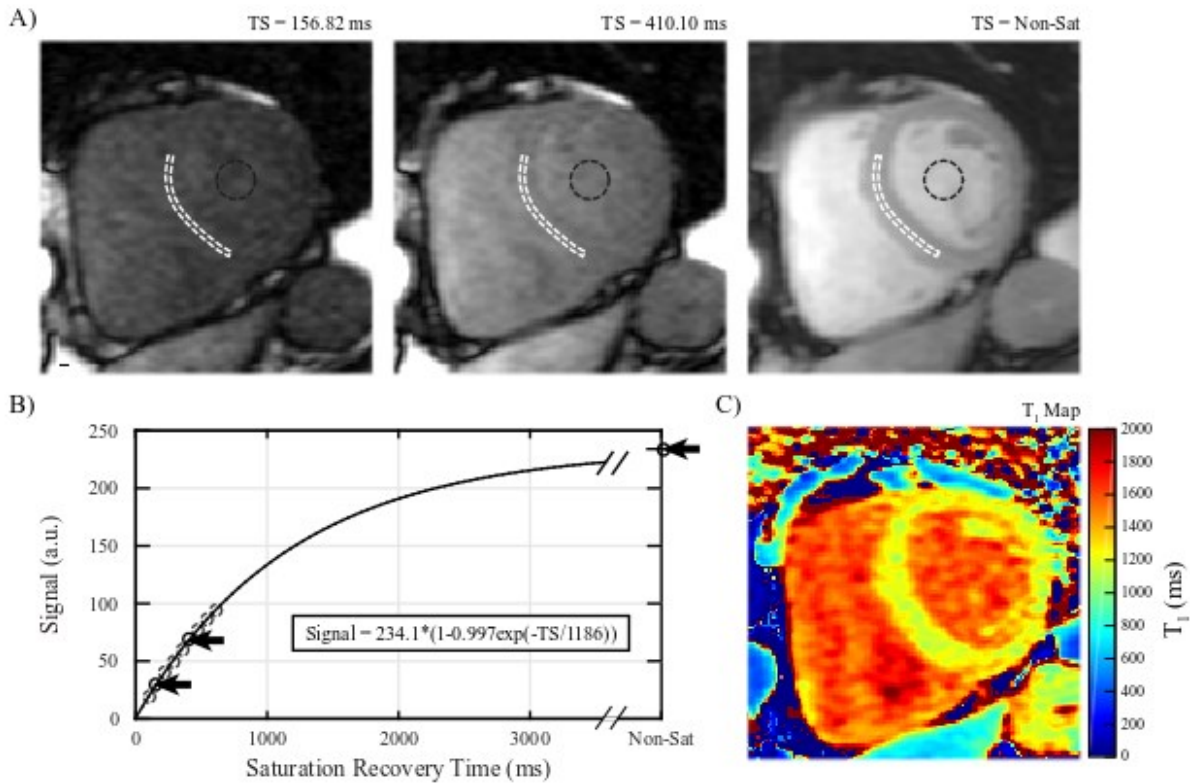


Figure 3.1: Example SASHA image set from a healthy male participant. A) Representative sample of T_1 -weighted images, including typical septal (white dash) and blood pool (black dash) regions of interest (ROI). B) Mean septal ROI signal intensity is plotted (circles) with the corresponding saturation recovery times (TS), along with the best fit saturation recovery curve (line) defined by the equation shown. The arrows depict the corresponding images shown in A). C) T_1 map for this subject, where T_1 values are calculated on a pixel-wise basis.

3.2.4 Statistical Analysis

Data are presented as mean \pm standard deviation or count (%), where appropriate. Sex-related comparisons were performed within each of the healthy and at-risk groups (i.e. healthy men vs. healthy women; at-risk men vs. at-risk women). Comparisons between risk groups were

performed by sex (i.e. healthy men vs. at-risk men; healthy women vs. at-risk women). An a priori decision was made to not compare all female to all male subjects, as the objective was to examine the interaction of sex and risk factors. Continuous variables were assessed using either a two sample t-test or the Mann-Whitney U test. Categorical data were compared using a chi-squared test or Fisher's exact test, depending on the frequency of observed data. Correlation between age and individual T_1 measurements, such as native T_1 or ECV, were assessed using linear regression for each sex and risk group independently. Multiple linear regression was used to further evaluate the relationship between age and T_1 measurements when controlling for heart rate, BMI, current smoking status, and indexed left ventricular (LV) mass. In the at-risk group, further multiple linear regression was performed adding diabetes, hypertension, hyperlipidemia, and LGE status to the previously mentioned model. Significance was set at $p < 0.05$. Adjustment of p-values, based on the number of pairwise comparisons, was not performed, to maximize statistical power. STATA statistical software (Version 11.2, Stata Corporation, College Station, USA) was used for statistical analysis.

3.3 Results

Contrast-enhanced CMR studies were performed in 224 subjects. Image artifacts precluded analysis in 9 cases, with an additional 28 cases excluded due to acquisition/protocol errors precluding analysis. Baseline characteristics of the final 187 subjects comprising the study population are shown in Table 3.1, with a histogram plot of age for the respective cohorts in Figure 3.2. The healthy men were a younger group than their at-risk male counterparts ($p=0.0001$), however both groups of women were of similar age ($p=0.1957$). Healthy women were slightly older than their male counterparts ($p=0.0206$), while men and women were of similar age for those with risk factors ($p=0.8456$). Women with risk factors for heart failure had higher values for weight and BMI than their healthy counterparts ($p=0.0000$ and $p=0.0000$, respectively). The proportion of diabetes, hypertension, hyperlipidemia, and atrial fibrillation were similar between sexes ($p=0.1240$, $p=0.2080$, $p=0.0800$, $p=0.9530$, respectively) in the at-risk group. There were no sex differences in the proportion of those taking specific medications ($p=0.2580$ for statins, $p=1.0000$ for other antihyperlipidemic medications, $p=0.4210$ for ACE-I/ARB class, $p=0.1040$ for beta-blockers, $p=0.8880$ for calcium channel blockers, $p=0.1020$ for diuretics, respectively).

Table 3.1: Study group characteristics

	Healthy		At-Risk	
	Men	Women	Men	Women
n	30	38	54	65
Age (years)	48.3±15.8*† (42.4-54.2)	56.8±13.8 (52.3-61.4)	59.8±9.7 (57.2-62.5)	60.2±12.1 (57.2-63.2)
Age range (years)	21-80	22-77	41-81	29-82
Height (cm)	177.2±6.3† (174.8-179.5)	164.7±6.6 (162.6-166.9)	177.6±7.3† (175.6-179.6)	163.3±8.4 (161.2-165.4)
Weight (kg)	82.6±14.3† (77.3-88.0)	68.2±12.0* (64.2-72.1)	87.7±14.5 (83.8-91.7)	82.2±18.2 (77.7-86.7)
BMI (kg/m ²)	26.2±3.7 (24.8-27.6)	25.1±4.0* (23.8-26.4)	27.8±4.2† (26.7-29.0)	30.8±6.6 (29.2-32.5)
BSA (m ²)	2.0±0.2† (1.9-2.1)	1.8±0.2* (1.7-1.8)	2.1±0.2† (2.0-2.1)	1.9±0.2 (1.9-2.0)
iBSA (m ²)	1.8±0.1† (1.8-1.9)	1.6±0.1 (1.6-1.6)	1.9±0.1† (1.8-1.9)	1.6±0.1 (1.6-1.6)
HR (bpm)	65.4±10.7 (61.4-69.4)	69.0±11.2 (65.4-72.7)	69.0±13.5 (65.3-72.6)	69.1±10.4 (66.5-71.7)
SBP (mmHg)	126.9±12.1* (122.4-131.4)	126.3±18.7* (120.1-132.5)	134.1±16.2 (129.6-138.5)	135.0±17.6 (130.6-139.4)
DBP (mmHg)	79.5±8.6† (76.3-82.7)	74.8±10.1* (71.4-78.1)	81.2±11.3 (78.2-84.3)	80.0±12.2 (77.0-83.0)
Diabetes	-	-	25(44.4%)	20(30.8%)
Hypertension	-	-	35(64.8%)	49(75.4%)
Hyperlipidemia	-	-	18(33.3%)	32(49.2%)
Atrial Fibrillation	-	-	4(7.4%)	5(7.7%)
Current Smoker	2(6.7%)	1(2.6%)	6(11.1%)	3(4.6%)
Medications				
Hyperlipidemia				
Statin	-	-	17(31.5%)	27(41.5%)
Other	-	-	2(3.7%)	2(3.1%)
Blood pressure				
ACE-I / ARB	-	-	31(57.4%)	42(64.6%)
Beta-blocker	-	-	5(9.3%)	13(20.0%)
CCB	-	-	7(13.0%)	9(13.8%)
Diuretic	-	-	11(20.4%)	22(33.8%)

BMI = body mass index, BSA = body surface area, iBSA = BSA based on ideal body weight, HR = heart rate, SBP = systolic blood pressure, DBP = diastolic blood pressure, ACE-I = ace inhibitor, ARB = angiotensin receptor blocker, CCB = calcium channel blocker

Data is presented as mean±SD (95% confidence intervals), or n(%) where applicable

*p<0.05 between Healthy and At-Risk group

†p<0.05 between sex within a given risk group

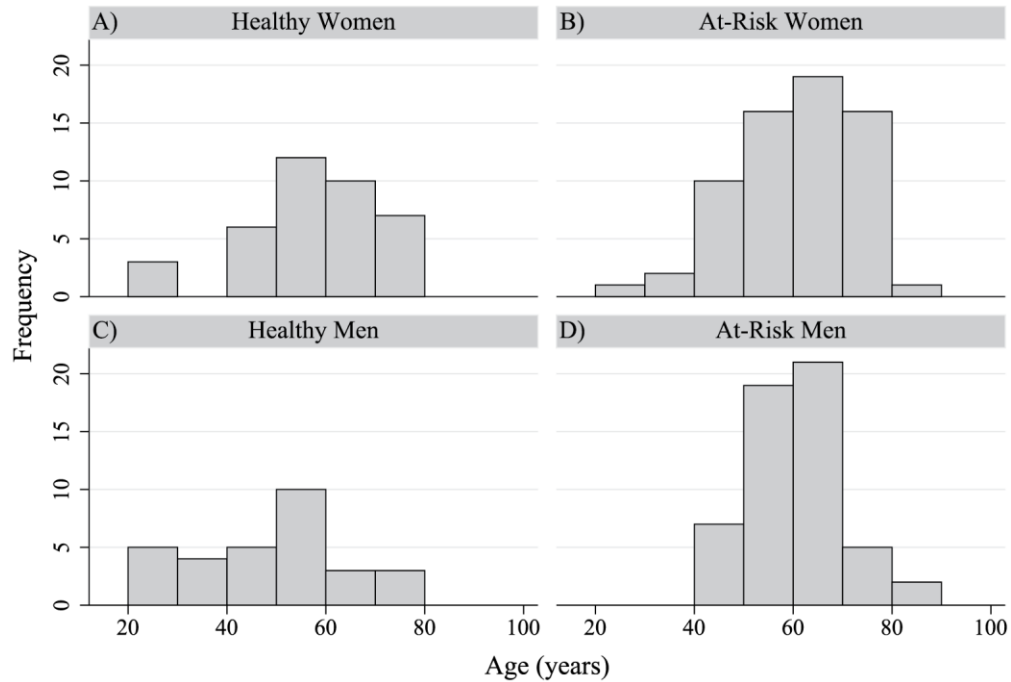


Figure 3.2: Distribution of age by sex and risk group

The cardiac MR findings are shown in

Table 3.2. For a given sex, there were no differences in standard cardiac MR metrics of structure and function between healthy individuals and those at risk for heart failure, except a slight increase in indexed LV mass in females ($p=0.0348$). Not surprisingly, both healthy and at-risk men had an increased indexed LV mass compared to women ($p=0.0000$ and $p=0.0004$, respectively). Healthy men and women, along with those with risk factors for heart failure, showed small differences in left ventricular ejection fraction (LVEF) ($p=0.0458$ and $p=0.0008$, respectively) and end-systolic volume ($p=0.0182$ and $p=0.0003$, respectively), with increased indexed end-systolic volumes and lower LVEF in men. No healthy subjects had positive LGE images. Of the 18 at-risk subjects who showed evidence of non-ischemic LGE, no LGE was located in the interventricular septum. Sixteen had small areas of midwall or subepicardial LGE in the lateral or inferolateral wall. In the other two subjects, one had a small amount of non-ischemic LGE of the LV apex, while the other subject had a small area of midwall LGE of the mid-anterior segment. There was no difference in the proportion of men or women with positive LGE in the at-risk group ($p=0.3460$).

In healthy subjects, sex differences were seen for all measures of T_1 , including higher native myocardial T_1 , blood T_1 , and ECV in women ($p=0.0000$, $p=0.0000$, and $p=0.0089$, respectively) as shown in

Table 3.2. However, these sex differences were not identified in the at-risk group for native T_1 ($p=0.6556$) or ECV ($p=0.5039$) (Figure 3.3A and Figure 3.3B). Native T_1 values were higher in at-risk men as compared to the healthy men ($p=0.0070$), however ECV was similar ($p=0.4572$) (Figure 3.3C). Native blood T_1 was higher in at-risk men as compared to healthy men ($p=0.0020$), despite no group difference in hematocrit ($p=0.1004$). No difference existed between at-risk or healthy women for ECV ($p=0.1026$), native T_1 ($p=0.6344$), or blood T_1 ($p=0.9298$) (Figure 3.3D). There was no correlation with native myocardial T_1 and blood T_1 , or hematocrit, for either sex or risk status (Table 3.3)). Additionally, no differences existed in ECV between those with and without positive LGE for at-risk men or at-risk women (Table 3.4). Similarly, no differences existed in native T_1 between those with and without positive LGE for at-risk men or at-risk women (Table 3.4). There were no statistical differences in ECV measurements when between gadolinium agent type used based on either sex or risk group, other than a weak difference in the group of at-risk women (0.0436).

Table 3.2: Comparison of cardiac magnetic resonance values between groups

	Healthy		At-Risk	
	Men	Women	Men	Women
n	30	38	54	65
LVEF (%)	60.4±5.3† (58.4-62.4)	63.0±5.3 (61.3-64.8)	60.9±6.0† (59.2-62.5)	65.4±6.5 (63.8-67.0)
LVEDVi‡ (mL/m ²)	80.7±14.5 (75.3-86.1)	75.9±12.5 (71.8-80.0)	84.6±19.3 (79.3-89.9)	78.4±15.2 (74.7-82.2)
LVESVi‡ (mL/m ²)	32.7±8.7† (29.4-35.9)	28.2±6.6 (26.0-30.4)	33.3±10.1† (30.6-36.1)	27.2±7.8 (25.3-29.2)
LVSVi‡ (mL/m ²)	48.5±8.2 (45.4-51.5)	47.7±8.1 (45.1-50.3)	51.3±11.6 (48.1-54.5)	51.3±10.9 (48.6-54.0)
LVmassi‡ (g/m ²)	63.7±10.5† (59.8-67.7)	52.6±8.2* (49.9-55.3)	65.8±12.8† (62.4-69.3)	57.4±12.3 (54.4-60.5)
Non-ischemic LGE n(%)	0(0.0%)	0(0.0%)	10(18.5%)	8(12.3%)
Native Myocardial T ₁ (ms)	1167±36*† (1153-1180)	1202±30 (1192-1212)	1193±45 (1181-1205)	1197±55 (1184-1211)
Native Blood T ₁ (ms)	1576±69*† (1550-1601)	1664±62 (1644-1685)	1635±88† (1611-1659)	1666±77 (1647-1685)
Post-contrast Myocardial T ₁ (ms)	600±38† (586-615)	539±46 (524-554)	599±59† (583-615)	540±51 (528-553)
Post-contrast Blood T ₁ (ms)	355±36† (342-369)	300±44 (286-314)	356±55† (341-371)	297±55 (284-311)
Hematocrit Available n(%)	22(73.3%)	32(84.2%)	36(66.7%)	53(81.5%)
Hct	0.46±0.03† (0.44-0.47)	0.40±0.03 (0.39-0.41)	0.44±0.03† (0.43-0.45)	0.41±0.03 (0.40-0.42)
ECV (%)§	20±2† (19-22)	22±2 (21-23)	21±3 (20-22)	21±2 (21-22)

LVEF = left ventricular ejection fraction, LVEDVi = left ventricular end diastolic volume indexed, LVESVi = left ventricular end systolic volume indexed, LVSVi = left ventricular stroke volume indexed, LVmassi = left ventricular mass indexed, ECV = extracellular volume fraction, Hct = hematocrit

‡indexed to idealized body surface area

§calculated only for those in whom a hematocrit was available

Data is presented as mean±SD (95% confidence intervals), or n(%) where applicable

*p<0.05 between Healthy and At-Risk group; †p<0.05 between sex within a given risk group

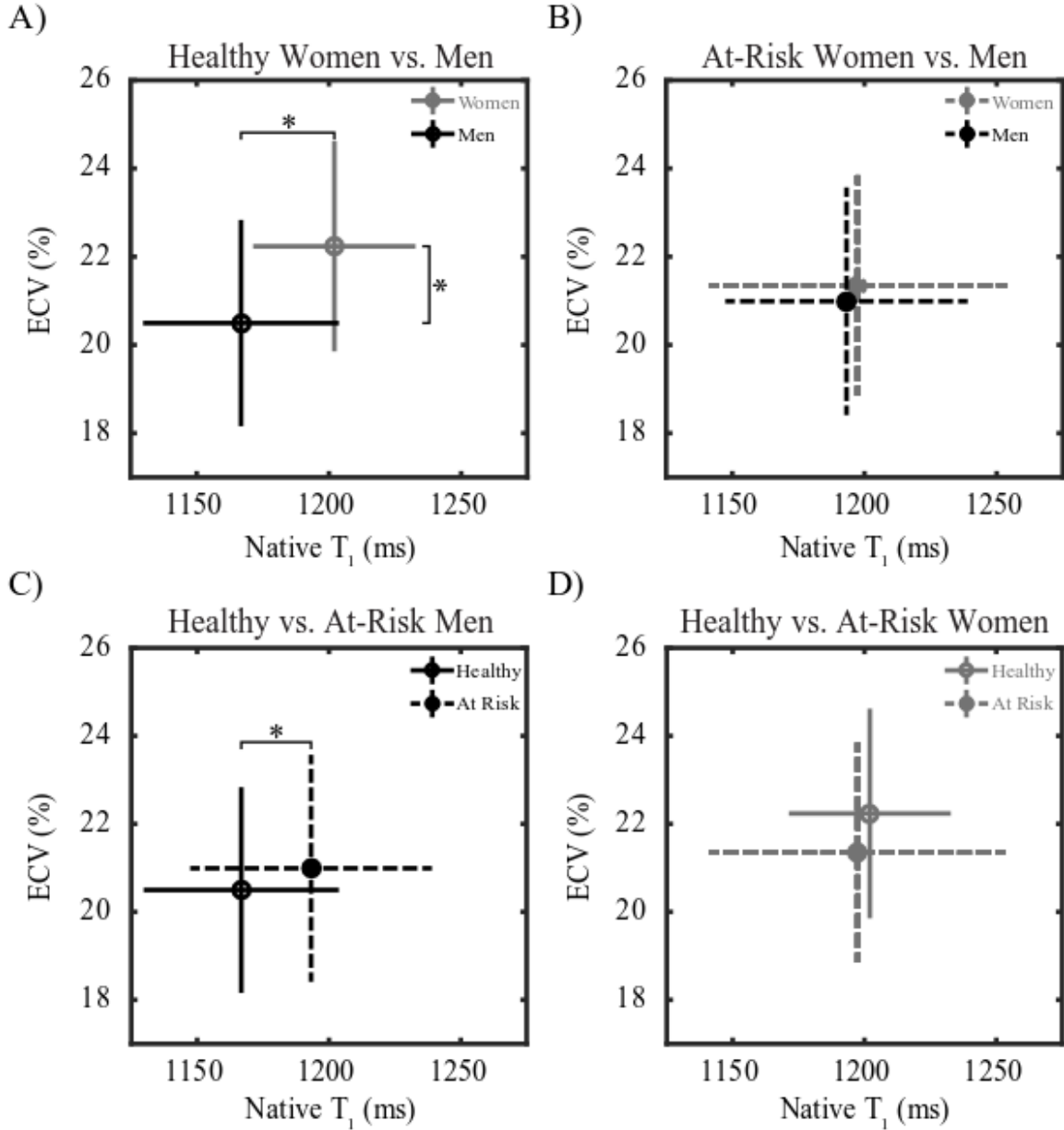


Figure 3.3: Native T₁ and ECV between sex and risk factor groups. Sex-related differences in both native T₁ and ECV are seen in healthy individuals (A), but are lost in those with risk factors for heart failure (B), partially on the basis of an increase in native T₁ in men with risk factors (C). No differences are seen between women with and without risk factors. Data is presented as mean value (circle) with bars representing one standard deviation. P-value <0.05 denoted by *.

Table 3.3: Relationship between native myocardial T₁ and native blood T₁ or hematocrit

		Coefficient (95% CI)	R ²	p-value
Blood T ₁ (ms)	Healthy Women	0.104 (-0.054-0.263)	0.0470	0.191
	Healthy Men	0.099 (-0.099-0.298)	0.0360	0.315
	At-Risk Women	0.052 (0.232-0.005)	0.0052	0.570
	At-Risk Men	0.043 (0.184-0.007)	0.0069	0.549
Hematocrit	Healthy Women	314.699 (-7.074-636.473)	0.1174	0.055
	Healthy Men	-101.776 (-815.023-611.471)	0.0044	0.769
	At-Risk Women	-158.441 (344.807-0.008)	0.0078	0.530
	At-Risk Men	-58.412 (357.508-0.002)	0.0024	0.777

Table 3.4: Comparison of native T₁ and ECV based on the presence or absence of late gadolinium enhancement

		At-Risk Women	At-Risk Men
Native T ₁ (ms)	No LGE	n=57	n=44
		1196±55 (1182-1211)	1194±47 (1180-1208)
	With LGE	n=8	n=10
		1204±57 (1157-1252)	1189±34 (1165-1214)
	p-value	0.7193	0.7384
	ECV (%)	No LGE	n=46
22±3 (21-22)			21±3 (20-22)
With LGE		n=7	n=7
		20±1 (19-22)	21±2 (19-23)
p-value		0.1090	0.9204

Data presented as mean±SD and (95% confidence interval)

Both native myocardial T_1 and ECV did not vary with age in either sex, both for healthy and at-risk groups (Figure 3.4 and Figure 3.5, Table 3.5). Similarly, native blood T_1 did not vary with age, irrespective of sex or risk group (Table 3.5). Independence of T_1 values and ECV versus age was maintained in all groups following correction for heart rate, BMI, current smoking status, and indexed LV mass, with the exception of ECV in women with risk factors for heart failure (Table 3.5), where a decrease in ECV was seen with increasing age. In the at-risk group, further inclusion of diabetes, hypertension, hyperlipidemia, and LGE status showed no age dependence for ECV, native myocardial T_1 , or native blood T_1 in either sex (Table 3.5).

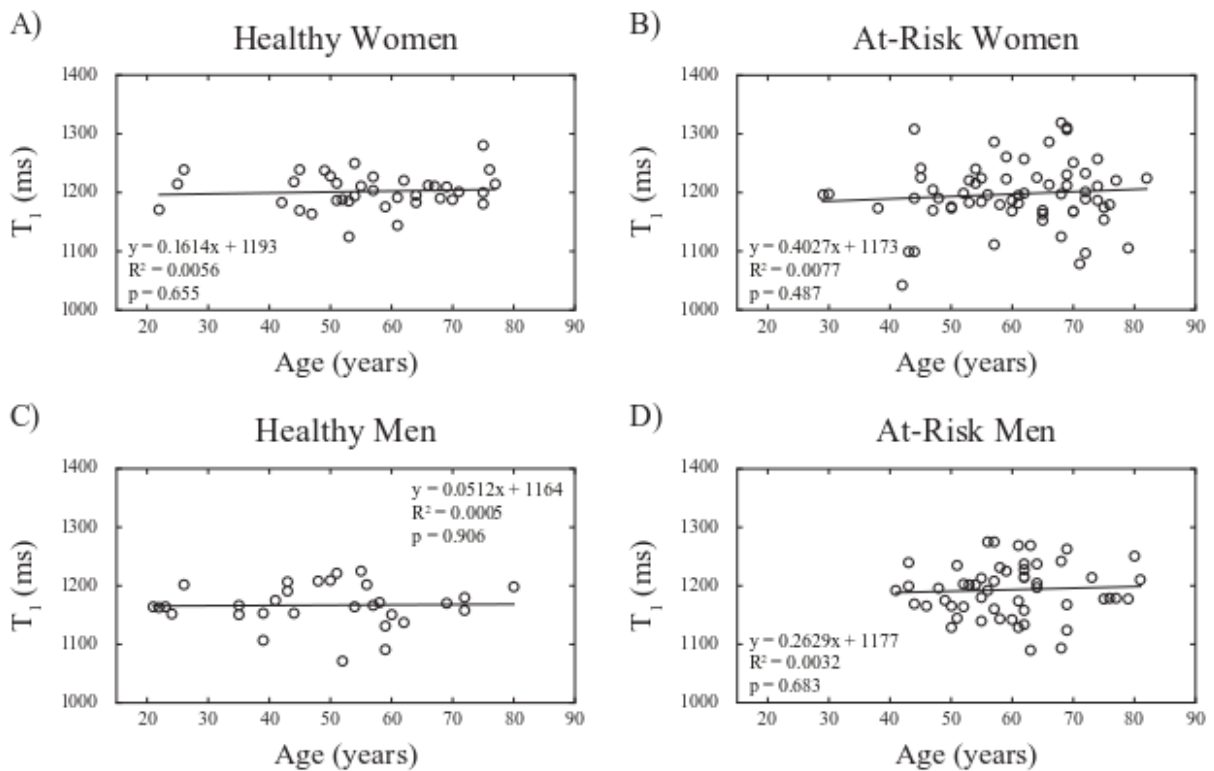


Figure 3.4: Correlation between age and native T_1 values. Comparisons are shown for A) healthy females, B) females with risk factors for heart failure, C) healthy males, and D) males with risk factors for heart failure. No statistically significant relationship exists with age in any group.

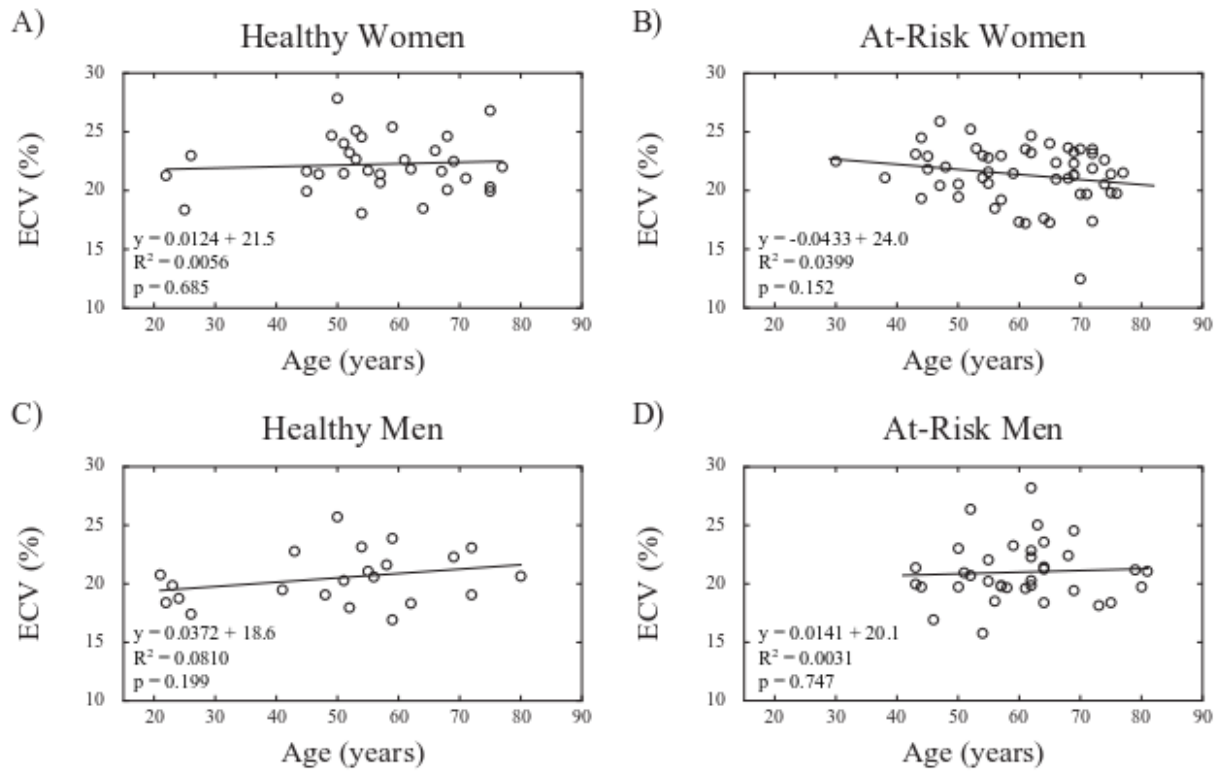


Figure 3.5: Correlation between age and ECV values. Comparisons are shown for A) healthy females, B) females with risk factors for heart failure, C) healthy males, and D) males with risk factors for heart failure. No statistically significant relationship exists with age in any group.

Table 3.5: Relationship between age and T_1 measures

			Coefficient (95% CI)	R^2	p-value
Age alone	Healthy Women	Native T_1	0.161 (-0.565-0.888)	0.0056	0.655
		Blood T_1	-0.469 (-1.974-1.036)	0.0110	0.531
		ECV	0.012 (-0.049-0.074)	0.0056	0.685
	Healthy Men	Native T_1	0.051 (-0.832-0.935)	0.0005	0.906
		Blood T_1	1.228 (-0.396-2.852)	0.0789	0.133
		ECV	0.037 (-0.021-0.096)	0.0810	0.199
	At-Risk Women	Native T_1	0.403 (-0.747-1.553)	0.0077	0.487
		Blood T_1	0.106 (-1.499-1.712)	0.0003	0.895
		ECV	-0.043 (-0.103-0.016)	0.0399	0.152
	At-Risk Men	Native T_1	0.263 (-1.024-1.549)	0.0032	0.683
		Blood T_1	1.158 (-1.341-3.657)	0.0164	0.357
		ECV	0.014 (-0.074-0.102)	0.0031	0.747
Model 2	Healthy Women	Native T_1	0.043 (-0.727-0.812)	0.1857	0.910
		Blood T_1	-0.141 (-1.843-1.562)	0.0758	0.867
		ECV	0.027 (-0.045-0.099)	0.0583	0.448
	Healthy Men	Native T_1	0.688 (-0.562-1.938)	0.1230	0.267
		Blood T_1	0.929 (-1.426-3.283)	0.1510	0.424
		ECV	0.047 (-0.044-0.138)	0.2722	0.291
	At-Risk Women	Native T_1	0.181 (-1.067-1.430)	0.0456	0.772
		Blood T_1	0.553 (-1.146-2.252)	0.0865	0.518
		ECV	-0.063 (-0.125--0.001)	0.1809	0.045
	At-Risk Men	Native T_1	0.523 (-0.777-1.823)	0.1190	0.422
		Blood T_1	1.578 (-1.015-4.172)	0.0825	0.227
		ECV	0.030 (-0.060-0.119)	0.1776	0.504
Model 3	At-Risk Women	Native T_1	0.407 (-0.972-1.786)	0.1278	0.556
		Blood T_1	1.264 (-0.636-3.163)	0.1444	0.188
		ECV	-0.033 (-0.105-0.040)	0.2415	0.371
	At-Risk Men	Native T_1	0.385 (-1.047-1.818)	0.1646	0.590
		Blood T_1	2.137 (-0.689-4.963)	0.1500	0.135
		ECV	0.024 (-0.074-0.121)	0.2532	0.623

Model 2 includes age plus heart rate, BMI, current smoking status, and indexed LV mass.

Model 3 includes model 2 plus diabetes, hypertension, hyperlipidemia, and late gadolinium enhancement status

3.4 Discussion

Our study indicates that among patients without established cardiovascular disease, myocardial native T_1 and extracellular volume fraction, as assessed with SASHA, do not depend on age, irrespective of sex or the presence of risk factors for heart failure. Further, while healthy women show higher values for native T_1 and ECV compared to healthy men, this difference is lost among subjects with risk factors, largely due to the increased T_1 and ECV values in the men with risk factors.

The definition of normal ranges for native T_1 and ECV as a function of age and sex are necessary to identify pathology. Systematic differences in T_1 values between different imaging sequences necessitates method-specific studies to define normative values. The native T_1 measured in the current study for the SASHA method at 1.5T (1167 ± 36 ms for men, 1202 ± 30 ms for women) and ECV values ($20 \pm 2\%$ for men, $22 \pm 2\%$ for women) are similar to those previously reported in healthy subjects using saturation recovery techniques, such as SASHA, with values ranging from 1170-1220ms and 18-22%, respectively.(51, 60, 73, 146) Look-Locker corrected techniques yield significantly different values as compared to SASHA, with typical native T_1 and ECV values around 940-1050ms and 23-28%, respectively.(63, 65, 81, 86, 121, 122, 146, 147) With regards to the study population variability of the different T_1 -mapping methods, the standard deviations of values for T_1 (± 30 -56ms) and ECV ($\pm 2\%$) for the healthy controls in the current study are similar to those reported in previous studies using MOLLI and ShMOLLI methods.(63, 65, 81, 86, 121, 122, 146, 147)

While saturation recovery based T_1 -mapping sequences have been shown to be less dependent on factors such as the T_1 , T_2 , and magnetization transfer than inversion recovery based sequences,(50, 64) it has been postulated that the combined alterations in these parameters may culminate in changes in T_1 that may not otherwise be noted using a saturation recovery approach without a larger study population.(64) While T_2 values have been shown to increase with age,(148) changes in magnetization transfer with aging are not well known, and thus more research is required to appreciate if an inversion recovery based approach may be more sensitive to these effects with increased age.

While a small number of studies have shown age dependence in healthy individuals, for example a decrease in native T_1 in women with increasing age(65, 149) or an age related increase in ECV,(125) the findings of the current study are in line with multiple publications that show an

absence of age-related changes for native T_1 and/or ECV in healthy cohorts free of cardiovascular risk factors.(86, 119, 121, 122, 126)

While the current study showed that the independence of native T_1 and ECV with age was also maintained in the at-risk group for either sex, previous studies have shown a positive correlation between ECV and age in patients with risk factors for cardiovascular disease, suggesting increasing fibrosis with aging with exposure to risk factors.(87, 121, 126) However, direct comparisons between studies is hampered by heterogeneity between the study populations, with potential differences in prevalence and/or duration of risk factors. Myocardial tissue characteristics and ventricular function of the at-risk population in the current study was similar to the healthy group, with no significant differences in volumes, mass or function. It was recently shown that while hypertensive individuals without LV hypertrophy had similar ECV and native T_1 values as compared to controls, those with hypertrophy did have significantly increased ECV and T_1 values.(150) Similar findings were shown when comparing milder concentric remodelling and more severe concentric left ventricular hypertrophy to controls, with increased T_1 and ECV values only in those with concentric hypertrophy.(151) Thus, it is likely that more detailed characterization of at-risk individuals would be necessary to untangle age related changes from other direct disease effects, with consideration of the duration and severity of disease, including changes in ventricular structure and function.

The findings of the current study show that in healthy individuals without risk factors for the development of heart failure, women have higher native myocardial T_1 and ECV values, and thus sex has to be factored into the definition of their normal ranges. These findings are in agreement with previous studies examining healthy individuals without risk factors that have also shown increased ECV(86) or native T_1 values(65, 119) in women as compared to men, using the EQ-CMR, 5(3)3 MOLLI acquisition, and ShMOLLI techniques, respectively. However, there are previous studies that have not identified a sex difference,(122, 125) using the original 3(3)3(3)5 MOLLI acquisition and a cine Look-Locker sequence, respectively. The exact etiology of the sex differences are not known, however there is data supporting differences in preservation of the myocardium in women, such as myocyte number and volume, with differing rates of apoptosis, all of which is likely related to differences in sex hormones.(128) Thus, these differing numbers and sizes of myocytes may be reflected by our measures of T_1 and ECV.

Perhaps the most interesting finding in the current study is the different myocardial response to risk factors between men and women. Sex-related differences in ECV and native T_1 were measured in the healthy group, but were no longer present in those with risk factors, reflecting the increase in both native T_1 and ECV between healthy and at-risk men (though only native T_1 was statistically different). The lack of correlation between native myocardial T_1 and either blood T_1 or hematocrit would support remodeling altering myocardial T_1 and not other possible confounding factors. These findings suggest that the male myocardium may be more prone to extracellular matrix remodeling in the presence of cardiovascular risk factors, in keeping with a recent cardiac MR study showing differences only in men at-risk.(126) These findings are also reflected in reports of morphologic, functional, and cellular differences in sex-related remodeling.(128) In line with these findings, the at-risk male subjects in our study had significantly larger LVESV and lower LVEF as compared to at-risk women, a difference which was not observed in the healthy groups. Importantly, male and female subjects had similar distributions of risk factors and medications, mitigating any potential disease exposure effects in these findings.

Men and women with risk factors for heart failure had an equal proportion of non-ischemic LGE, with no evidence of LGE in the interventricular septum. Native T_1 and ECV in the septal region did not differ between those with and without LGE, suggesting the pathological process giving rise to the remote LGE may be limited to the enhancing regions.

3.4.1 Limitations

The current study has several important limitations. First, a cross-sectional study design was used to infer the temporal influence of aging. This is of particular importance when considering the potential additive effects of cardiovascular risk factors, where the duration of exposure is an important consideration and not always known, as is the case in this study. Additionally, without knowledge of the duration of exposure, relative contribution of individual risk factors was not considered in the analysis. Unfortunately, menopausal status was not available, and thus could not be factored into analysis. While cardiac MR measures of fibrosis have been shown to be correlated in a variety of disease states,(81, 82, 85, 141) the invasiveness of biopsies required to obtain histological measurements ethically precludes such measures in the healthy heart; nevertheless, we lack of histological corroboration of the measures of ECV. Due to our modest sample size, we may not have a complete representation of a healthily aging population. Similarly, though we do not have race/ethnicity information for our study subjects, the distribution

in our study may not reflect other North American or European cities, possibly affecting the generalizability of the results. As mentioned above, values reported in this study, particularly the T_1 values themselves, are not directly comparable to others obtained using other T_1 -mapping techniques, thus limiting direct comparisons to previous work using other methods. We chose to perform analysis in the interventricular septum, which may limit comparisons to other studies. This analysis method was chosen to minimize errors from unintentional inclusion of artifacts from regions commonly affected,(51) and given the diffuse nature of any changes we sought to measure are not expected to be regionally distributed in this cohort. Finally, ECV is preferred over post-contrast T_1 times as a measure of fibrosis due to its relative insensitive to dose, timing and type of contrast agent.(152) While no statistical differences in ECV were noted between the different gadolinium agents used in the study, this may be an additional source of variability in our results.

3.5 Conclusion

In conclusion, native T_1 and ECV measured with SASHA do not vary significantly with age, regardless of sex in healthy individuals or those with risk factors for heart failure, but otherwise normal structure and function. In healthy subjects, native T_1 and ECV are significantly higher in women than in men, but do not differ with sex in the presence of risk factors, suggesting a different myocardial response to risk factors between men and women. Larger, longitudinal, prospective studies, where the duration and severity of risk factors can be assessed, would be beneficial in confirming the findings of this study.

Chapter 4

Sex Differences in Native T_1 and Extracellular Volume Fraction in Heart Failure

4.1 Introduction

Heart failure (HF) is a multifactorial disease with a significant global presence.(153) An estimated 600,000 Canadians,(6) 6.5 million Americans,(7) and millions worldwide are affected by HF. It is now widely recognized that there are different phenotypes of heart failure, most commonly characterized by the left ventricular ejection fraction (LVEF). These distinctions are important, as the underlying etiology, natural history, and therapeutic options differ significantly between those with heart failure and reduced ejection fraction (HFrEF) and those with preserved ejection fraction (HFpEF). However, in patients with HF the association between LVEF and mortality only holds up to an LVEF of 45%, after which any increase in LVEF does not predict further improvements in mortality.(154) Therefore, simply relying on this metric will not provide adequate characterization of the risks for patient with HF.

Myocardial fibrosis is a common pathological finding in heart failure, particularly at end-stages. Assessing myocardial fibrosis non-invasively using cardiac magnetic resonance imaging (CMR) via T_1 -mapping, including estimation of the extracellular volume fraction (ECV), has been associated with outcomes, such as heart failure hospitalizations or death, for patients with HFrEF(99) and HFpEF,(101, 103, 155) with data demonstrating improved predictive power over LVEF and additive benefit of ECV.(99) Additionally, studies have demonstrated differences in ECV between patients with HFrEF and HFpEF, though differences in native T_1 were smaller and non-significant.(78, 89, 156, 157) However, detailed comparisons between these groups, along with healthy individuals and those at risk for heart failure, are lacking, particularly when considering the additional impact of sex. There is increasing evidence of differences in the incidence, clinical course, morbidity, and mortality between the sexes.(128) How sex-related

differences in T_1 and ECV relate to sex-related differences in cardiovascular disease and heart failure is not well known and requires further investigation.

In this study we aim to better characterize differences in myocardial T_1 and ECV across a spectrum of healthy individuals, those with significant risk factors for heart failure, and those with either HFpEF or HFrEF, considering sex-related variances. Additionally, we aim to examine the predictive nature of these CMR metrics of fibrosis, along with other conventional predictors, for the risk of hospitalization and death.

4.2 Methods

4.2.1 Study Subjects

Subjects enrolled in a multicentre, province wide study with the purpose of developing novel strategies for the diagnosis, treatment, and prognostication of patients with heart failure (Alberta HEART(143)) who underwent comprehensive, contrast-enhanced CMR examinations with T_1 -mapping, were included in this study. In brief, subjects enrolled included: 1) healthy individuals free of cardiovascular disease; 2) individuals with risk factors for the development of heart failure including hypertension (defined as a history of hypertension or antihypertensive medication use), diabetes, obesity (body mass index [BMI] > 30 kg/m²), atrial fibrillation, hyperlipidemia, and coronary artery disease or a history of myocardial infarction; 3) individuals with known heart failure with preserved ejection fraction (LVEF > 50%); or 4) individuals with known heart failure with reduced ejection fraction (LVEF < 50%). Data from the healthy subjects, along with 89 of the individuals with risk factors for the development of heart failure, have been presented as a portion of the previous chapter.(158) All subjects provided written, informed consent, and the study was approved by both the University of Alberta Health Research Ethics Office and the University of Calgary Research Ethics Board.

4.2.2 Cardiac MRI Protocol

Imaging was performed on 1.5T Siemens MRI systems (Siemens MAGNETOM Sonata or Avanto, Siemens Healthcare, Erlangen, Germany). Cardiac gated, segmented bSSFP cine imaging was performed in standard long axis and short axis planes for assessment of ventricular volumes and function. Late gadolinium enhancement (LGE) imaging was performed using a phase-sensitive inversion recovery sequence in standard long axis and short axis planes, in keeping with

the volumetric assessment, starting approximately 7 minutes following intravenous administration of 0.15 mmol/kg gadobutrol (Gadovist; Bayer HealthCare Pharmaceuticals, Montville, NJ).

T₁-mapping was performed using the SATuration-recovery single-SHot Acquisition (SASHA) pulse sequence(51) at basal and mid-ventricular short axis slice locations. T₁-mapping was performed before, and approximately 15 minutes post-contrast administration.

4.2.3 Image analysis

Ventricular volumes, function, and myocardial mass were analyzed in the standard fashion with manual contouring of epicardial and endocardial contours using commercially available software (cvi42, Circle Cardiovascular Inc., Calgary, Canada, or Syngo Argus, Siemens Healthcare, Erlangen, Germany). Papillary muscles, and right ventricular trabeculations, were included in the blood pool. Analysis of the LGE imaging was performed qualitatively, for the presence of areas of high signal intensity.

Analysis of the T₁-mapping images was performed separately for each slice and time point (i.e. pre/post-contrast) using custom software (The MathWorks, Natick, MA, United States).(51) Non-rigid motion correction of the T₁ weighted images prior to T₁ calculation was performed to minimize in-plane translation due to imperfect breath-holding.(51) Regions of interest (ROIs) were drawn in the interventricular septum and LV blood pool, with manual adjustments made for residual in-plane motion following motion correction. The septal ROI was drawn as a line, which was then expanded radially to a width of 2 mm. For blood pool a circular ROI was drawn in the LV blood pool, avoiding papillary muscles and trabeculations. For each slice location, ROIs were copied between pre- and post-contrast time points to minimize variability, with adjustments performed as needed due to variations in breath-hold location.

Average signal intensities from the ROI were fit to a 3-parameter mono-exponential recovery curve:

$$Signal(TS) = k \left(1 - \eta e^{-TS/T_1} \right)$$

with scaling constant k, saturation efficiency g, longitudinal relaxation time T₁, and saturation recovery time TS.(51)

Extracellular volume was calculated using the standard relationship(79):

$$ECV = (1 - hematocrit) \left(\frac{\left[\frac{1}{T_{1Gd}} - \frac{1}{T_1} \right]_{tissue}}{\left[\frac{1}{T_{1Gd}} - \frac{1}{T_1} \right]_{blood}} \right)$$

T_1 and ECV were calculated for each slice independently and averaged per patient. Note was made if LGE was present in corresponding septal regions, allowing for analysis of T_1 and ECV without the inclusion of focal fibrosis.

4.2.4 Outcome Data Collection

As previously outlined,(143) study subjects were followed via review of the external databases administrated by the provincial health authority. Outcomes of interest include hospital admission for cardiovascular causes (defined by International Classification of Diseases codes version 10), including heart failure, all-cause mortality, or a composite end-point of hospital admission for cardiovascular cause or mortality. Follow-up included events up to a maximum of 5 years.

4.2.5 Statistics

Data are presented as mean \pm standard deviation or count (%), as applicable. Comparisons were performed between groups within a sex (ex: women with HFpEF vs. women with HFrEF), with continuous variables evaluated with the two-sample t-test, while the Chi-squared, or the Fisher's exact test, was used for categorical data depending on the observed frequency.

Kaplan-Meier analysis, with log-rank testing, was performed to examine the temporal pattern associated with the outcomes of CV admission, all-cause mortality, or the composite end-point of CV admission or all-cause mortality, with an elevated native T_1 or ECV ($>2SD$ sex normal values), and the presence of LGE.

Univariate Cox regression analysis was performed on clinical and imaging parameters, with any parameter demonstrating significance < 0.1 to be included in multivariate Cox regression analysis. Native T_1 and ECV were analyzed in two approaches, considering it as a continuous variable (per 10 ms for native T_1 , and per 1% for ECV) or as a categorical condition if the value is two standard deviations above sex specific normal values.(158)

P-values were not corrected for multiple comparisons to preserve power. Statistical analysis was performed using STATA statistical software (version 11.2, Stata Corporation, College Station, TX).

4.3 Results

Contrast-enhanced CMR studies, including T₁-mapping were available in 392 individuals. Image artifacts precluded analysis in 30 subjects, and acquisition/protocol errors precluded analysis in 38 subjects, resulting in a final group of 324 individuals (66±11 years, 163 male). Characteristics of the included groups, separated by sex, are presented in Table 4.1 and Table 4.2.

4.3.1 Native T₁

In women (Figure 4.1A), there are no differences in native myocardial T₁ between healthy controls and those at-risk (p=0.8213) or those with HFpEF (p=0.1118), nor between those at-risk and those with HFpEF, though there is a trend towards higher values (p=0.0537). Native myocardial T₁ is increased in those with HFrEF versus healthy controls (p=0.0007) and those at-risk (p=0.0004), however not statistically different between the types of HF (p=0.1159).

When considering septal native T₁ when regions that include LGE are excluded (Figure 4.2A), the findings remain similar, with significant differences only noted between those with HFrEF and healthy controls (p=0.0164) or those at-risk (p=0.0198).

In men (Figure 4.1B), there are no differences in native myocardial T₁ between healthy controls and those at-risk (p=0.2278) or those with HFpEF (p=0.1086), nor between those at-risk and those with HFpEF (p=0.5210). Men with HFrEF demonstrate an increased native T₁ compared to all other groups, including those with HFpEF (p<0.001 for all).

These relationships persist when septal regions containing LGE are removed (Figure 4.2B), with statistical differences only found between men with HFrEF and all other groups (p<0.025 for all).

Table 4.1: Participant characteristics and CMR data

	Women				Men			
	Healthy	At-Risk	HFpEF	HFrEF	Healthy	At-Risk	HFpEF	HFrEF
	n=29	n=78	n=33	n=21	n=11	n=79	n=32	n=41
Age (yrs)	61±10	64±12	74±9	67±10	61±11	65±9	68±12	65±13
BMI (kg/m ²)	24.6±2.8	30.1±6.7	31.3±6.9	28.3±5.7	25.3±2.4	29.3±4.5	30.5±4.5	29.5±4.6
Hypertension	0 (0%)	52 (67%)	26 (79%)	14 (67%)	0 (0%)	54 (68%)	21 (66%)	22 (54%)
Diabetes	0 (0%)	15 (19%)	16 (48%)	5 (24%)	0 (0%)	22 (28%)	10 (31%)	16 (39%)
Hyperlipidemia	0 (0%)	44 (56%)	22 (67%)	11 (52%)	0 (0%)	46 (58%)	24 (75%)	37 (90%)
Atrial fibrillation	0 (0%)	7 (9%)	11 (33%)	9 (43%)	0 (0%)	12 (15%)	19 (59%)	15 (37%)
CAD or MI	0 (0%)	6 (8%)	8 (24%)	5 (24%)	0 (0%)	30 (38%)	13 (41%)	25 (61%)
Etiology of Heart Failure								
Undefined	0 (0%)	0 (0%)	2 (6%)	0 (0%)	0 (0%)	0 (0%)	1 (3%)	1 (2%)
Ischemic	0 (0%)	0 (0%)	3 (9%)	3 (14%)	0 (0%)	0 (0%)	7 (22%)	23 (56%)
Non-Ischemic	0 (0%)	0 (0%)	18 (86%)	18 (86%)	0 (0%)	0 (0%)	24 (75%)	17 (41%)
Sarcoidosis			0 (0%)	1 (4%)			1 (4%)	0 (0%)
Alcohol-induced			0 (0%)	1 (4%)			1 (4%)	2 (12%)
Dilated Cardiomyopathy			14 (78%)	16 (67%)			16 (67%)	10 (59%)
Hypertensive								
Cardiomyopathy			0 (0%)	0 (0%)			0 (0%)	0 (0%)
Infectious			1 (6%)	1 (4%)			1 (4%)	1 (6%)
Valvular			1 (6%)	0 (0%)			0 (0%)	1 (6%)
Medications								
Hyperlipidemia								
Statin	0 (0%)	34 (44%)	19 (58%)	9 (43%)	0 (0%)	40 (51%)	22 (69%)	31 (76%)
Other	0 (0%)	4 (5%)	2 (6%)	1 (5%)	0 (0%)	2 (3%)	1 (3%)	3 (7%)
Blood pressure								
ACE-I / ARB	0 (0%)	45 (58%)	29 (88%)	19 (90%)	0 (0%)	54 (68%)	29 (91%)	37 (90%)
Beta-blocker	0 (0%)	20 (26%)	22 (67%)	18 (86%)	0 (0%)	24 (30%)	28 (88%)	37 (90%)
CCB	0 (0%)	14 (18%)	13 (39%)	2 (10%)	0 (0%)	18 (23%)	9 (28%)	7 (17%)
Diuretic	0 (0%)	27 (35%)	27 (82%)	17 (81%)	0 (0%)	17 (22%)	21 (66%)	31 (76%)

BMI = body mass index; CAD = coronary artery disease; MI = myocardial infarction; ACE-I = ace inhibitor, ARB = angiotensin receptor blocker, CCB = calcium channel blocker

Table 4.2: Comparison of cardiac magnetic resonance values between groups

	Women				Men			
	Healthy	At-Risk	HFpEF	HFrEF	Healthy	At-Risk	HFpEF	HFrEF
	n=29	n=78	n=33	n=21	n=11	n=79	n=32	n=41
LV mass (g/m ²)	48±6	49±10	55±14	67±15	55±10	62±13	63±13	77±24
LVEDVi (ml/m ²)	69±10	65±12	68±16	93±27	70±10	74±18	71±16	118±36
LVESVi (ml/m ²)	25±5	22±6	25±8	56±21	27±7	29±11	30±9	78±32
LVSVi (ml/m ²)	43±7	42±9	43±11	37±8	44±7	45±10	41±8	40±13
LVEF (%)	63±5	66±7	63±6	41±7	62±6	61±8	58±6	35±10
RVEDVi (ml/m ²)	65±11	62±12	63±19	62±15	74±17	71±15	74±20	87±25
RVESVi (ml/m ²)	24±7	23±7	27±12	28±9	33±11	30±8	34±11	47±21
RVSVi (ml/m ²)	41±8	39±10	36±11	33±10	41±9	41±11	40±12	40±11
RVEF (%)	63±7	63±8	58±10	54±10	56±7	58±8	55±8	47±11
Native T ₁ (ms)	1204±31	1202±52	1223±58	1249±55	1178±35	1197±51	1204±48	1252±63
ECV (%)	22.6±2.4	21.5±2.5	23.3±3.5	24.7±3.6	22.0±2.0	21.3±3.4	22.4±3.8	26.3±6.5
LGE present	0 (0%)	14 (18%)	8 (24%)	11 (52%)	0 (0%)	33 (42%)	12 (38%)	32 (78%)
<i>No LGE in ROI</i>								
Native T ₁ (ms)	1204±31	1202±52	1219±54	1236±56	1178±35	1197±50	1201±49	1235±63
ECV (%)	22.6±2.4	21.4±2.4	23.3±3.5	23.2±2.6	22.0±2.0	21.1±3.3	21.9±3.5	23.0±3.3
Hematocrit available	24 (83%)	75 (96%)	30 (91%)	19 (90%)	10 (91%)	75 (95%)	32 (100%)	41 (100%)
Hematocrit	0.39±0.03	0.41±0.03	0.38±0.04	0.39±0.03	0.45±0.01	0.44±0.04	0.43±0.05	0.42±0.04

LV = left ventricle; LVEDVi = indexed left ventricular end-diastolic volume; LVESVi = indexed left ventricular end-systolic volume; LVSVi = indexed left ventricular stroke volume; LVEF = left ventricular ejection fraction; RVEDVi = indexed right ventricular end-diastolic volume; RVESVi = indexed right ventricular end-systolic volume; RVSVi = indexed right ventricular stroke volume; RVEF = right ventricular ejection fraction; ECV = extracellular volume fraction

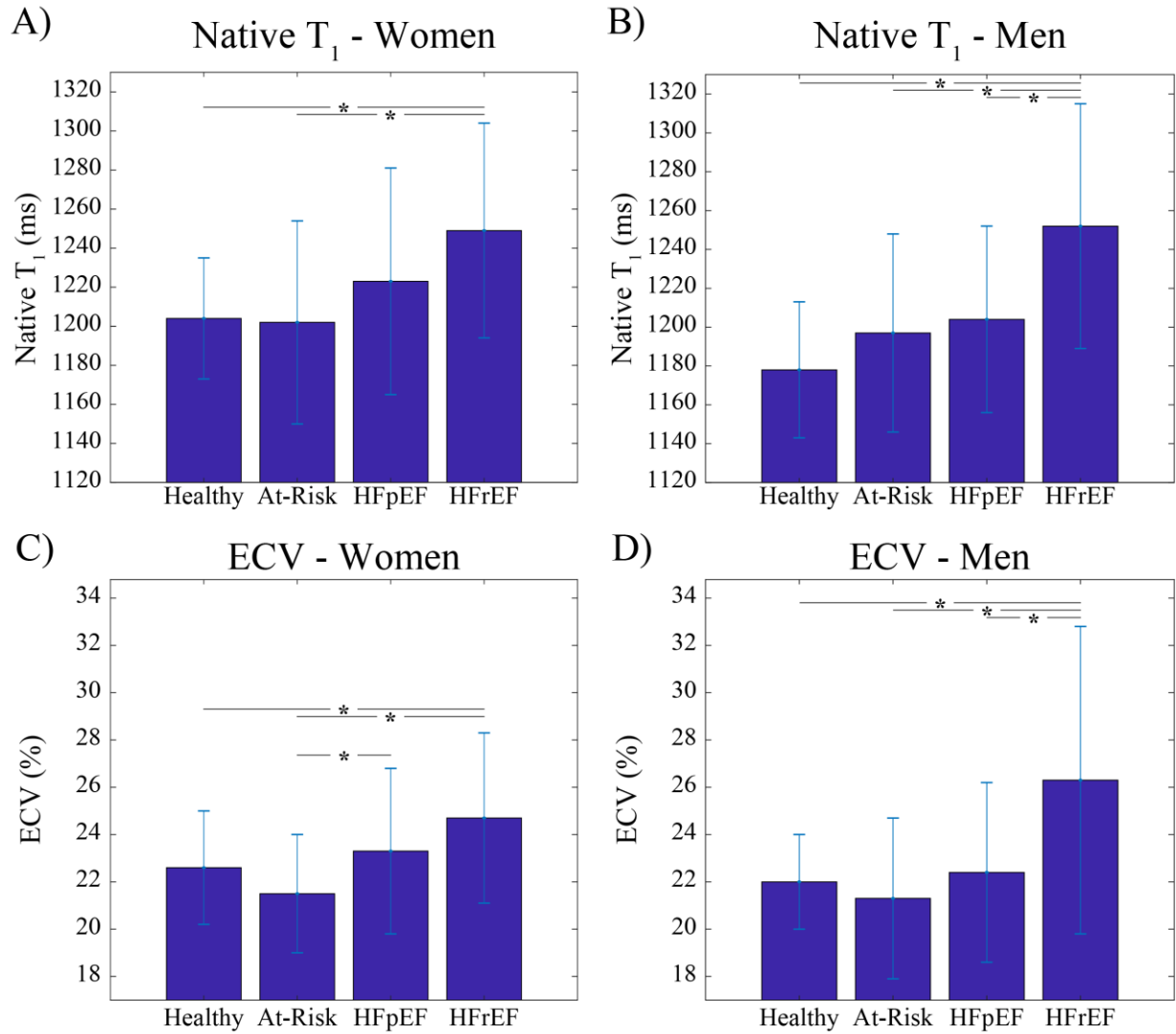


Figure 4.1: Mean \pm standard deviation plots shown for septal regions for native T₁ and ECV by sex, for the four subject groups. * denotes $p < 0.05$ between group.

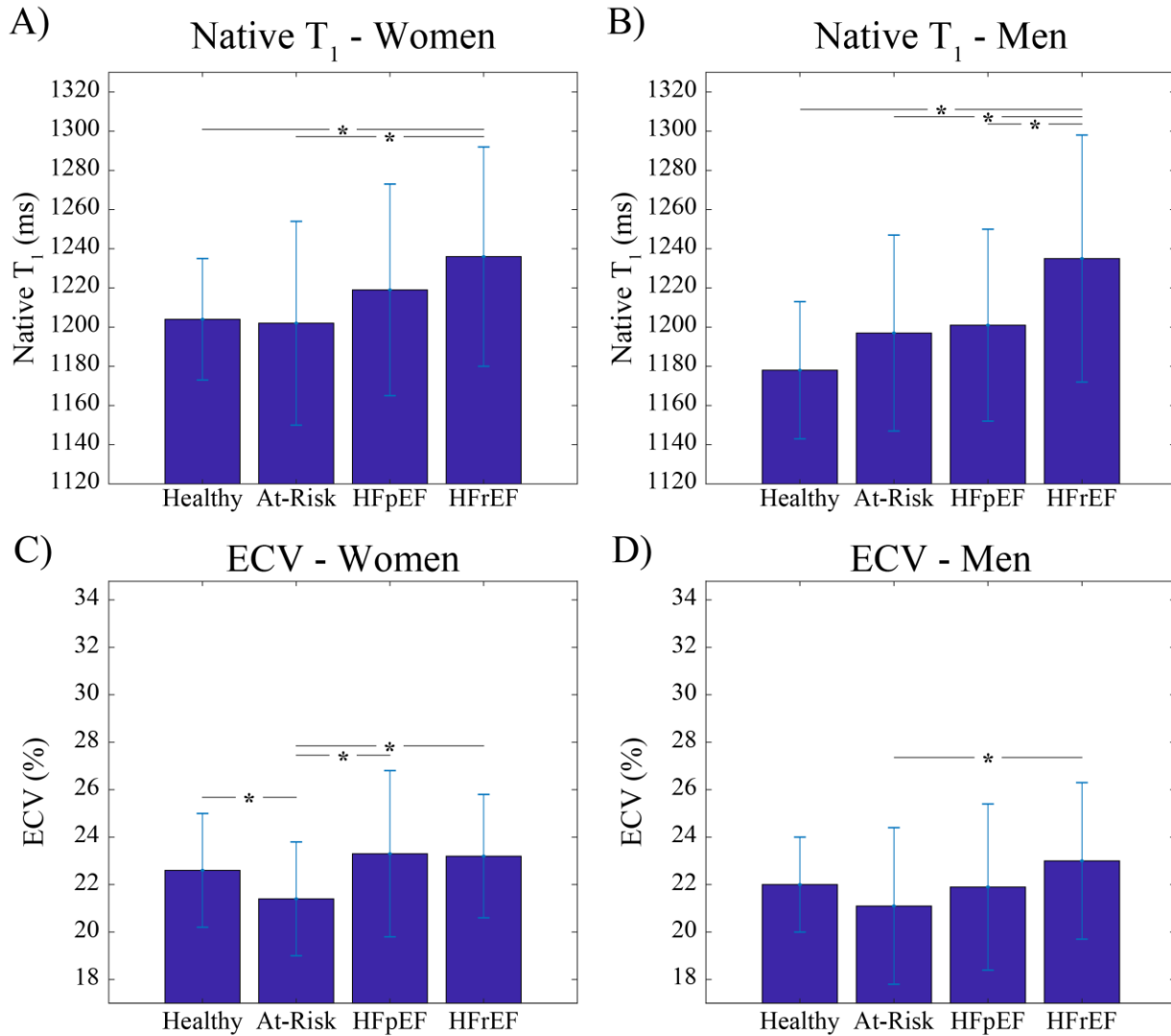


Figure 4.2: Mean \pm standard deviation plots shown for septal regions for native T₁ and ECV by sex when septal regions with LGE are excluded from analysis, for the four subject groups. * denotes $p < 0.05$ between group.

4.3.2 ECV

In women (Figure 4.1C), there are no differences in ECV between healthy controls and those at-risk ($p=0.0564$) or those with HFpEF ($p=0.4032$). However, unlike native T₁, ECV was statistically increased in those with HFpEF compared to those at risk ($p=0.0033$). Similar to the native T₁ findings, women with HFrEF showed increased ECV compared to healthy controls ($p=0.0258$) and those at-risk ($p < 0.0001$), however not statistically different between the types of HF ($p=0.1737$).

When removing septal regions containing LGE (Figure 4.2C), there is now a slight difference between healthy controls and those at-risk ($p=0.0438$) and no longer an increase in ECV between those with HFrEF and healthy controls (0.5029). There remains a significant increase in between those with either HFpEF or HFrEF and those at-risk ($p=0.0023$ and $p=0.0176$, respectively).

In men (Figure 4.1D), findings for ECV are similar to native T_1 . There are no differences in between healthy controls and those at-risk ($p=0.5323$) or those with HFpEF ($p=0.7727$), nor between those at-risk and those with HFpEF ($p=0.1580$). Men with HFrEF demonstrate and increased native T_1 compared to all other groups, including those with HFpEF ($p<0.05$ for all).

Following exclusion of septal regions including LGE (Figure 4.2D), the only statistically significant difference between groups was an increased ECV in men with HFrEF compared to those at-risk ($p=0.0082$).

4.3.3 Outcomes

In the entire cohort of 324 individuals, there were 48 individuals had a cardiovascular admission (average time from CMR to admission of 789 days), with only 15 of those admissions being for heart failure (average time from CMR to HF admission of 932 days). During the study period, there were 21 deaths, occurring on average 756 days from the CMR study. Considering the composite end-point of CV admission or all-cause mortality, there were 62 events, occurring on average 763 days following the CMR. The breakdown of events by risk group and sex are presented in

Table 4.3. Overall, there are higher frequencies of CV admissions for those with heart failure, in particular for women with HFpEF and men with HFrEF. The frequency of mortality appears higher in men with HF of either type and for women with HFpEF. Considering the composite end-point, the frequency of events is most common in women with HFpEF and men with HFrEF.

Table 4.3: Outcome occurrence, by subject group and sex

	Women				Men			
	Healthy	At-Risk	HFpEF	HFrEF	Healthy	At-Risk	HFpEF	HFrEF
	n=29	n=78	n=33	n=21	n=11	n=79	n=32	n=41
CV Admission	n=1 (3.4%)	n=3 (3.8%)	n=10 (30.3%)	n=3 (14.3%)	n=1 (9.1%)	n=14 (17.7%)	n=4 (12.5%)	n=12 (29.3%)
HF Admission	n=0 (0%)	n=0 (0%)	n=4 (12.1%)	n=0 (0%)	n=0 (0%)	n=1 (1.3%)	n=3 (9.4%)	n=7 (17.1%)
Mortality	n=1 (3.4%)	n=1 (1.3%)	n=3 (9.1%)	n=1 (4.8%)	n=0 (0%)	n=2 (2.5%)	n=5 (15.6%)	n=8 (19.5%)
CV Admission or Mortality	n=2 (6.9%)	n=3 (3.8%)	n=12 (36.4%)	n=4 (19.0%)	n=1 (9.1%)	n=15 (19.0%)	n=9 (28.1%)	n=16 (39.0%)

CV = cardiovascular; HF = heart failure

Native T₁ is increased in women who had a cardiovascular admission (1242 vs. 1209 ms, p=0.0129) or the composite end-point (1242 vs. 1208 ms, p=0.0056), however it was not statistically different for mortality alone (1231 vs. 1212 ms, p=0.3707). These findings generally remained when excluding septal regions containing LGE (women who had cardiovascular admission 1237 vs. 1206 ms, p=0.0221; women who died 1198 vs. 1210 ms, p=0.6660; women with composite end-point 1231 vs. 1207 ms, p=0.0564).

Meanwhile, there was increased native T₁ in men who died (1239 vs. 1208 ms, p=0.0490) or met the composite end-point (1229 vs. 1204 ms, p=0.0165), with a trend in those with a cardiovascular admission (1228 vs. 1207 ms, p=0.0651). However, these differences become only a non-significant trend when regions containing LGE are removed (men who had cardiovascular admission 1219 vs. 1201 ms, p=0.1266; men who died 1228 vs. 1202 ms, p=0.1296; men with composite end-point 1219 vs. 1200 ms, p=0.0671).

There were no statistically significant differences in ECV between women with respect to those who had a cardiovascular admission (23.1 vs. 22.4%, p=0.4031), died (23.9 vs. 22.4%, p=0.2838), or met the composite point (23.7 vs. 22.3, p=0.0572). There is no change to these findings when excluding septal regions containing LGE (women who had cardiovascular admission 22.8 vs. 22.1%, p=0.3809; women who died 21.7 vs. 22.2%, p=0.7292; women with composite end-point 23.0 vs. 22.1%, p=0.2151).

In contrast, men showed increased ECV in those who had a cardiovascular admission (23.5 vs. 22.7%, p=0.04134), died (26.7 vs. 22.5%, p=0.0010), or met the composite end-point (24.4 vs. 22.3% ms, p=0.0198). These findings remained (men who died 24.8 vs. 21.4%, p=0.0009; men

with composite end-point 22.8 vs. 21.4%, $p=0.0298$), other than for men who had a cardiovascular admission (22.1 vs. 21.6%, $p=0.5353$) when septal regions containing LGE were excluded.

Freedom from cardiovascular admission, mortality, or the composite end-point was statistically different between those with a native T_1 or ECV value greater than two standard deviations of the sex normal values (Figure 4.3A and Figure 4.3C). When removing septal regions containing LGE, these findings persisted for CV admissions and the composite end-point, but an abnormal native T_1 did not distinguish differences in mortality (Figure 4.3B and Figure 4.3D). The freedom from cardiovascular admission was significantly different between individuals with and without the presence of LGE (Figure 4.3E).

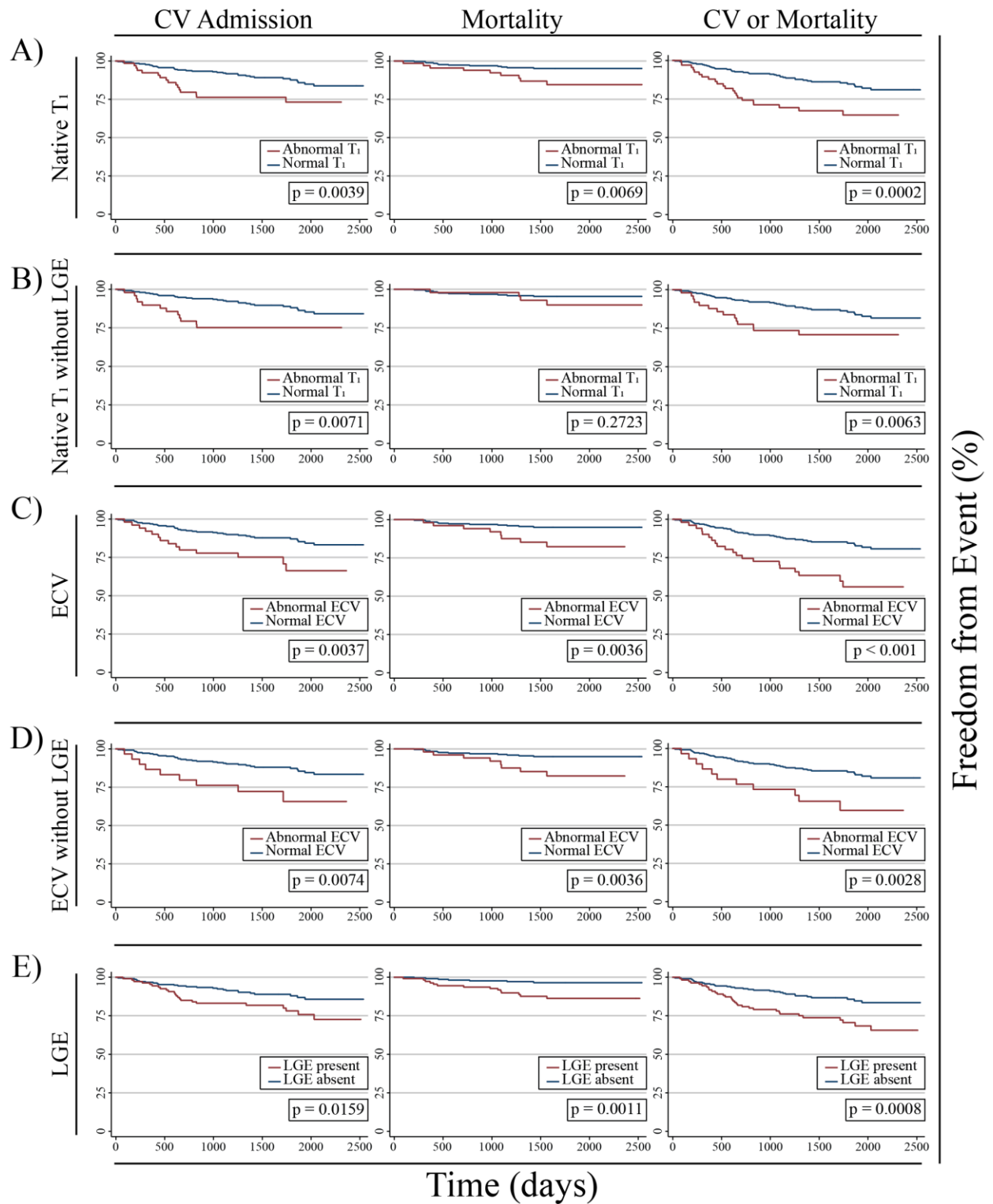


Figure 4.3: Kaplan-Meier survival analysis plots for outcome analysis, including cardiovascular admission (first column), all-cause mortality (middle column), and composite end-point (last column). A) and C) represent subjects with (red curves) or without (blue curves) a native T₁ or ECV, respectively, two standard deviations above normal values for sex. B) and C) similarly

represent subjects with (red curves) or without (blue curves) a native T₁ or ECV, respectively, when septal regions with positive late gadolinium enhancement is excluded, that is two standard deviations above normal values for sex. E) demonstrates subjects with (red curves) or without (blue curves) positive late gadolinium enhancement. Log rank p-values are provided.

The result of univariate and multivariate Cox regression analysis are presented in

Table 4.4 and

Table 4.5, when considering native T₁ (or ECV) as a continuous variable or when greater than two standard deviations of the sex normal values, respectively. Univariate regression demonstrates significance for the majority of the parameters included, however most were not significant in multivariate testing. Patient age was the only parameter to remain significantly associated with all outcome metrics, be it CV admission, mortality, or the composite end-point, irrespective if T₁ or ECV was treated as a continuous variable or a cut-off based on normal values. Native T₁ (per 10 ms) and a diagnosis of CAD or previous MI were associated with CV admissions and the composite end-point, but not mortality alone. Besides age, RVEF remained the only other metric significantly associated with mortality. In the model including native T₁ above sex normal values, findings were overall similar other than the loss of significance for the association of CAD or MI with CV admission, and the association of increased native T₁ with CV admission or the composite end-point.

Table 4.4: Univariate and multivariate Cox regression analysis, considering T₁ and ECV as continuous variable

Variable	Univariate				Multivariate			
	HR	[95% CI]		P-value	HR	[95% CI]		P-value
Cardiovascular admission								
Age	1.06	1.03	1.09	0.00	1.06	1.02	1.09	0.00
Sex	1.87	1.04	3.38	0.04	1.60	0.81	3.14	0.17
CAD	3.11	1.77	5.48	0.00	2.21	1.15	4.25	0.02
LVMi	1.01	1.00	1.03	0.09	0.99	0.97	1.01	0.20
LVEF	0.97	0.95	0.99	0.00	0.99	0.96	1.03	0.72
RVEF	0.97	0.94	1.00	0.04	0.98	0.95	1.02	0.39
T ₁ (per 10 ms)	1.08	1.03	1.14	0.00	1.07	1.02	1.13	0.01
ECV	1.05	0.99	1.11	0.12				
LGE present	1.98	1.12	3.49	0.02	0.99	0.49	1.99	0.98
Mortality								
Age	1.11	1.05	1.17	0.00	1.11	1.05	1.18	0.00
Sex	2.52	0.98	6.50	0.06	1.56	0.50	4.82	0.44
CAD	4.11	1.73	9.76	0.00	1.62	0.53	4.90	0.40
LVMi	1.01	0.99	1.03	0.45				
LVEF	0.96	0.93	0.99	0.01	1.02	0.97	1.07	0.41
RVEF	0.92	0.88	0.96	0.00	0.91	0.86	0.97	0.01
T ₁ (per 10 ms)	1.09	1.02	1.17	0.01	1.01	0.92	1.12	0.78
ECV	1.14	1.07	1.22	0.00	1.04	0.95	1.15	0.39
LGE present	4.21	1.70	10.45	0.00	1.77	0.55	5.68	0.34
Cardiovascular admission or mortality								
Age	1.07	1.04	1.10	0.00	1.07	1.04	1.10	0.00
Sex	2.00	1.18	3.38	0.01	1.59	0.86	2.94	0.14
CAD	3.33	2.02	5.48	0.00	2.14	1.20	3.85	0.01
LVMi	1.02	1.00	1.03	0.02	0.99	0.97	1.01	0.28
LVEF	0.97	0.95	0.99	0.00	1.00	0.97	1.03	0.87
RVEF	0.96	0.94	0.99	0.00	0.98	0.95	1.01	0.16
T ₁ (per 10 ms)	1.09	1.04	1.13	0.00	1.07	1.01	1.13	0.01
ECV	1.08	1.03	1.13	0.00	0.99	0.93	1.06	0.73
LGE present	2.29	1.39	3.77	0.00	1.13	0.60	2.13	0.71

Table 4.5: Univariate and multivariate Cox regression analysis, considering T₁ and ECV as binary variable, being above or below two standard deviations of normal values for sex

Variable	Univariate				Multivariate			
	HR	[95% CI]		P-value	HR	[95% CI]		P-value
Cardiovascular admission								
Age	1.06	1.03	1.09	0.00	1.06	1.02	1.09	0.00
Sex	1.87	1.04	3.38	0.04	1.37	0.70	2.70	0.36
CAD	3.11	1.77	5.48	0.00	1.92	0.99	3.70	0.05
LVMi	1.01	1.00	1.03	0.09	0.99	0.97	1.01	0.32
LVEF	0.97	0.95	0.99	0.00	0.99	0.96	1.02	0.63
RVEF	0.97	0.94	1.00	0.04	0.98	0.95	1.02	0.36
T ₁ Above Norm	2.36	1.29	4.31	0.01	1.53	0.74	3.17	0.25
ECV Above Norm	2.44	1.31	4.56	0.01	1.46	0.69	3.11	0.33
LGE present	1.98	1.12	3.49	0.02	0.99	0.48	2.02	0.98
Mortality								
Age	1.11	1.05	1.17	0.00	1.10	1.05	1.17	0.00
Sex	2.52	0.98	6.50	0.06	1.45	0.45	4.62	0.53
CAD	4.11	1.73	9.76	0.00	1.49	0.49	4.54	0.48
LVMi	1.01	0.99	1.03	0.45				
LVEF	0.96	0.93	0.99	0.01	1.02	0.97	1.07	0.42
RVEF	0.92	0.88	0.96	0.00	0.92	0.86	0.97	0.00
T ₁ Above Norm	3.10	1.30	7.35	0.01	1.32	0.48	3.62	0.59
ECV Above Norm	3.48	1.42	8.51	0.01	1.63	0.57	4.63	0.36
LGE present	4.21	1.70	10.45	0.00	1.64	0.51	5.30	0.41
Cardiovascular admission or mortality								
Age	1.07	1.04	1.10	0.00	1.06	1.04	1.09	0.00
Sex	2.00	1.18	3.38	0.01	1.45	0.79	2.67	0.23
CAD	3.33	2.02	5.48	0.00	2.02	1.13	3.62	0.02
LVMi	1.02	1.00	1.03	0.02	0.99	0.98	1.01	0.44
LVEF	0.97	0.95	0.99	0.00	1.00	0.97	1.03	0.83
RVEF	0.96	0.94	0.99	0.00	0.98	0.95	1.01	0.18
T ₁ Above Norm	2.60	1.54	4.37	0.00	1.47	0.78	2.77	0.24
ECV Above Norm	2.89	1.69	4.94	0.00	1.69	0.88	3.24	0.12
LGE present	2.29	1.39	3.77	0.00	1.01	0.54	1.91	0.97

4.4 Discussion

In this study, we have shown that there are small, but often significant, differences between SASHA-derived myocardial native T_1 and ECV amongst healthy controls, those at risk for heart failure, and the different phenotypes of heart failure, specifically those with preserved or reduced ejection fraction. Additionally, differences exist between the freedom from adverse events, including cardiovascular admissions and mortality, between those with and without elevated native T_1 or ECV.

Differences in cardiovascular risks and outcomes have been demonstrated between the sexes,(159-161) and we have previously shown that the sexes exhibit differences in myocardial native T_1 and ECV between healthy controls and those at risk of heart failure.(158) In this study, these sex-related differences in the findings for native T_1 and ECV are extended into the heart failure population, further highlighting this important principle. In the current study, we find that in women the T_1 and ECV values for those with HFpEF appear more similar to those with HFrEF, while for men there appears to be more similarity between those with HFpEF and controls or those at-risk. It is unclear if these patterns of T_1 and ECV are the cause of, or simply reflective of, sex-related differences between myocardial adaptations to the stressors leading to the development of HFpEF.

The proportion of outcomes, particularly for cardiovascular admissions, appears higher in women with HFpEF compared to their HFrEF counterparts, while in men the opposite relationship appears. However, the overall occurrence of mortality in either HF phenotype appears higher in men, even those with HFpEF. These sex related differences in outcomes are in line with other published data for both HFrEF(160) and HFpEF(161) subtypes.

Interestingly, there is an increase in native T_1 , even when septal LGE was excluded, between women who had a cardiovascular admission, but not mortality, whereas the opposite pattern (more difference between those who died but not those admitted for cardiovascular causes) was present in men. While this pattern remained similar for ECV in men, no significant differences were present between those with/without outcomes in women. Whether this is indicative of native T_1 and ECV showing differing sensitivity to pathophysiological alterations remains to be elucidated. While a different predictive nature of T_1 vs. ECV has been shown,(101, 155) there is limited data on whether one marker may prove more advantageous.

We have demonstrated that freedom from adverse outcomes, including cardiovascular-related admission or mortality, are different in those with either increased myocardial native T₁ or ECV. However, there is undoubtedly an influence from the presence of LGE, as there was no longer a difference in mortality curves for native T₁ when septal ROIs with LGE were excluded from the analysis.

Determining predictors of adverse outcomes is of important clinical significance. Considering any of the outcome measures, including the composite end-point, increasing age was the only predictor that remained significant in multivariate Cox regression analysis for all outcomes. While this is in keeping with other publications that also included ECV in their analysis,(85, 99) others have not necessarily found this age related association when including ECV or native T₁.(98, 101, 103, 159) Unfortunately, in contrast to other publications(85, 96, 99, 101, 103, 155) where ECV was associated with outcomes after multivariate regression, this was not repeated in our study. It is not clear why these differences exist; it may be related to different patient groups, or differences in included variables. For example, in the study from Duca et al. MOLLI-ECV was significant in multivariate analysis when considering only CMR parameters, but was no longer significant when non-CMR variables were combined in the multivariable model.(101)

When considering T₁ as a continuous variable, myocardial native T₁ was a significant predictor on multivariate Cox regression for cardiovascular-related admissions and the composite end-point. This finding of potentially improved prognostic performance of native T₁ over ECV is similar to a previous publication by Puntmann et al.,(96) though other studies have seen the opposite.(101, 155) The specific reason for this finding is difficult to ascertain. While native T₁ and ECV are related, perhaps there are subtle differences in what in the myocardial milieu they are reflecting. Additionally, there are multiple measures required for the calculation of ECV, which may contribute errors or variability. This may also be compounded as hematocrit was unavailable in 5.6% of the study subjects, though the number is small.

Other than age, right ventricular ejection fraction (RVEF) was the only other significant predictor of all-cause mortality. Previous literature has shown a similar predictive nature of RVEF for mortality, but not hospitalizations using radionuclide ventriculography.(162) When considering T₁ data, our study found similar findings to that of Puntmann et al., who also found an association with RVEF.(96) This is also in line with other studies that have found associations

with RV remodelling,(85, 101) though again there is disparity in the literature, as not all studies including native T_1 metrics have demonstrated this.(103)

4.4.1 Limitations

Like many outcome studies, the overall small number of events limits extensive multiparameter assessments of potential associations and predictor variables. The overall number of subjects with heart failure is modest, when subgrouping by sex and heart failure type the smaller group sizes mean complex comparisons between groups becomes more problematic. This also meant that further dividing the HFrEF group to consider the emerging phenotype of heart failure with mid-range ejection fraction (HFmEF; LVEF 40-50%) was not feasible in the current study. Additionally, the data is derived from a single centre, and institution-related biases cannot be excluded, whether they are related to recruitment or management practices. As previously described,(158) the septal region was chosen to minimize unintentional inclusion of artifacts often found over the anterior or inferolateral walls.(51)

The exclusion of patients with pacemakers, or implanted defibrillators, and the requirements for administration of gadolinium-based contrast agents, for assessment of LGE and ECV, meant that those with devices and/or significant renal dysfunction were not included in the study, and thus generalizing the results to all patients with heart failure is not possible. However, the predictive performance of native T_1 in this study, and others,(96) highlight that there may not be a need for contrast administration, which is important given recent concerns about the clearance of these agents.(163)

The use of the SASHA T_1 -mapping sequence, which is known to have less sensitivity to other parameters such as T_2 , flip angle, and off-resonance, is less prevalent in the literature, and therefore more challenging to directly compare group values and cut-offs to other published data. However, to our knowledge this is the first published report of patient related outcomes using the SASHA pulse sequence.

4.5 Conclusions

Subtle differences in native T_1 and ECV are present between healthy individuals and those with heart failure, with sex-related differences in the patterns between heart failure phenotypes. While increased T_1 and ECV were associated with an increased incidence of adverse outcomes, between the measures only native T_1 remained a significant predictor for cardiovascular

admissions or the combined end-point in multivariate testing. Further study is warranted to better understand the nature and significance of potential differences of T₁ and ECV in the development of heart failure and for their relevance to prognosis, particularly considering different responses between the sexes.

Chapter 5

Reduced Right Ventricular Native Myocardial T_1 in Anderson-Fabry Disease: Comparison to Pulmonary Hypertension and Healthy Controls

5.1 Introduction

Anderson-Fabry disease (AFD), an X-linked lysosomal storage disease, is characterized by progressive multiorgan accumulation of intracellular sphingolipids due to α -galactosidase A enzyme deficiency.(164, 165) Cardiac involvement can result in progressive ventricular hypertrophy leading to heart failure, arrhythmias and is now the most common cause of mortality in patients with AFD.(164, 165) Due to inherent risks and limitations of endomyocardial biopsy,(166) non-invasive measures are sought as surrogates for sphingolipid deposition.(167, 168) While the focus has been primarily on global changes in cardiac structure and function, such as increasing ventricular mass,(169) atrioventricular uncoupling,(170) and reduced myocardial function,(171-173) recent studies using cardiac magnetic resonance T_1 -mapping techniques show promise in providing improved diagnostic differentiation between other causes of ventricular hypertrophy, as well as the prospect of an earlier marker of disease involvement.(73, 74, 174)

Measurement of native myocardial T_1 (longitudinal relaxation) time using cardiac magnetic resonance imaging (CMR) has revealed increased values in individuals with numerous cardiac conditions, including cardiomyopathies, acute myocarditis, and acute myocardial infarction.(66, 67, 175) In contrast, significantly reduced left ventricular (LV) T_1 values have been measured in patients with AFD, with average values >100 ms lower than healthy subjects, and larger magnitude changes compared to other conditions presenting with similar LV hypertrophy.(73, 74) T_1 -mapping is thus a promising tool in differentiating distinct manifestations of hypertrophy and has been proposed as a quantitative biomarker to follow for response to therapy, such as enzyme replacement in AFD.(73, 74)

While left ventricular hypertrophy is a hallmark of AFD, right ventricular (RV) involvement is also commonly seen, including ventricular hypertrophy and dysfunction.(176-179) Right ventricular dysfunction likely contributes to the presence of heart failure symptoms in those with preserved LV ejection fraction.(176) While autopsy studies have shown sphingolipid deposition in both ventricles,(180) it is important to note that despite studies which have shown beneficial effects from enzyme replacement therapy on LV metrics, there have been inconsistent changes seen in the RV.(178, 179) This may indicate subtle differences in the pathophysiological mechanisms behind ventricular remodelling and dysfunction in Anderson-Fabry disease. Due to the ability of native T_1 to differentiate those with Anderson-Fabry disease from other cases of LV hypertrophy, it offers a non-invasive metric that may help understand if the RV involvement mirrors that of the LV. However, the assessment of RV T_1 values in AFD have not previously been reported. Thus, the goal of the current study was to evaluate quantitative T_1 -mapping in the RV of patients with AFD. To aid in the understanding of the underlying mechanism of RV involvement in AFD, RV T_1 values were compared to LV values in patients with AFD and RV T_1 values in a group of patients with idiopathic pulmonary hypertension (PH), in whom changes in T_1 values are representative of increased RV afterload.(181)

5.2 Methods

5.2.1 Subjects

The primary study patient cohort consisted of 32 subjects with clinically and genetically confirmed AFD and 11 subjects with pulmonary hypertension, in whom T_1 -mapping was performed as part of existing studies. Average left ventricular T_1 values from the healthy controls and subjects with AFD have previously been published.(73) Subjects with AFD were recruited from both the University of Alberta and University of Calgary, from May 2010 to November 2012. Subjects were included if they had clinically and genetically confirmed AFD, and excluded if they were unable to provide informed consent or had contraindication to CMR. Subjects with PH were recruited from the University of Alberta from March 2010 to June 2013. Subjects were included if they had PH due to familial conditions, associated with anorexic medications, or idiopathic PH, and excluded if they were unable to provide informed consent, had abnormal renal function (GFR <30 mL/min/1.73 m²), or had a contraindication to CMR. Pulmonary hypertension was defined by catheter measured mean pulmonary artery pressure ≥ 25 mmHg, pulmonary capillary wedge

pressure ≤ 15 mmHg, and pulmonary vascular resistance > 240 dynes \cdot sec/cm⁵. Subjects with PH also needed to have had no changes within 2 months to medications approved for treatment of pulmonary hypertension, with stable New York Heart Association class of III-IV. Normal LV T₁ values were obtained from a healthy control (HC) group (n=21) from an ongoing study of heart failure with preserved ejection fraction (Alberta Heart Failure Etiology and Analysis Research Team [HEART]),(143) who were recruited from the region around Edmonton, Alberta, between January 2010 and October 2014. Healthy controls had no evidence of heart disease or significant cardiovascular risk factors, including coronary artery disease, hypertension, diabetes mellitus, inflammatory or autoimmune diseases, and could not be on any cardiac medication or have contraindication to CMR. The studies were approved by the University of Alberta and University of Calgary health research ethics boards. Informed written consent was obtained from all subjects.

5.2.2 CMR Imaging

CMR was performed on 1.5T systems (Siemens Sonata or Avanto, Siemens Medical Solutions, Erlangen, Germany). Short- and long-axis ventricular cines were performed using balanced steady-state free precession (bSSFP) imaging. Typical scan parameters were 1.24 ms echo time, 2.48 ms repetition time, 51° flip angle, 8 mm slice thickness, 2 mm gap, 400×275 mm field of view, 256×132 acquisition matrix, 75% phase resolution, 14 views per segment, rate 2 parallel imaging (GRAPPA), and 30 reconstructed cardiac phases. T₁-mapping was performed on a mid-ventricular short-axis slice during diastasis using the SATuration-recovery single-SHot Acquisition (SASHA) pulse sequence with a bSSFP readout, as previously described.(51, 73) Typical SASHA parameters were 1.36 ms echo time, 2.72 ms repetition time, 70° flip angle, 9 images spanning 100–650 ms saturation recovery times plus a non-saturated image, 8 mm slice thickness, 360×270 mm field of view, 192×108 acquisition matrix before interpolation, and 75% phase resolution. Acquired in-plane spatial resolution was 1.9 mm, and was interpolated to 0.94 mm for analysis. Either rate 2 parallel imaging (GRAPPA) or 6/8 partial Fourier was used for image acceleration. A phase sensitive inversion recovery sequence was used for conventional late gadolinium enhancement (LGE) imaging, typically starting 7 minutes following gadolinium-based contrast injection, with coverage matching cine locations. Typical LGE parameters were 4.18 ms echo time, 25° flip angle, 8 mm slice thickness, 380×285 mm field of view, 256×173 acquisition matrix, 90% phase resolution, and 25 views per segment. Subjects with AFD, along with healthy controls, received 0.15 mmol/kg gadobutrol (Gadovist; Bayer HealthCare Pharmaceuticals,

Montville, NJ), while subjects with PH received 0.1 mmol/kg gadolinium-diethylenetriaminepentaacetic acid (Gd-DTPA, Magnevist; Bayer Healthcare, Toronto, Canada).

5.2.3 Data Analysis

Manual endocardial tracing of both ventricles was performed for quantification of ventricular end-systolic volume and end-diastolic volume. Ejection fraction was calculated as $(\text{end-diastolic volume} - \text{end-systolic volume}) / \text{end-diastolic volume}$. Manual epicardial tracing of the left ventricle, excluding papillary muscles, was performed for quantification of ventricular mass, calculated as the ventricular muscle volume corrected for specific gravity of the tissue (1.05 g/mL). Masses and volumes were indexed to body surface area.

Late gadolinium enhancement images were assessed for the presence of positive enhancement, with specific assessment of the interventricular septum, inferior RV wall, inferior LV wall, and the inferior RV insertion point at the slice location nearest to the corresponding T₁-mapping images. Additional LGE short and long axis slices were used to corroborate the presence or absence of positive enhancement in these locations of interest. Nine subjects with Anderson-Fabry disease did not receive gadolinium contrast, either due to research protocol (n=8) or renal dysfunction (n=1).

Inferior RV wall thickness (RVI thickness), interventricular septal wall thickness (IVS thickness), and inferior LV wall thickness (LVI thickness) was measured in all subjects at a diastasis cardiac phase on short-axis cine images (Figure 5.1), for a slice location matching the T₁-mapping slice location. In subjects with AFD or PH, a minimum RVI of 4 mm was selected as an inclusion criterion for further analysis. This RVI thickness was selected for the T₁-mapping data to mitigate potential partial volume contamination of myocardial tissue T₁ values from neighbouring epicardial fat and/or blood pool pixels, based on a typical non-interpolated in plane resolution of approximately 1.9 mm. As healthy individuals were not expected to have increased RV wall thickness, their LV T₁-mapping data was included if the septal or inferior LV wall thickness was at least 4 mm.

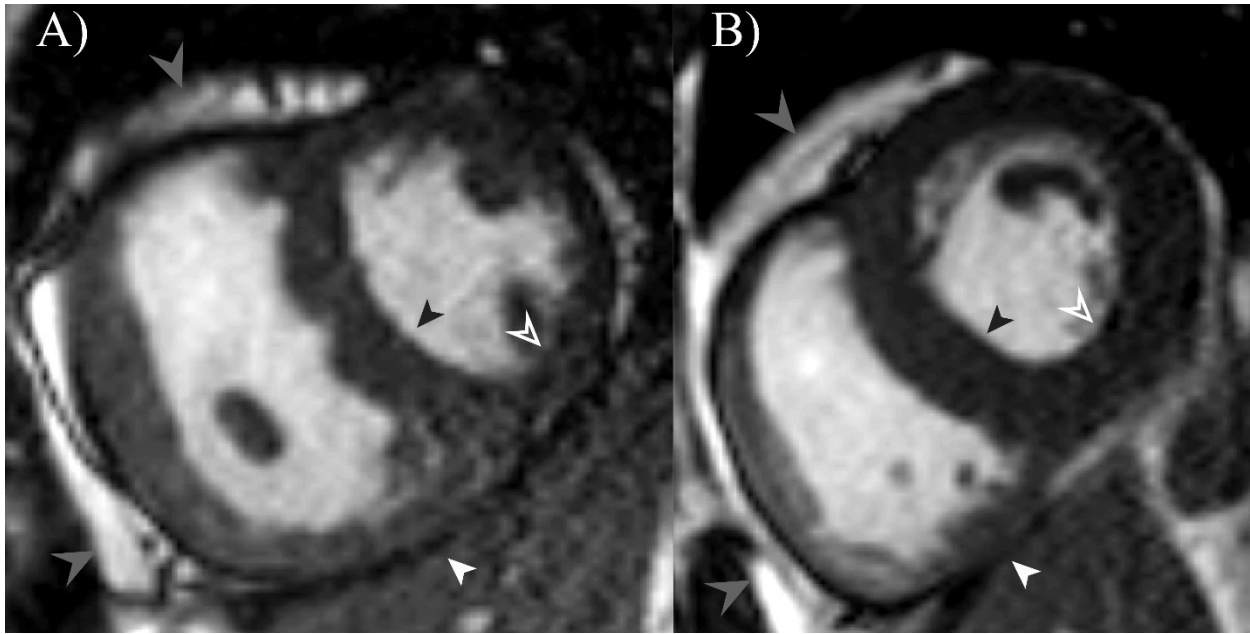


Figure 5.1: Example of bSSFP cine images in diastole used for wall thickness measurements. Measurement locations are shown at the inferior RV wall (RVI thickness, white arrowhead), interventricular septum (IVS thickness, black arrowhead), and inferior LV wall (LVI thickness, open arrowhead) for a subject with pulmonary hypertension (A) and Anderson-Fabry disease (B). Light grey arrows show areas of RV epicardial fat. Note the absence of readily visible epicardial fat along the inferior RV wall.

In all healthy controls, along with subjects with AFD or PH who met the criteria for minimum inferior RV wall thickness of 4 mm, the 10 images in the T_1 -mapping acquisition were registered to correct for in-plane motion occurring during the breath-hold.(51, 182) Region of interest (ROI) tracing was then completed on the inferior RV wall, interventricular septum, and inferior LV wall with sample ROI placements shown in Figure 5.2. Care was taken to minimize potential contamination by blood or epicardial fat by avoiding the endocardial and epicardial borders, as well as avoiding the RV insertion point where positive LGE is commonly observed, particularly in PH.(183) Manual adjustment of ROI placement on the 10 images was performed if residual motion was noted following image registration. Signal intensities within ROIs were averaged prior to fitting a 3-parameter mono-exponential recovery curve, $S(TS) = k(1 - \eta \exp(-TS/T_1))$, where k denotes a scaling constant, η represents the saturation efficiency, TS represents the saturation recovery time, and T_1 represents the longitudinal relaxation time. For the assessment of reproducibility, analysis was performed on each subject twice, independently by two observers (JP and RBT). Subjects' images were loaded randomly, with blinding between repeated

observations and observers. T_1 analysis was performed offline using custom software (MATLAB R2012a, The MathWorks, Natick, MA, USA).

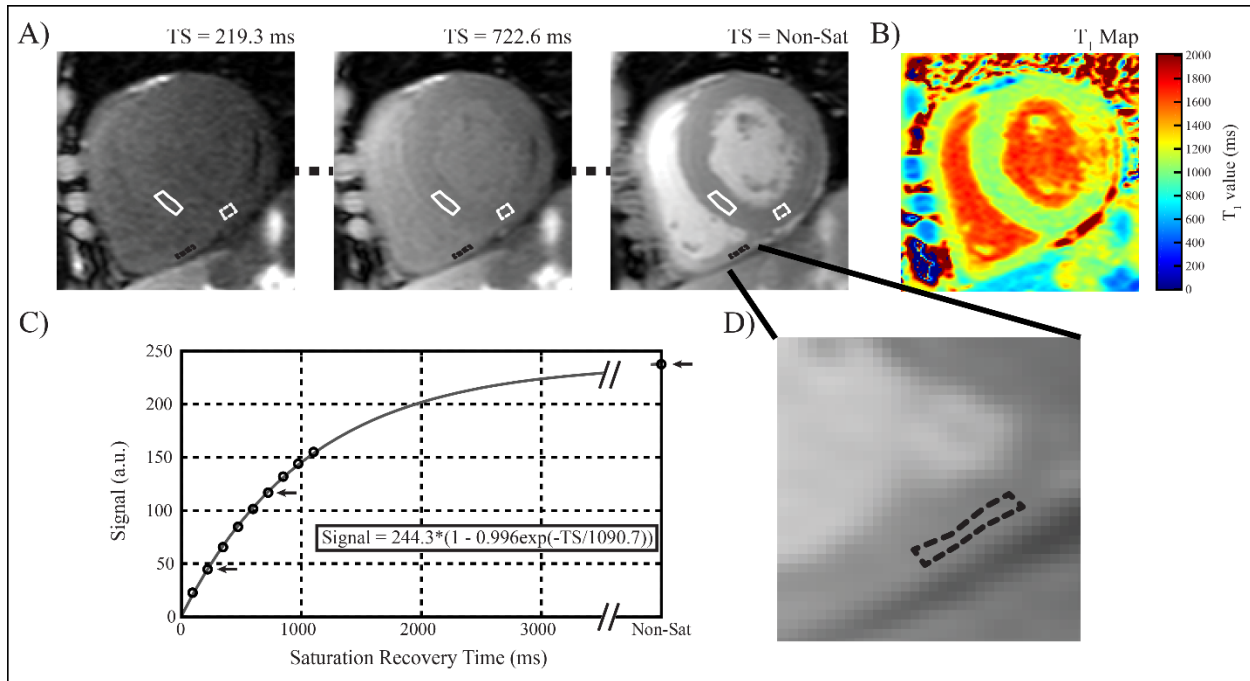


Figure 5.2: Example SASHA T_1 -mapping case. A) Sample SASHA T_1 -mapping images in a subject with Anderson-Fabry disease, showing septal (solid white), inferior right ventricle (dashed black), and inferior left ventricle (dashed white) regions of interest (ROI). B) Sample T_1 map is shown. C) Mean signal intensity from the right ventricle ROI from this subject are plotted with the corresponding saturation recovery time (TS), along with a best-fit saturation recovery curve defined by the displayed equation. Black arrows indicate the saturation recovery images shown in A). D) A zoomed in portion showing the inferior RV wall, along with the corresponding ROI. Note the absence of visible pericardial fat in this location. The dark signal in the left ventricle lateral wall is a site of positive late gadolinium enhancement.

5.2.4 Statistical Analysis

Subject characteristics and CMR variables, including wall thickness and ventricular T_1 values are presented as mean \pm standard deviation. Group differences, except with respect to sex, were compared using Kruskal-Wallis One-Way ANOVA, with multiple pair-wise comparisons performed using the Mann-Whitney U Test. Sex-related differences between groups were compared using Chi-squared analysis. Ventricular T_1 values within subjects were compared using the Friedman test, with multiple pair-wise comparisons performed using the Wilcoxon signed rank test. Reliability was measured using Coefficient of Variation (CoV), defined as the standard deviation of the differences between repeated measurements divided by the measurement mean. Significance was set at $p < 0.05$, with a Bonferroni correction where applicable. Statistical analysis

was performed using STATA statistical software (Version 11.2, Stata Corporation, College Station, TX, USA).

5.3 Results

Of the subjects included initially in the study, 6 subjects with AFD, 7 subjects with PH, and 0 healthy controls had inferior RVI thickness ≥ 4 mm and were therefore included for further T₁-mapping analysis. One subject with PH had unanalyzable T₁ datasets due to significant image artifact and was excluded and two HC subjects LVI T₁ values were excluded due to LVI thickness < 4 mm. The characteristics of those included in T₁ analysis are included in Table 5.1. Four of the six subjects with AFD were on enzyme replacement therapy, for a minimum of 4 years. Values derived from CMR scans are presented in Table 5.2. The average RVI thickness was not different between those with AFD and PH, but was thinner in HC than both AFD and PH (adjusted $p < 0.05$, respectively). The average LVI thickness was larger in those with AFD compared to both PH and HC (adjusted $p < 0.05$, respectively), while the IVS thickness was different between all groups, with the largest in AFD and the thinnest in HC (adjusted $p < 0.05$ for all comparisons).

Table 5.1: Subject characteristics

	AFD (n=6)	PH (n=6)	HC (n=21)
Age (yrs)	46.7±8.1	49.7±17.6	40.5±15.9
Sex (M)	4	1	10
Weight (kg)	74.9±18.0	84.4±20.8	70.5±15.9
Height (m)	1.7±0.1	1.7±0.1	1.7±0.1
BSA (m ²)	1.9±0.3	2.0±0.3	1.8±0.2
BMI (kg/m ²)	25.1±5.5	29.8±6.0	24.8±5.4
HR (bpm)	65.8±12.8	78.0±14.1	64.7±7.2

AFD = Anderson-Fabry disease; PH = pulmonary hypertension; HC = healthy control; BSA = body surface area; BMI = body mass index; HR = heart rate; bpm = beats per minute

* $p < 0.05$ compared to HC, † $p < 0.05$ AFD vs. PH

Table 5.2: CMR variables

	AFD (n=6)	PH (n=6)	HC (n=21)
IVS thickness (mm)	13±2*, †	10±1*	8±2
LVI thickness (mm)	10±3*, †	5±1	6±1
LV mass (g/m ²)	97.7±32.9*, †	50.8±4.0	58.2±12.4
LV EF (%)	67.5±7.4	63.0±7.1	62.2±5.3
LVEDVi (mL/m ²)	81.7±14.7†	57.0±8.5*	77.2±15.6
LVESVi (mL/m ²)	26.2±6.1	21.2±5.8	29.3±8.0
IVS-T ₁ (ms)	1053±41*, †	1280±123	1180±60
LVI-T ₁ (ms)	1072±44*, †	1274±57*	1183±45
RVI thickness (mm)	5±1*	6±2*	2±0
RV EF (%)	69.3±8.3†	37.8±6.9*	58.1±7.3
RVEDVi (mL/m ²)	71.0±18.2	123.3±47.9*	76.7±20.7
RVESVi (mL/m ²)	22.5±9.3†	79.0±37.3*	32.6±11.9
RVI-T ₁ (ms)	1096±49†	1239±41	

AFD = Anderson-Fabry disease; PH = pulmonary hypertension; HC = healthy control; RVI = inferior right ventricle wall; IVS = interventricular septum; LVI = inferior left ventricular wall; EF = ejection fraction; LVEDVi = left ventricular end-diastolic volume indexed; LVESVi = left ventricular end-systolic volume indexed; RVI = inferior right ventricular wall; RVEDVi = right ventricular end-diastolic volume indexed; RVESVi = right ventricular end-systolic volume indexed

*p<0.05 compared to HC, †p<0.05 AFD vs. PH

As shown in Table 5.2, irrespective of ventricular location, myocardial T₁ is shorter in subjects with AFD (RVI-T₁=1096±49 ms, IVS-T₁=1053±41 ms, LVI-T₁=1072±44 ms) compared to those with PH (RVI-T₁=1239±41 ms, IVS-T₁=1280±123 ms, LVI-T₁=1274±57 ms) and HC (IVS-T₁=1180±60 ms, LVI-T₁=1183±45 ms) (adjusted p<0.05 for all comparisons). Subjects with PH had longer LVI-T₁ than HC (adjusted p=0.02), but the IVS-T₁ was not statistically different (adjusted p=0.24), with a wide range of values (1140 to 1477 ms). T₁ values for all groups are shown in Figure 5.3.

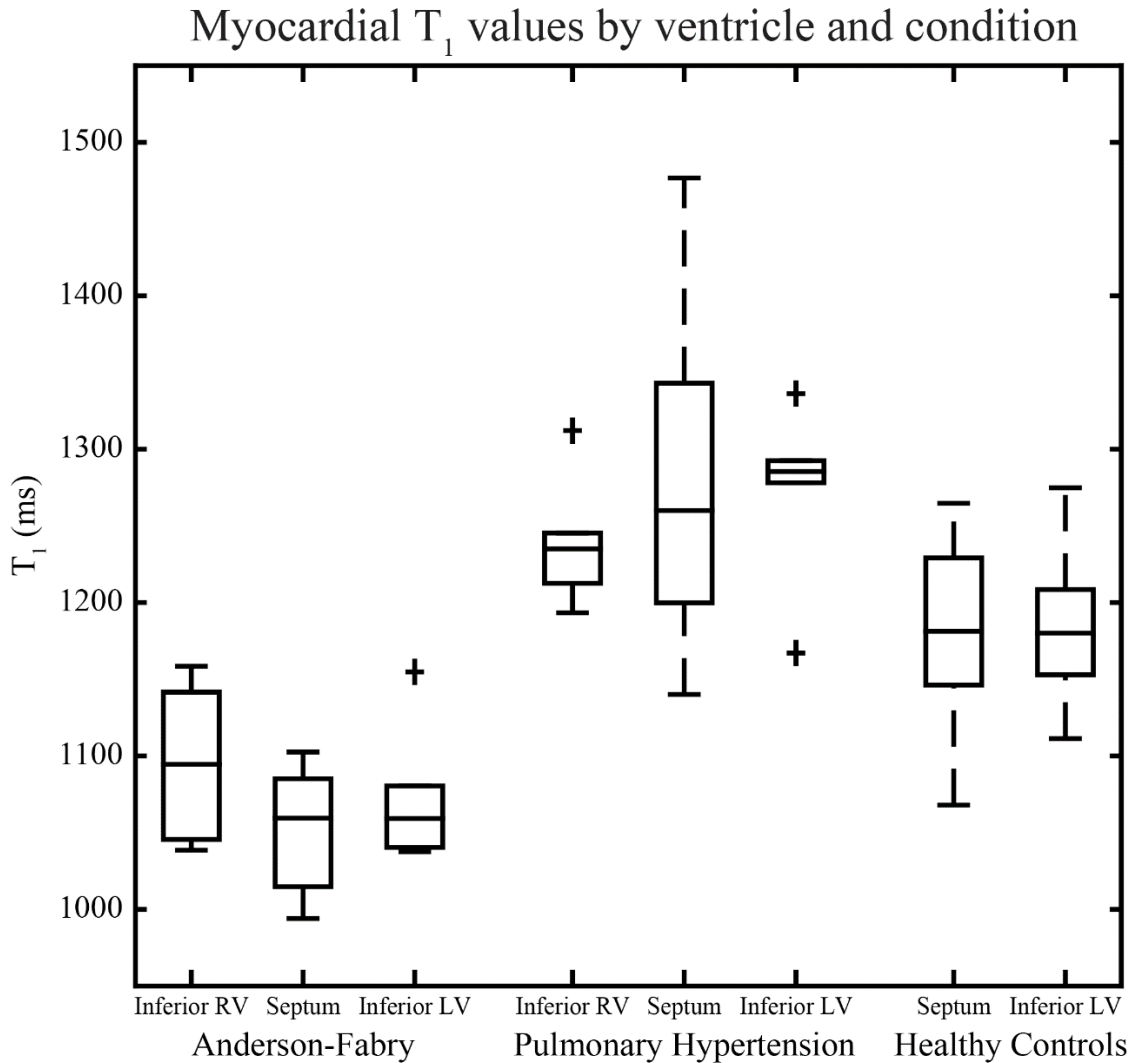


Figure 5.3: Myocardial T_1 values by ventricle and condition. Data is presented as boxes representing the 25th, 50th, and 75th percentiles, and fences representing $1.5\times$ interquartile range.

Comparing regions in subjects with AFD, T_1 values were not statistically different between the two LV and RV locations ($p=0.31$). Similarly, subjects with PH also showed non-significant differences between regional ventricular T_1 values ($p=0.51$).

In subjects with AFD, the IVS and LVI T_1 values were non-significantly shorter in those with thicker RV walls compared to those without (IVS- T_1 : 1053 ± 41 ms vs. 1112 ± 64 ms respectively, adjusted $p=0.2352$; LVI- T_1 : 1072 ± 44 ms vs. 1105 ± 76 ms respectively, adjusted $p=1$). Compared to healthy controls, the septal and inferior T_1 values remain statistically reduced irrespective of the presence or absence of increased RVI thickness (adjusted $p<0.05$ for all

comparisons). In subjects with PH, the septal and inferior LV T₁ values were not statistically different in those with thicker RV walls compared to those without (IVS-T₁: 1280±123 ms vs. 1258±60 ms respectively, adjusted p=1; LVI-T₁: 1274±57 ms vs. 1343±74 ms respectively, adjusted p=1). Compared to healthy controls, the inferior T₁ values remain statistically larger irrespective of the presence or absence of increased RVI thickness (adjusted p<0.05 for all comparisons), however septal T₁ values are no longer statistically different (adjusted p>0.05 for all comparisons).

Of the subjects with AFD who received contrast agents (n=3), none were positive for LGE in the inferior RV, septal, or inferior LV regions. One subject showed positive enhancement at the inferior RV insertion point. One subject with PH showed inferior RV wall enhancement, 2 showed septal enhancement, and 1 showed enhancement at the inferior LV. All subjects with PH showed enhancement at the inferior RV insertion point.

Coefficient of Variability (CoV) for the repeated analyses by observer 1 was 1.4%, 0.9%, and 1.5% for the RVI, IVS, and LVI, respectively. For observer 2, the CoV was 1.2%, 0.6%, and 2.7% for the RVI, IVS, and LVI, respectively. For interobserver agreement, the CoV was 1.7%, 1.5%, and 1.8% for the RVI, IVS, and LVI, respectively.

5.4 Discussion

The primary finding of the current study is the similar native T₁ values in the right and left ventricle of patients with AFD and thickened right ventricles, both of which are reduced in comparison to LV T₁ values in the healthy heart and as compared to patients with pulmonary hypertension. Reduced LV native T₁ values were reported previously in patients with AFD,(73, 74, 174) but this is the first report in the RV. Right ventricular involvement in subjects with AFD is common,(176-179) typically manifesting as hypertrophy and/or myocardial dysfunction, and the findings of the current study suggest that the underlying changes in tissue characteristics are also similar in both ventricles. Autopsies studies have shown biventricular cellular hypertrophy, vacuolization and sphingolipid accumulation,(180) thus the reduced RV T₁ values in the current study likely reflect the same pathology and mechanisms as within the LV.

The exact cause and mechanism of the reduced native T₁ in AFD values still requires further elucidation. Reduced LV T₁ values have also been seen in individuals with iron overload,(55) however this is unlikely the etiology in those with AFD. The effects of lipids on T₁-

mapping in general has not been systematically characterized, with one report of normal LV lipid content in AFD patients using ^1H NMR spectroscopy.(184) Interestingly, a mixed RV response has been seen with enzyme replacement therapy.(178, 179) In a study by Wuest et al., 14 patients with AFD who received enzyme replacement therapy for approximately 1 year showed beneficial effects for both ventricles, including a decrease in RV mass and end-diastolic volume.(179) However, a study by Niemann et al. of 57 patients with AFD treated with enzyme replacement therapy for more than 3 years showed no decrease in RV wall thickness or end-diastolic dimension.(178) This suggests there may be additional factors involved in the development of RV hypertrophy in addition to deposition of sphingolipids or that therapy is less effective in the RV. The T_1 differences noted in this study between AFD and PH suggests different origins of RV thickening between the conditions, indicating that RV thickening in AFD is not primarily related to increased RV afterload. Larger, and ideally longitudinal, studies including T_1 -mapping in the LV and RV would be useful in further elucidating the nature of RV involvement in subjects with AFD. Certainly, there is excitement in the community of the promise of T_1 -mapping, in either the LV or RV, to offer a potential biomarker to follow patients with AFD, particularly with respect to responses to enzyme replacement therapy.

In contrast, the increased native RV T_1 values in PH (1239±41 ms versus 1096±49 ms in AFD) likely reflect fibrosis, or more specifically the increased water mobility associated with increased extracellular volume fraction, related to long standing pressure overload. In this study we also show that LV and RV native T_1 values appear to be increased in those with PH and thickened RVs as compared to healthy control LV T_1 values. There is limited existing literature to corroborate this finding, however a recent publication also showed increased native T_1 , along with extracellular volume fraction, in the RV of subjects with PH versus healthy controls.(181) Elevated native T_1 values have been demonstrated at the RV insertion points in an animal model of chronic pulmonary hypertension,(185) though septal values were not statistically different than controls. Our septal native T_1 values were increased, though not statistically, likely reflecting pathological remodelling including a degree of interstitial and replacement fibrosis, evident by cases with positive late enhancement and reduced RV ejection fraction.

Quantitative T_1 -mapping, using native T_1 values, has been used for non-invasive tissue characterization in a variety of disease conditions(66, 67, 175); however, its use has generally been restricted to the left ventricle due in part to the limitations of spatial resolution. T_1 -mapping

sequences typically have an in-plane spatial resolution of approximately 2 mm, thus making it difficult to apply in the right ventricle, where, in normal hearts the mean diastolic wall thickness of the RV is $\leq 4\text{-}5$ mm,(186, 187) compared to 6-10 mm for the interventricular septum.(187) The most relevant data comes from studies by Mehta et al., using the accelerated and navigator-gated look-locker imaging for cardiac T_1 estimation (ANGIE) technique.(181, 188) Using this advanced technique, including optional fat-saturation, high-resolution RV T_1 -mapping was performed at end-systole, the authors found healthy control RV T_1 and extracellular volume fraction values are similar to those found in the LV. Unfortunately, the high-resolution ANGIE sequence takes much longer than standard T_1 -mapping sequences (~ 3 minutes vs. 9-17 heartbeats), may still be subject to partial volume contamination effects, and more practically is not yet widely available.

In the present study, the effects of partial volume contamination by either blood or epicardial fat was mitigated by selecting individuals with an increased RVI thickness, which is a cardinal feature of patients with Anderson-Fabry disease and pulmonary hypertension (5 ± 1 mm and 7 ± 2 mm, respectively, in the current study). Importantly, both patient groups' RVI thickness were similar to the inferior LV thickness of healthy controls (6 ± 1 mm), suggesting a similar small risk of partial volume contamination for parts of the LV. Subjects with PH were shown to have elevated T_1 values in the LV and RV, while those with Anderson-Fabry disease have T_1 values that are reduced in both ventricles. The primary technical concern with RV tissue characterization is systematic artifactual bias of these values from partial volume errors with epicardial fat or blood pool (which would be expected to decrease or increase T_1 values, respectively). The consistently increased native T_1 values in the PH group and reduced values in the AFD group, as compared to controls, and the excellent reproducibility of T_1 values by two observers in the blinded analysis suggest that partial volume errors did not confound the major findings of the current study. Nonetheless, in the absence of robust techniques to remove the signal from blood and fat, the potential for signal contamination remains.

5.4.1 Limitations

Our study is primarily limited by its small numbers and lack of normal RV T_1 values for comparison. However, Mehta et al., showed similar normal LV and RV native T_1 values using a high spatial resolution fat-suppressed method,(181, 188) suggesting our healthy control LV values may be used as a reference surrogate. Unfortunately, due to spatial and temporal resolution limitations of currently available T_1 -mapping methods, we limited our investigation to patients

with thickened RV walls and therefore were unable to study the RV of healthy volunteers. This fact also limits the generalizability of our findings to other patients with Anderson-Fabry disease or pulmonary hypertension without a thickened RV. Also, while the inferior RV wall was consistently the most clearly discernible location with least amount of trabeculation and epicardial fat content (as observed on bSSFP cines), leading to our decision to perform analysis in that location, performing analysis on a small region at a single slice location may not accurately represent the entire ventricle. There is currently no data to suggest that there are intrinsic differences in native T_1 values regionally within the RV.

Unfortunately, LGE imaging was not performed in all of the subjects with Anderson-Fabry disease so replacement fibrosis, and its potential to alter our reported T_1 values, could not be ruled out. Previous reports typically describe elevated native T_1 values in areas of positive LGE(73, 74, 174) where the basal inferolateral wall is most typically affected.(189-191) Thus, the reduced values seen in those with Anderson-Fabry disease in this study would not be typical if the ROI included a region with positive enhancement. However, we cannot rule out replacement fibrosis in other regions of the RV, where T_1 analysis was not performed. Due to the lack of contrast administration, we are also not able to provide extracellular volume fraction estimates, which require native and post-contrast T_1 measurement in the blood and tissue for calculation.

Further study, including clinical and function correlates, would add important diagnostic and prognostic significance to T_1 measurements, however without significant improvements to T_1 -mapping techniques, larger scale RV imaging studies are not feasible.

5.5 Conclusion

Though normal values for native T_1 in the RV are still unknown, native T_1 values appear similarly reduced in the left and right ventricles of individuals with AFD and right ventricular wall thickening, likely driven by the same pathological processes. In contrast, individuals with pulmonary hypertension and right ventricular wall thickening show increased native T_1 values in both the LV and RV, suggestive of fibrosis. While T_1 -mapping is emerging as a useful marker in the diagnosis and monitoring of numerous cardiac conditions, its use in the right ventricle remains a challenge given this ventricle's relative thinness and potential for blood pool or epicardial fat contamination.

Chapter 6

End-Systolic Imaging of Myocardial Extracellular Volume Fraction with Contrast Level Assessment using Intensity Ratios (CLAIR)

6.1 Introduction

Recent advancements in the development and application of contrast-enhanced quantitative myocardial T_1 -mapping have allowed for the quantitative evaluation of myocardial extracellular volume fraction (ECV) for the detection of diffuse myocardial fibrosis using cardiac magnetic resonance imaging (CMR).(80-82, 141) Measurement of ECV using CMR is based on the estimation of blood and tissue concentrations of injected gadolinium contrast agents using the known relationship between the longitudinal relaxation time constant (T_1) and contrast agent concentrations.(145, 192) However, T_1 -mapping acquisitions are typically limited in spatial resolution due to the need to acquire several T_1 -weighted images for T_1 -quantification, typically single-shot acquisitions, in the duration of a breath-hold. Importantly, motion during the relatively long single-shot image acquisition window may reduce the acquired spatial resolution, which is exacerbated with higher heart rates.(50)

Commonly used spatial resolutions of 1.4 to 2.3 mm for T_1 -mapping acquisitions, in combination with potential motion blurring effects, increase the possibility of partial volume effects(50) from neighboring epicardial fat and/or intraventricular blood, with no method to determine the magnitude of these effects in a given study, if present. Quantitative assessment of regional wall thickness in populations of healthy individuals using CMR have shown an average minimum thickness as low as 3.5 ± 1.0 mm in women and 4.1 ± 1.1 mm for men, for the inferolateral region of the left ventricle at the mid-ventricular level, with multiple regions averaging 4-5 mm.(193) In order to avoid potential bias of ECV values on partial volume effects, it is desirable to acquire images with increased resolution and reduced acquisition durations. It has been

proposed that acquisition during the end-systolic cardiac phase will mitigate partial volume errors due to increased wall thickness relative to the typically targeted diastasis cardiac phase.(194-196) However, this approach places higher demands on a shorter acquisition window due to the short duration of the end-systolic cardiac phase.

This study introduces an alternative method to traditional T₁-mapping based assessment of contrast agent concentration for estimation of ECV, with the aim of providing higher spatial resolution and a shorter acquisition window allowing for end-systolic imaging of the heart. The proposed method is based on signal intensity ratios between images acquired pre-contrast and post-contrast agent delivery, with the estimation of contrast agent concentration using Bloch equation derived look-up tables (CLAIR - Contrast Level Assessment using Intensity Ratios). The primary goal of the current study was to evaluate the accuracy of the CLAIR method using numerical simulations, phantom experiments, and in vivo experiments in individuals without significant cardiovascular disease.

6.2 Methods

6.2.1 Theory

Contrast Level Assessment using Intensity Ratios (CLAIR)

Myocardial ECV is estimated based on the ratio of contrast agent concentrations in the tissue and blood pool, referred to as the partition coefficient (λ), with a correction for hematocrit.

$$\lambda = \frac{[Gd]_{tissue}}{[Gd]_{blood}}$$

$$ECV = \lambda \times (1 - hematocrit)$$

The relaxivity equation describes the changes in T₁ and T₂ as a function of concentration of gadolinium contrast agent.

$$\frac{1}{T_{1Gd}} = \frac{1}{T_1} + r_1[Gd]$$

$$\frac{1}{T_{2Gd}} = \frac{1}{T_2} + r_2[Gd]$$

where [Gd] represents the concentration of the gadolinium-based contrast agent (mM), while r_1 and r_2 denote the contrast agent's proton relaxivity ($\text{mM}^{-1}\text{s}^{-1}$) for longitudinal and transverse magnetization, respectively.

It can be seen that measurement of T_1 values with and without gadolinium would allow for estimation of the contrast agent concentration, for example within the myocardial tissue.

$$[Gd]_{tissue} = r_1^{-1} \left[\frac{1}{T_{1Gd}} - \frac{1}{T_1} \right]_{tissue}$$

Considering an ideal saturation recovery image, the signal intensity (I) can be estimated.

$$I = M_0 \left(1 - e^{-\frac{TS}{T_1}} \right)$$

M_0 is the net magnetization at equilibrium and TS is the saturation recovery time.

The ratio between a pre- and post-contrast image can be calculated.

$$\frac{I_{Gd}}{I} = \frac{\left(1 - e^{-\frac{TS}{T_{1Gd}}} \right)}{\left(1 - e^{-\frac{TS}{T_1}} \right)}$$

Furthermore, it can be modified to incorporate the relaxivity equation.

$$\frac{I_{Gd}}{I} = \frac{\left(1 - e^{-TS\left(\frac{1}{T_1} + r_1[Gd]\right)} \right)}{\left(1 - e^{-\frac{TS}{T_1}} \right)}$$

Finally, it can be written in a modified format.

$$\frac{I_{Gd}}{I} = \frac{\left(1 - e^{-\frac{TS}{T_1}} e^{-TS r_1 [Gd]} \right)}{\left(1 - e^{-\frac{TS}{T_1}} \right)}$$

Therefore, the ratio between two images will be related to changes in T_1 , proportional to the amount of contrast agent present.

Given this, as an alternative to direct quantification of T_1 values, the change in signal intensity in T_1 -weighted images with contrast agent delivery is proposed as a method to estimate the contrast agent concentration, using a Bloch equation-based look-up table approach (CLAIR - Contrast Level Assessment using Intensity Ratios) to account for effects of the imaging readout on the expected signal. The proposed pulse sequence for the CLAIR method and the Bloch equation simulation approach are described below.

It is proposed that the relative change in myocardial signal intensity between pre-contrast and post-contrast scans will depend predominantly on the contrast agent concentration in the tissue, $[Gd]_{\text{tissue}}$, which can subsequently be used to estimate ECV, as shown above, utilizing $[Gd]_{\text{blood}}$ from conventional T_1 -mapping.

6.2.2 Pulse Sequence

In order to provide predominantly T_1 -weighting, as well as sufficient temporal resolution to capture the end-systolic cardiac phase, a saturation recovery gated-segmented balanced steady-state free-precession pulse sequence (bSSFP), similar to the previously published multi-contrast late enhancement (MCLE) sequence,(197, 198) was used. While the MCLE sequence uses an inversion preparation prior to a gated-segmented cine-acquisition, the CLAIR sequence uses an adiabatic non-slice selective BIR4 saturation pulse occurring at the time of the ECC trigger, to ensure predominantly T_1 -weighting in the acquired signal intensities, without dependence on magnetization history. Saturation-based imaging also increases scan efficiency as there is no requirement for full recovery of magnetization, as is the case for inversion-recovery imaging. A delay between the saturation pulse and the acquisition beginning near end-systole allows for pure T_1 -recovery prior to the onset of image acquisition (Figure 6.1). Imaging throughout this recovery interval prior to the frames of interest was avoided to minimize the number of radiofrequency (RF) pulses to center of k-space, as bSSFP signal intensities are a complex function of flip angle, T_1 and T_2 (approaching T_2/T_1 weighting with increasing number of RF pulses).(199) Additionally, potential effects of through-plane motion, which can increase signal intensities independently of T_1 recovery, were also minimized by limiting the number of RF pulses prior to the centre of k-space. To minimize artifacts arising from the approach to steady-state, linearly ramping the bSSFP flip angle for the first 13 RF pulses was performed. A segmented acquisition significantly reduced the acquisition window to mitigate motion effects at the targeted end-systolic cardiac phase and provided a cine time-series of images.

Numerical simulations, phantom, and in-vivo experiments used identical image acquisition parameters for pre-contrast and post-contrast agent acquisitions. Typical pulse sequence parameters were field-of-view = 340 x 340 mm, 8 mm slice thickness, echo time (TE) = 1.59 ms, repetition time (TR) = 3.18 ms, acquisition matrix = 256 x 192, phase resolution = 75%, views per segment = 13 (41.3 ms acquisition window per phase), linearly increasing RF pulses = 13, flip angle = 73°, pixel bandwidth = 890 Hz/pixel, a saturation recovery time (TS) = 300 ms, and a total acquisition time of 15 heartbeats. Typically, 6 images were reconstructed spanning end-systole to early-diastole, depending on the heart rate. Parallel imaging was not used but could be incorporated to reduce breath-hold durations.

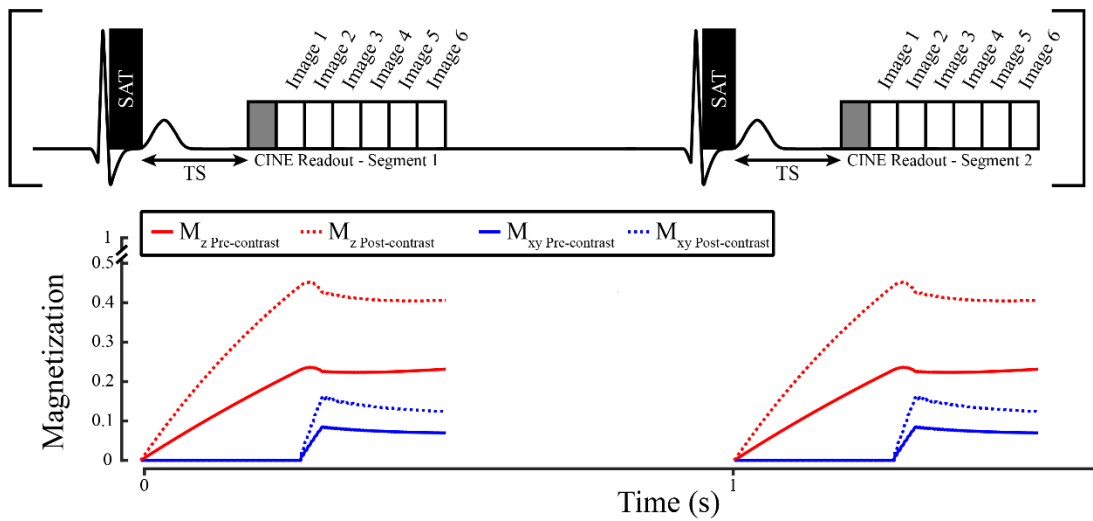


Figure 6.1: Schematic representation of the CLAIR pulse sequence, including simulation based plots of the magnetization (M_z – red; M_{xy} – blue) over the first 2 heartbeats, given a set of input parameters (T_1 1175 ms, T_2 50 ms, flip angle 73°, on resonance, B_1^+ scale 1, TE 1.59 ms, TR 3.18 ms, saturation recovery time (TS) 300 ms, saturation efficiency 100%, 13 view per segment). The post-contrast simulation uses a tissue [Gd] of 0.2 mM. The grey section in the cine readout reflects the ramped dummy pulses.

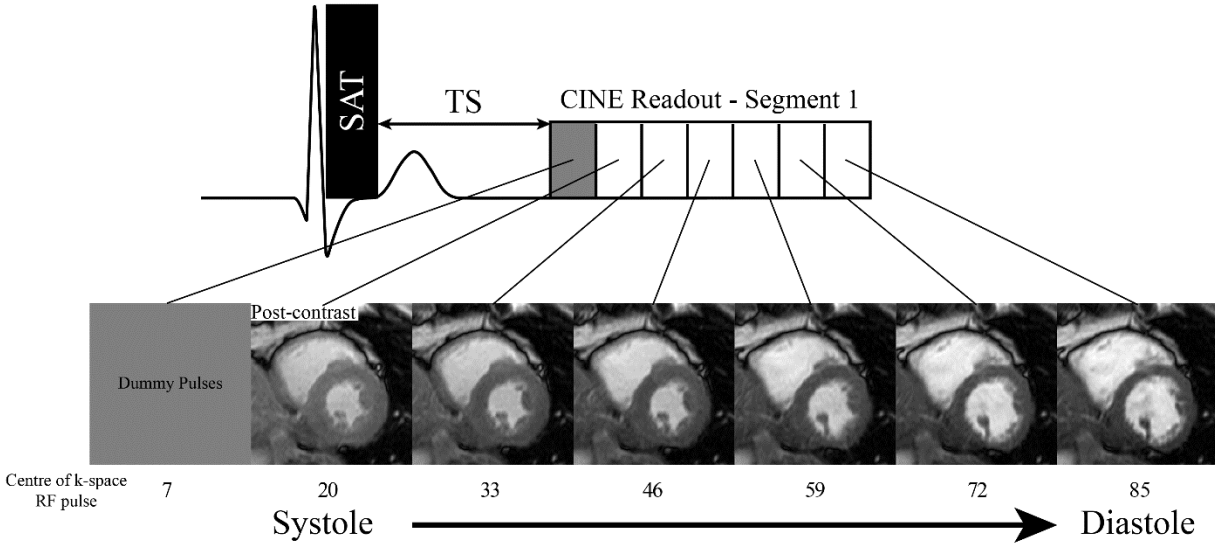


Figure 6.2: Schematic representation with example in vivo images, illustrating the initial acquisition at end-systole. Subsequent acquired segments correspond to images associated with progression through the cardiac cycle, from systole to diastole, with the typical radiofrequency (RF) pulse associated with the centre of k-space for the corresponding image, for the typical case of a 13 views per segment acquisition

6.2.3 Bloch Equations Simulations and Lookup Table Generation

Bloch equation simulations (custom software in MATLAB, The MathWorks, Natick, MA, United States) of the saturation-recovery bSSFP pulse sequence were used to generate a library of signal intensities for given input parameters including TE, TR, T_1 , T_2 , flip angle, excitation efficiency (B_1^+), off-resonance, saturation recovery time (TS), saturation pulse efficiency and contrast agent concentrations, along with their respective relaxivities, r_1 and r_2 . Simulations included the distribution of flip angles from the actual Sinc-Gaussian RF pulse (time-bandwidth product of 1.6), determined from Bloch-equation simulations of the excitation pulse waveform from the MRI scanner. As shown in Figure 6.1, the transverse (observable) and longitudinal magnetization are calculated continuously following saturation preparation, for a given contrast agent concentration. The signal intensity in each image phase (ex: images 1, 2, and 3 in Figure 6.1) was assumed to be equal to the transverse magnetization at the centre line of k-space. Other factors

that determine the acquired signal intensities such as spin density and receiver coil sensitivity are assumed to be unchanged between image acquisitions.

Lookup table simulations incorporated standard idealized input parameters, including an ideal saturation pulse efficiency of 100%, a homogeneous B_1^+ field, a spatially uniform static magnetic field (B_0) and non-contrast tissue T_1 values of 1175 ms and T_2 values of 50 ms. Evaluation of the effects of errors in these assumed input parameters was addressed using numerical simulations (below). A sample lookup table, relating the ratio of signals intensities and the corresponding tissue contrast agent concentration, using these assumed parameters, along with a 300 ms TS, and an r_1 of $5.3 \text{ mM}^{-1}\text{s}^{-1}$ is shown in Figure 6.3. Comprehensive numerical simulations were used to calculate the dependence of the lookup table on all pulse sequence and tissue parameters.

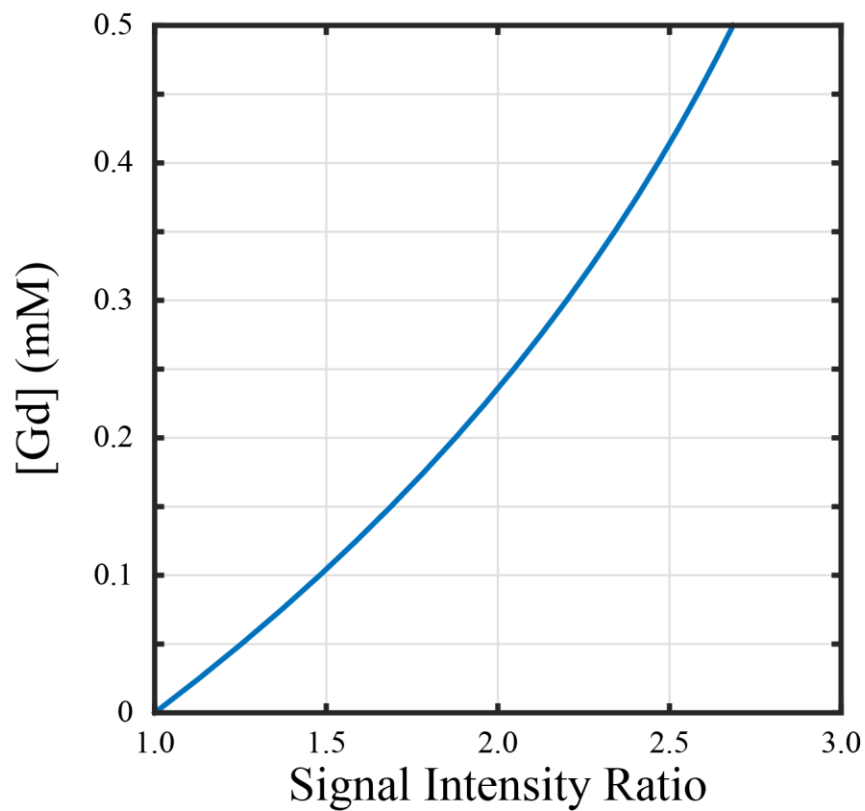


Figure 6.3: Sample lookup table, relating a signal intensity ratio of post- and pre-contrast images to the estimated tissue contrast agent concentration ($[Gd]$).

6.2.4 Numerical Simulations

Bloch equation simulations were performed to validate the proposed CLAIR approach, for the estimation of contrast agent concentrations based on ratios of signal intensities, and to evaluate the dependence of the CLAIR method on the parameters incorporated into the lookup table, including a range of T_1 (1000-1300 ms), T_2 (45-55 ms), B_1^+ (70-100% relative B_1^+), off-resonance (0-120 Hz), and saturation efficiencies (90-100%), based on the range of expected values.(113, 200) Specifically, the error in the lookup table-derived contrast agent concentrations was calculated as a function of error in the assumed input values for T_1 , T_2 , B_1^+ , off-resonance, and saturation efficiency. The proton relaxivities ($r_1 = 5.3 \text{ mM}^{-1}\text{s}^{-1}$ and $r_2 = 5.4 \text{ mM}^{-1}\text{s}^{-1}$) used were based on that of gadobutrol (Gadovist; Bayer HealthCare Pharmaceuticals, Montville, NJ) in blood at 1.5T.(Rohrer, Bauer et al. 2005) The range of [Gd] considered was limited to between 0.15-0.25 mM, in keeping with our typical in vivo tissue concentrations results. While the experiments typically considered the 20th RF pulse, corresponding to the first cardiac phase acquired, simulations were completed for 95 RF pulses following the 13 opening ramped pulses, to allow evaluation of the CLAIR method for several cardiac phases. The error in the [Gd] as a function of the RF pulse number was evaluated, considering cases of errors in assumed baseline T_1 or T_2 values and an input [Gd] of 0.2 mM.

6.2.5 Phantom Experiments

The accuracy of CLAIR for the assessment of contrast agent concentrations was evaluated in a series of identical NiCl_2 -doped agarose phantoms with a range of concentrations of gadobutrol (0-0.5 mM). A Siemens Sonata 1.5T scanner (Siemens Healthcare; Erlangen, Germany) was used for all experiments with a simulated heart rate of 60 bpm. CLAIR pulse sequence parameters were as described in the Pulse Sequence section above. An inversion recovery spin echo experiment was used to obtain the gold-standard measure phantom T_1 values and contrast agent concentration for comparison to CLAIR. Spin echo experiments with $\text{TR} = 10$ seconds were repeated with 11 inversion times (22-4000 ms). As the spin echo experiment is not feasible for in vivo studies, an accurate breath-hold duration T_1 -mapping sequence, SATuration-recovery single-SHot Acquisition (SASHA),(51) was also performed in phantoms. Imaging parameters: field-of-view = 360 x 270 mm, 8 mm slice thickness, $\text{TE} = 1.39$ ms, $\text{TR} = 2.78$ ms, acquisition matrix = 192 x 108, phase resolution = 75%, partial Fourier = 6/8, flip angle = 70° , pixel bandwidth = 1000 Hz/pixel. T_2

values were measured using a series of spin echo images, with a 90° flip angle, TR 6000 ms, and 7 TE times (8.3 – 400 ms). For CLAIR and SASHA, all phantoms were imaged individually using a small flex loop coil, to ensure similar B_1^+ and B_0 values for all samples.

Linear regression was used to derive the r_1 and r_2 for gadobutrol in the phantoms, based on the prepared [Gd] along with the measured T_1 and T_2 values from the spin echo experiments.(201) For the phantom experiments, these relaxivities were used in the calculations of contrast agent concentrations in each phantom for the spin echo and SASHA sequences, and in the derivation of the CLAIR lookup table. The CLAIR lookup table also used the T_1 and T_2 spin echo values for the phantom without contrast agent as the assumed native T_1 and T_2 values.

The mean signal intensities from a single region of interest (ROI) drawn in the centre of each phantom was used for analysis.

6.2.6 In Vivo Experiments

Twelve patients, from an ongoing clinical study of heart failure (Alberta HEART, Alberta Heart Failure Etiology and Analysis Research Team(143)) were included in the CLAIR study. Participants were free from known coronary artery disease and heart failure, with no evidence of scar on late gadolinium enhancement imaging. Imaging was performed on the same Siemens Sonata as the phantom experiments, using a body transmit coil and surface receive coils. Subjects underwent a comprehensive CMR examination, including standard bSSFP cine imaging for volumetric analysis, and phase sensitive inversion recovery imaging for qualitative scar assessment. T_1 -mapping using SASHA was performed at a basal and mid-ventricular short axis slice location, during end-diastole, while CLAIR was prescribed at end-systole, at a single slice location. The selection of TS for acquisitions starting at end-systole was based on the four-chamber cine acquired earlier in the scan. Typically, the SASHA mid-ventricular slice location was copied for the CLAIR acquisition at end-systole, but the slice-location would generally fall between the basal and mid diastolic slices, depending on the amount of systolic annular excursion. Acquisition parameters were as described above, with field-of-view adjustments based on body habitus. Post-contrast imaging was performed starting approximately 15 minutes after administration of 0.15 mmol/kg gadobutrol. All patients provided written informed consent with approval from the University of Alberta Health Research Ethics Board.

6.2.7 In Vivo Image Analysis

All SASHA and CLAIR image analysis was performed offline by a single individual (JP) using MATLAB. T_1 weighted images from SASHA were registered using non-rigid motion correction,(51, 182) independently for each slice, as well as separately for pre- and post-contrast acquisitions. For both SASHA and CLAIR analysis, a single ROI was drawn on the interventricular septum on T_1 weighted images. The ROI was defined by a line drawn along the mid-line of the septum that was expanded in the radial dimension to define a region with a uniform thickness of 2 mm. Regions were copied between pre- and post-contrast acquisitions, for a given slice, to eliminate ROI size variability. Manual ROI adjustments were performed as needed to account for discrepancies in breath-hold location, cardiac phase differences, or if residual motion was present despite motion correction (SASHA acquisition). Only the first cardiac phase of the CLAIR data, at end-systole, was considered for comparison with SASHA, however all phases were analyzed to evaluate the dependency of the error in [Gd] as a function of cardiac phase. Figure 6.4 illustrates sample pre- and post-contrast T_1 weighted in-vivo images from CLAIR.

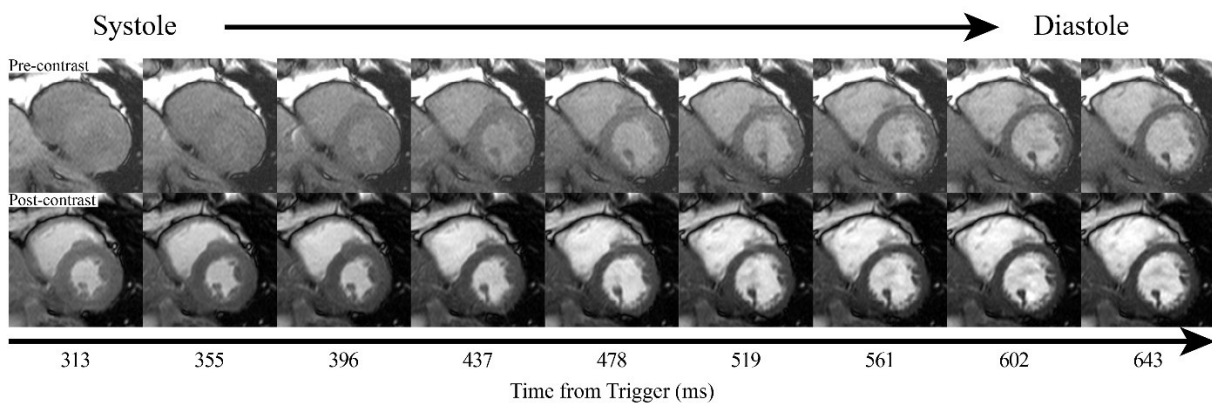


Figure 6.4: Example pre- and post-contrast CLAIR images illustrating the acquisition of multiple images over the cardiac cycle.

Analysis of the SASHA data also included a single ROI placed within the blood pool of the left ventricular cavity for blood pool pre- and post-contrast T_1 measurements, for the measurement of blood [Gd]. For the in vivo experiment calculations, the proton relaxivities of gadobutrol in blood ($r_1 = 5.3 \text{ mM}\cdot\text{s}^{-1}$ and $r_2 = 5.4 \text{ mM}\cdot\text{s}^{-1}$) were used for all cases.(202) Derivation of the CLAIR lookup table, performed on a per subject basis, also used patient specific acquisition parameters (TE, TR, flip angle, TS time, views per segment, and number of linearly increasing

initial RF pulses), along with an assumed pre-contrast T_1 of 1175 ms, T_2 of 50 ms, on-resonance, B_1^+ scale of 100%, and 100% saturation efficiency.

In addition to $[Gd]$, both λ and extracellular volume fraction were calculated in all subjects, as described in the Theory section. Specifically, measurements of $[Gd]_{\text{tissue}}$ were performed with CLAIR and SASHA, while $[Gd]_{\text{blood}}$ was measured with SASHA. T_1 and $[Gd]$ calculations were all performed using averaged ROI signal intensities from the T_1 -weighted images for both CLAIR and SASHA.

For demonstrative purposes, parametric maps were created for both sequences. For the SASHA acquisitions, T_1 maps were created at both slice locations based on registered T_1 weighted images, for pre- and post-contrast times. For a given slice location, the pre- and post-contrast T_1 maps were then registered and used to create λ and ECV maps. Non-rigid motion correction was also performed for the CLAIR pre- and post-contrast images to create a signal intensity ratio and $[Gd]_{\text{tissue}}$ map, and subsequently maps for λ and ECV using the average $[Gd]_{\text{blood}}$ from the basal and mid SASHA slices. An example is provided in Figure 6.5.

SASHA - mid

CLAIR

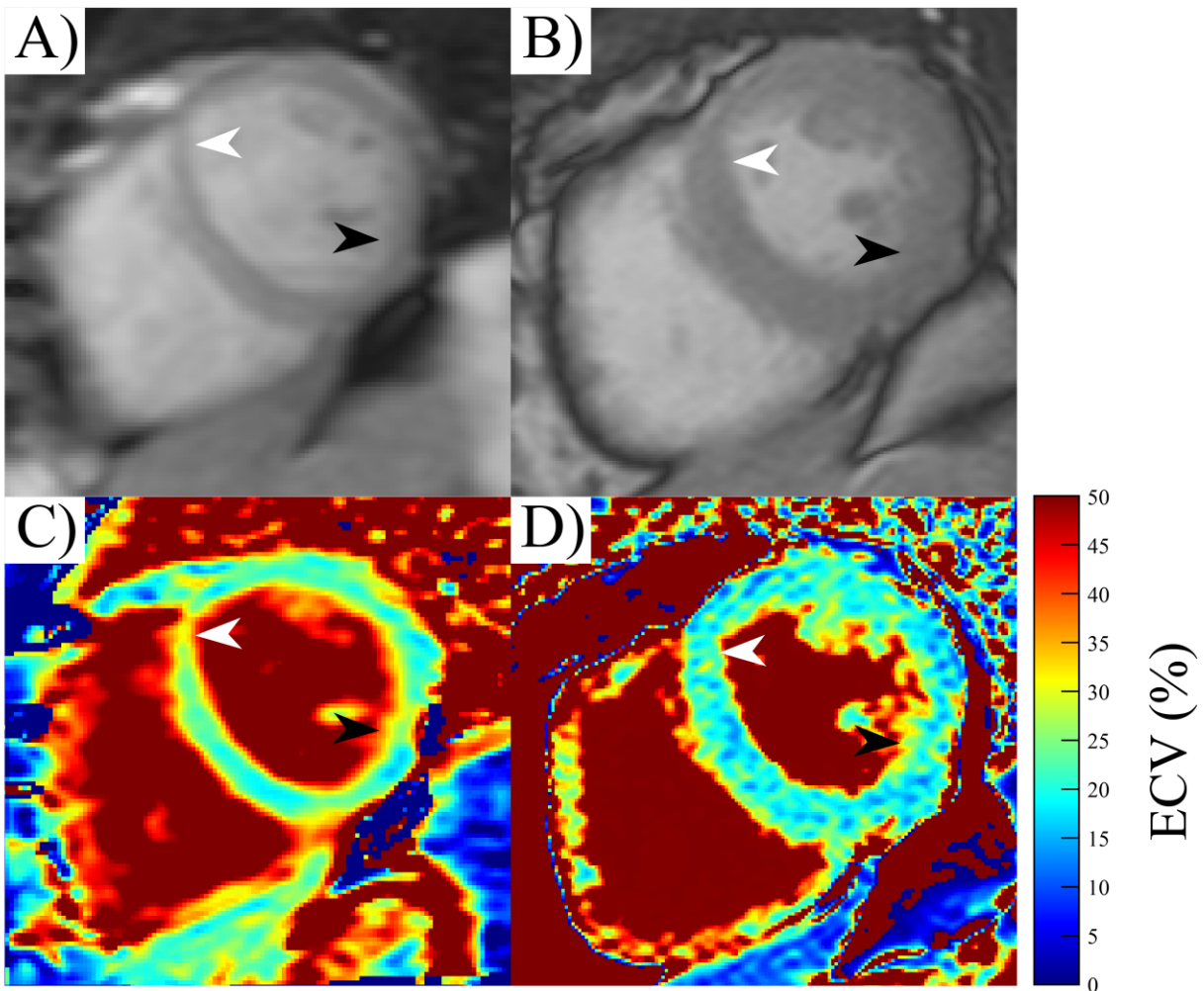


Figure 6.5: Example SASHA and CLAIR images. Upper panel demonstrates post-contrast T_1 weighted images, with the fully recovered SASHA images displayed. The lower panel demonstrates the corresponding ECV maps. Arrowheads note areas of thin myocardium that are better resolved on the systolic CLAIR images.

For both SASHA and CLAIR acquisitions, the number of interpolated pixels over the mid-ventricular septum was calculated based on the full-width half-maximum signal intensity profile across the septum.

6.2.8 Statistics

Data are presented as mean±standard deviation, or count (%), where applicable. SASHA values presented represent averages over both slices. Comparison of paired data for more than 2 groups was performed using the Friedman test. Comparison of paired data for 2 groups, including any pairwise comparison, was performed using the Wilcoxon Signed Rank test, with Bonferroni adjustment of p-values where applicable. Correlation between SASHA and CLAIR was assessed using linear regression. Significance was set at $p < 0.05$. Statistical analysis was performed using Stata statistical software (Version 11.2, Stata Corporation, College Station, TX, USA).

6.3 Results

6.3.1 Simulations

The results of the simulations of the CLAIR sequence revealed small errors in estimated [Gd] due to errors in the assumed input baseline $T_2 = 50$ ms ($< 0.05\%$ error in [Gd] for T_2 between 45-55ms), B_1^+ scale = 1.0 ($< 0.15\%$ error in [Gd] for B_1^+ scale between 0.7-1.0), and off-resonance = 0 Hz ($< 1\%$ error in [Gd] for 0-120 Hz). The errors in [Gd] derived from the lookup table are approximately 6% per 50 ms error in the real native T_1 value from the assumed input value of 1175 ms (Figure 6.6a). Importantly, there is a positive bias in [Gd], and thus a positive bias ECV, for the case of true native T_1 values that are greater than the assume value of 1175 ms. Thus, pathology associated with increased native T_1 values will also increase the derived ECV values using the CLAIR approach. Smaller errors in [Gd], of approximately 1% per 1% error in saturation efficiency, were also noted (Figure 6.6b). The effect of the readout on the error in estimated [Gd] is demonstrated in Figure 6.7, showing increasing error with additional RF pulses, as a function of errors in assumed native T_2 or T_1 , where errors are defined as true value minus assumed values of $T_2 = 50$ ms and $T_1 = 1175$ ms, for myocardium at 1.5T.

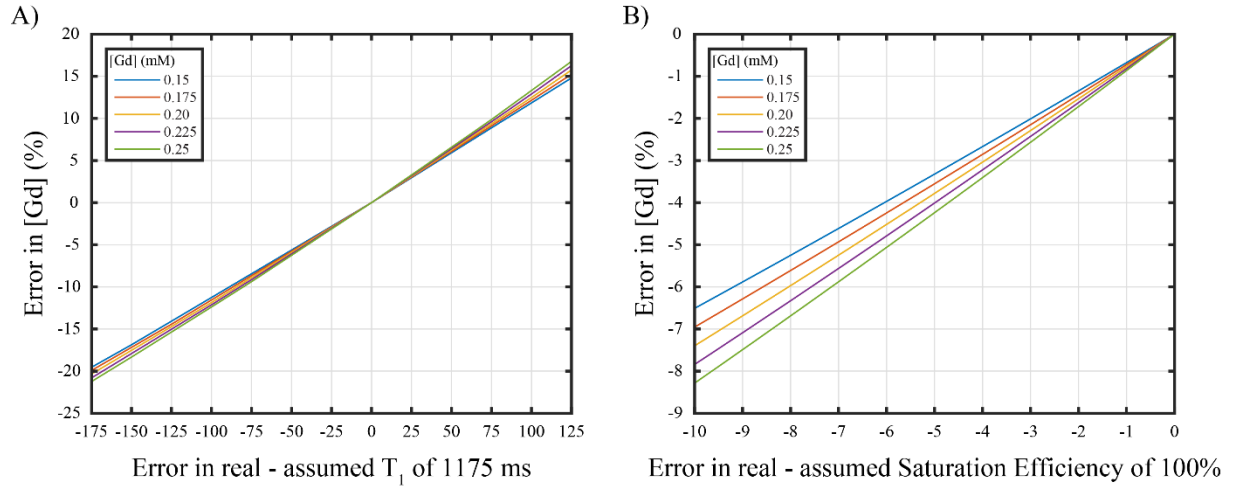


Figure 6.6: Simulation derived errors in estimated [Gd] as a function of errors in assumptions used in the lookup table derivation for A) T₁ and B) saturation efficiency, shown for different estimated [Gd] values.

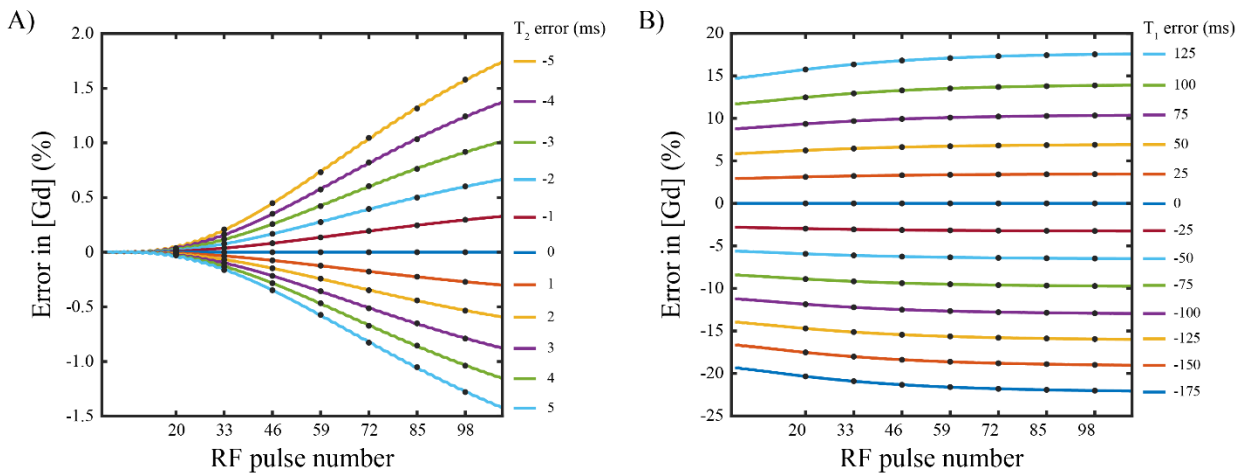


Figure 6.7: Simulation experiments showing an increase in error in contrast agent estimation as a function of radiofrequency (RF) pulse number, including the dummy pulses. A) Errors in assumed T₂ and B) errors in assumed T₁ in the CLAIR lookup table, considering an input [Gd] of 0.2 mM. Black dots represent typical centre lines of k-space for a 13 views per segment acquisition. Errors are defined as true value minus assumed values of T₂ = 50 ms and T₁ = 1175 ms, for myocardium at 1.5T.

6.3.2 Phantom Experiments

The T₁, T₂, and calculated [Gd] values for the phantoms are shown in Table 6.1. Relaxivities for T₁ and T₂ for the phantoms were derived based on the known [Gd] in each phantom and the measured spin echo changes in T₁ and T₂ with increasing [Gd],(201) with best-fit values of 6.2 and 7.3 mM⁻¹·s⁻¹, respectively. T₁ values from SASHA were systematically lower than those

from spin echo (p-value = 0.02), by an average of only 9 ms. Both SASHA and CLAIR showed mild non-significantly increased estimated [Gd] compared to spin echo values (adjusted p-value = 0.08, for both cases), with an average difference of approximately 4.3% and 6.2% respectively. Similarly, there is a non-significant increase of estimated [Gd] between SASHA and CLAIR (adjusted p-value = 0.08), with an average difference of approximately 1.8%. Figure 6.8 shows an increase in this average error in contrast agent estimation, between CLAIR and SASHA, for the phantoms as a function of the cine readout.

Table 6.1: T₁, T₂, and Calculated [Gd] values for the agarose phantoms

Phantom	Expected [Gd] (mM)	Spin Echo			SASHA		CLAIR
		T ₂ (ms)	T ₁ (ms)	[Gd] (mM)	T ₁ (ms)	[Gd] (mM)	[Gd] (mM)
1	0	44.7	1105	-	1105	-	-
2	0.05	44.0	797	0.057	786	0.059	0.060
3	0.1	43.5	643	0.105	633	0.109	0.112
4	0.15	41.6	530	0.159	518	0.165	0.167
5	0.2	41.7	450	0.213	440	0.221	0.226
6	0.25	41.4	396	0.262	386	0.272	0.280
7	0.5	38.4	249	0.501	240	0.526	0.529

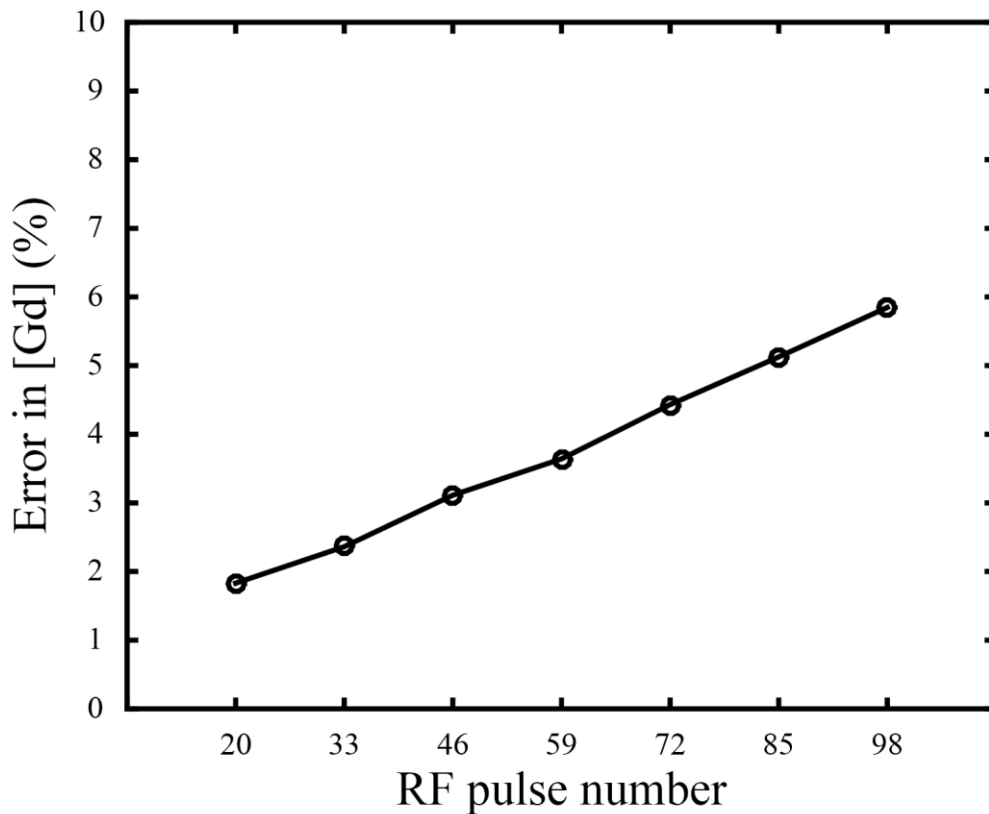


Figure 6.8: The error in average contrast agent estimation (CLAIR vs. SASHA) for phantom experiments as a function of the RF pulse number in the cine acquisition.

6.3.3 In Vivo

The characteristics of the subjects are shown in Table 6.2. One subject did not have a hematocrit drawn, so was assigned a healthy female value of 0.42. Values from the T_1 analysis of SASHA and CLAIR are shown in Table 6.3. Average CLAIR values for myocardial [Gd], λ , and ECV are all statistically increased as compared to SASHA (p-value 0.02 for all), with average relative differences of 4.8%, 4.6%, and 4.6% respectively, or absolute differences of 0.008 mM, 0.017, and 1.0%. Excellent correlation is seen between SASHA and CLAIR values for [Gd], λ , and ECV (Figure 6.9), and is statistically significant for all (p-value <0.0001 for all). No significant correlation is noted between a subject's native T_1 value and [Gd] error (Figure 6.10), defined by [Gd] from CLAIR minus [Gd] from SASHA, normalized to [Gd] from SASHA. Figure 6.11 summarizes the error of [Gd] as a function of cardiac phase, showing a box plot of the error in CLAIR estimates of ECV as compared to SASHA for all subjects, as a function of cardiac phase.

Table 6.2: Subject characteristics

n	12
Male n(%)	3 (25)
Age (yrs)	62±11
Height (m)	1.67±0.08
Weight (kg)	68.4±10.3
Heart Rate (bpm)	57±8
Systolic blood pressure (mmHg)	122±17
Diastolic blood pressure (mmHg)	70±14
Diabetes n(%)	1 (8.3)
Hypertension n(%)	8 (66.7)
Hyperlipidemia n(%)	4 (33.3)
Hematocrit	0.41±0.03
LVEF (%)	65±5
LVEDVi (mL/m ²)	70±8
LVESVi (mL/m ²)	25±5
LV Mass (g/m ²)	50±8
Positive LGE n(%)	0 (0)

LVEF = Left ventricular ejection fraction, LVEDVi = Indexed left ventricular end-diastolic dimension, LVESVi = Indexed left ventricular end-systolic dimension, LGE = Late gadolinium enhancement

Table 6.3: CMR values

	SASHA	CLAIR
Native τ_1 (ms)	1194±31	-
Blood τ_1 (ms)	1616±74	-
Post-Gd Myocardial τ_1 (ms)	537±55	-
Post-Gd Blood τ_1 (ms)	290±51	-
Myocardial [Gd] (mM)	0.20±0.04	0.20±0.03
Blood [Gd] (mM)	0.55±0.11	-
Lambda	0.36±0.04	0.38±0.05
ECV (%)	21±3	22±3

Gd = gadolinium, [Gd] = concentration of gadolinium, ECV = extracellular volume fraction

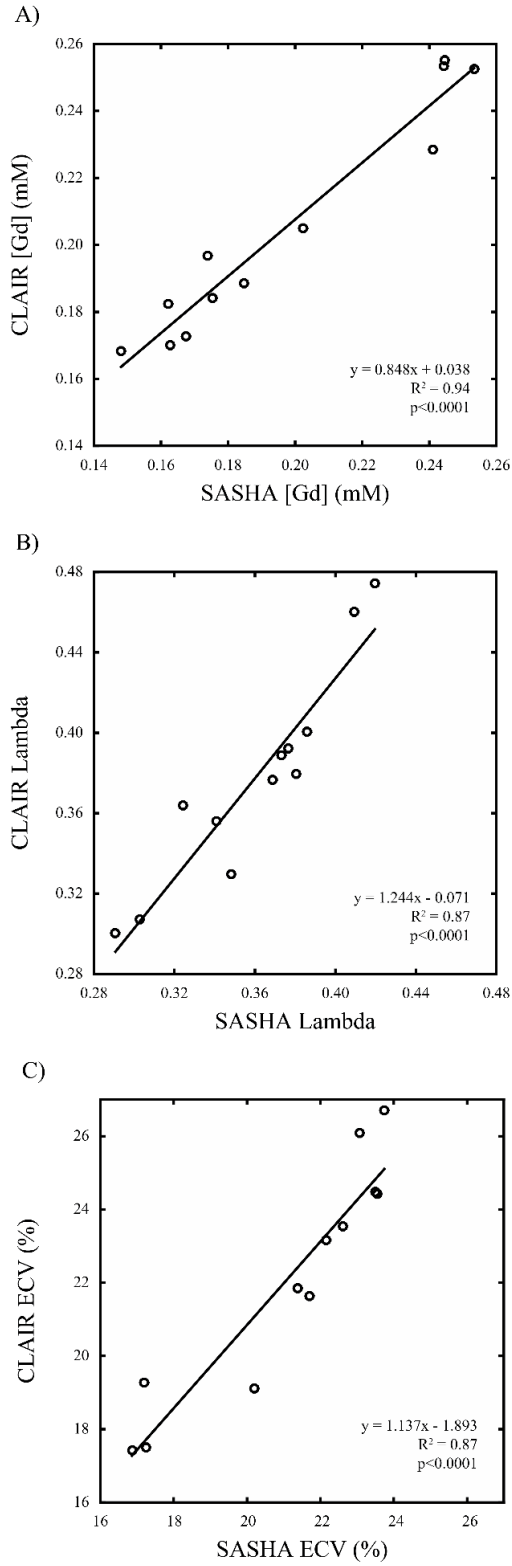


Figure 6.9: Correlation of in vivo SASHA and CLAIR values for A) [Gd], B) lambda, and C) ECV

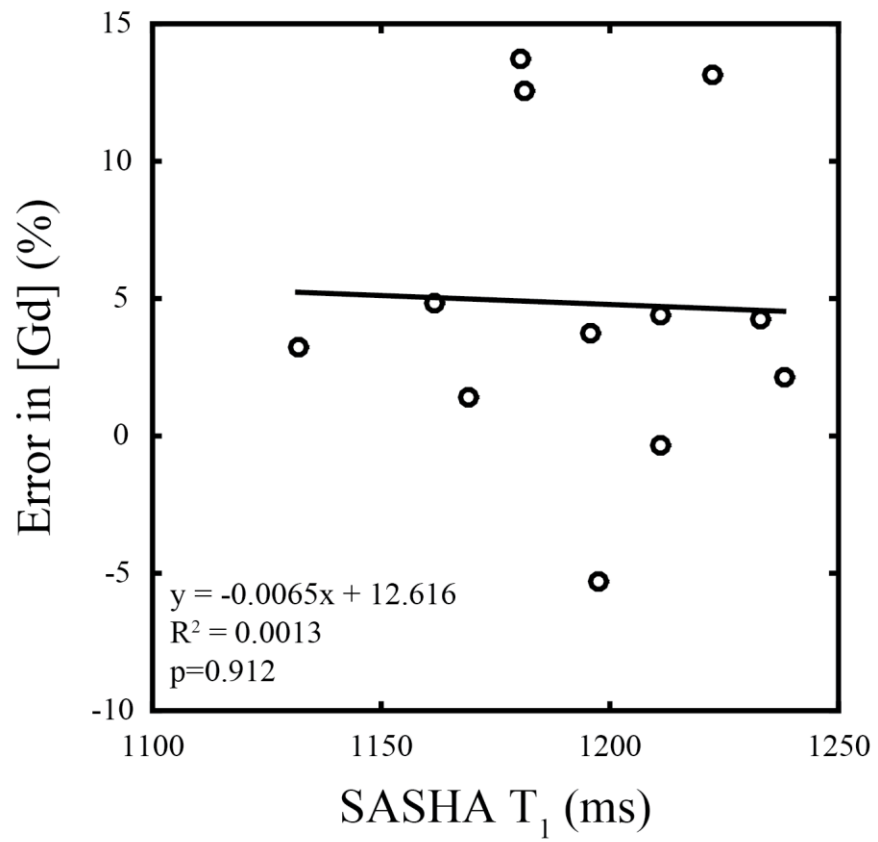


Figure 6.10: Relationship between in vivo contrast agent estimation errors vs. native T_1

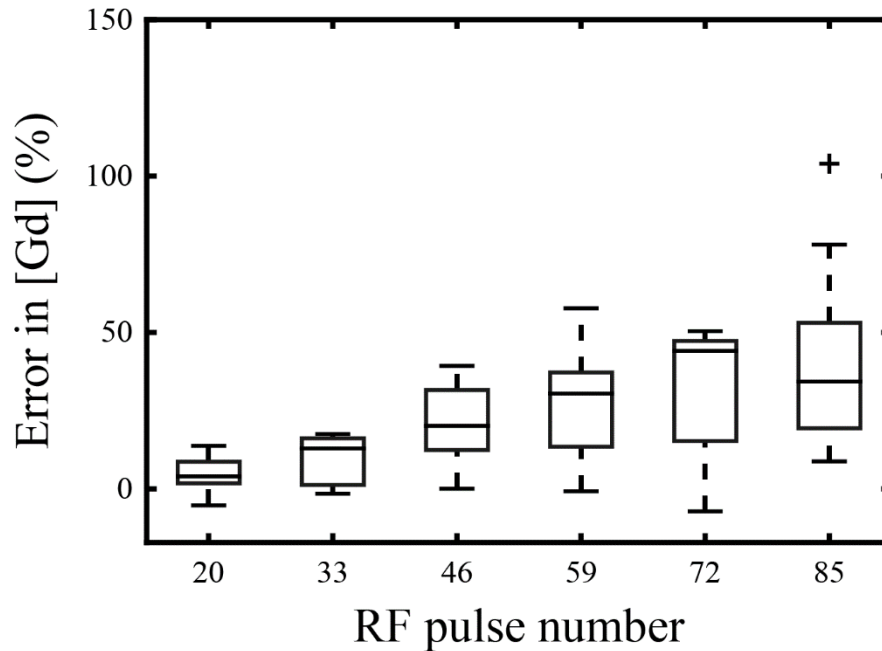


Figure 6.11: Error in in vivo average contrast agent estimation as a function of the RF pulse number in the cine acquisition.

On average there are twice as many pixels across the ventricular septum with CLAIR compared to SASHA (21.1 ± 2.9 vs. 10.1 ± 2.4 , p-value 0.0022).

6.4 Discussion

In this study, we presented CLAIR (Contrast Level Assessment using Intensity Ratios), a new method for estimation of myocardial contrast agent concentration and extracellular volume fraction using CMR. To minimize potential partial volume effects, CLAIR uses segmented acquisitions to enable increased spatial resolution in combination with sufficiently short imaging windows (~ 40 ms), capturing end-systolic frames, to both minimize potential motion-related blurring and yield an increased number of pixels across the myocardium. By comparison, conventional T_1 -mapping sequences typically have imaging windows of 150 to 200 ms.(50) CLAIR is based on a lookup table approach, where the ratio of pre- and post-contrast images is converted to contrast agent concentration. This approach was shown to have excellent experimental agreement with T_1 -mapping-derived contrast agent concentrations, in both phantoms and in vivo studies.

In recent years, the availability of, and demand for, non-invasive tests for diffuse myocardial fibrosis and other microstructural pathology have driven the field of T_1 -mapping. However, clinically applicable T_1 -mapping acquisitions require concessions to account for cardiac and respiratory motion and comfortable breath-hold duration. Specifically, the majority of T_1 -mapping methods use single-shot imaging performed at end-diastole, where cardiac motion is relatively quiescent and more tolerant of the longer imaging duration (150 to 200 ms), with typical in-plane resolutions of 1.4 to 2.3 mm.(50) However, residual motion in diastasis, particularly with higher heart rates, and the resulting loss in achieved spatial resolution is difficult to quantify and thus not well understood. The potential for blurring in this situation, leading to partial volume errors from surrounding epicardial fat or intraventricular blood, has previously been noted as a major concern.(50)

In a recent study of 300 subjects free from cardiovascular disease,(193) the average minimum left ventricular wall thickness at a basal level ranged between 4.3 to 5.7 mm in women, and 5.2 to 6.9 mm in men. These values were smaller at the mid-ventricular level, with average minimum wall thicknesses of 3.5 to 4.9 mm in women and 4.1 to 5.6 mm in men. Given the moderate true acquired spatial resolutions of ~ 2 mm that are common in T_1 -mapping protocols and the additional effects of motion over the imaging window, there is potential for significant partial volume effects even when the myocardium appears well resolved from neighboring fat and blood pools. Indeed, a recent study of the shortened MOLLI (ShMOLLI) method comparing end-diastolic and end-systolic image acquisitions found that the increased wall thickness with end-systolic imaging yielded lower native T_1 values, even in the thicker septal segments, which are ascribed by the authors to reduced partial volume effects from the longer- T_1 blood pool.(196) Other studies have shown a similar reduction in native T_1 with end-systolic imaging(194, 195); however standard diastasis imaging parameters were applied these studies to acquire images at end-systole, assumedly with conventional single-shot imaging windows of 150-200 ms. Like these previous studies, the use of end-systolic imaging in the current study was designed to minimize partial volume errors by increasing the number of pixels across the wall, averaging over double the numbers of pixels across the mid-ventricular septum. Additionally, the CLAIR method offers imaging windows that are ~ 3 -4 times shorter than attainable with single-shot imaging, and thus can mitigate the blurring effects of these longer acquisition windows. CLAIR offers the advantage of a time-resolved cine acquisition, as shown in Figure 6.4, which offers the ability to use the

motion of myocardium and trabeculation, as well as improved blood-tissue contrast, to aid in the differentiation of muscle, fat, and blood pool. While the CLAIR analysis can also be performed on any of the acquired frames, deviation from T_1 recovery weighting due to the bSSFP readout (Figure 6.7 and Figure 6.8) provide rationale for limiting the analysis to only the first acquired cardiac phase in the current study. Furthermore, through plane motion of unexcited myocardial tissue through the rest of the cardiac cycle may contribute to additional errors with increasing cardiac phase. Through-plane motion effects likely account for the larger error in calculated contrast agent concentration with advancing cardiac phase in-vivo (Figure 6.11) as compared to phantom experiments (Figure 6.8).

A potential additional feature of the CLAIR method is the simultaneous acquisition of cardiac function. CLAIR employs spatial and temporal resolution in keeping with guidelines for ventriculography.(203) Though CLAIR was acquired over 15 heartbeats, the use of parallel imaging, and/or increasing the number of lines per segment, could be used to reduce the breath-hold as needed. However, as our CLAIR acquisitions included cardiac phases only until mid-diastole, missing the important end-diastolic cardiac phase, we did not complete a head to head comparison in this study, as was performed for the MCLE sequence,(197, 198) so cannot speak to its performance in this respect. Nevertheless, there are no intrinsic limitations with the CLAIR method that would preclude the acquisition of cardiac phases to span the full cardiac cycle.

There is potential for the CLAIR method to be used to evaluate the more challenging right ventricular (RV). However, despite the short end-systolic imaging windows used in the current study, there was insufficient consistency between or within subjects to proceed with formal analysis of the right ventricle. This is likely the result of the combined effects of low RV wall thickness, prevalence of epicardial fat, and the additional confounding effects of trabeculation, which together make robust identification of pure RV muscle pixels particularly challenging.

6.4.1 Limitations

While CLAIR provides estimates of $[Gd]$, λ , and ECV using increased spatial resolution and end-systolic imaging, there are important limitations to this approach. Perhaps most importantly CLAIR does not directly calculate T_1 values, but instead uses a lookup table approach that requires assumed input values for several parameters. While it was shown that the resulting calculated contrast agent concentrations are largely independent of flip angle, magnetic field homogeneity and T_2 , the calculated concentrations do depend on the native T_1 values, with

approximately 6% overestimation of [Gd] per 50 ms error in the assumed T_1 value below the true value. Fortunately, pathology associated with increased ECV has consistently been associated with increased native T_1 values,(66, 67, 175, 204) such that CLAIR will tend to overestimate contrast agent concentrations, and thus ECV, when there is an increase in the native T_1 values, thus providing an additive contrast mechanism. Importantly, the error in myocardial [Gd] estimated with CLAIR in the current study was shown to be independent of native T_1 values, suggesting other factors dominate differences between CLAIR and T_1 -mapping estimation of ECV. Another limitation of CLAIR is that it is dependent on the use of contrast agents, and thus cannot be utilized in those unable to receive them. Also, the effects of inflow confound the applicability of CLAIR, where signal enhancement due to through-plane motion overwhelms the underlying T_1 changes based on contrast agent concentration. Thus, CLAIR requires the acquisition of a conventional T_1 -mapping sequence for a single slice for the estimation of blood pool contrast agent concentration. Finally, though CLAIR performed well in this small cohort of subjects, further work is required to evaluate its performance in larger studies with more diverse patient groups. Additionally, further work is needed to optimize the sequence to determine if CLAIR can provide estimates of ECV in the RV, potentially with optimization of sequence parameters to target the much thinner RV wall.

6.5 Conclusion

Utilizing a Bloch equation derived lookup table approach, the CLAIR sequence enables end-systolic estimation of contrast agent concentration and ECV. Numerical simulations show negligible dependence on assumed input parameters including T_2 , B_1^+ scale, and off-resonance, and small dependencies on native T_1 and saturation efficiency. In this preliminary work, good agreement was seen with a conventional T_1 -mapping approach in phantom experiments and in vivo. Further work, to evaluate its performance in larger, more diverse populations is warranted, along with exploring its potential for simultaneous assessment of ventricular function or its ability to accomplish assessment of the RV.

Discussion and Conclusions

7.1 Summary

In this thesis, T_1 -mapping is used to establish normative data spanning varying age ranges. Building upon this data, relationships are examined when the norm no longer exists, and the effects of chronic conditions, including risk factors for the development of heart failure and enzymatic deficiencies (Anderson-Fabry Disease), illustrate the benefit of non-invasive examination of changes to the cardiac extracellular environment. Finally, attempts to overcome some technical limitations of lower spatial and temporal resolutions approaches led to the development of a novel pulse sequence.

Chapter 2 provides important normative data for the young child, where the availability of such information is sparse. The importance of reference data is of particular significance in the pediatric sphere, as reliable and available non-invasive assessments are extremely valuable as the risks associated with invasive assessments affect decision making of clinicians and researchers. This chapter demonstrates similarities between adult and pediatric data, including sex-related differences in native T_1 and ECV, and highlights much of the challenges that exist within the pediatric population.

Chapter 3, like its preceding chapter, aims to establish critically important normative data, in this instance in the adult population. Building upon this, sex-related differences are observed, and importantly, differences between the myocardial response to chronic stressors, such as diabetes and hypertension, are suggested by the loss of sex-related differences in myocardial native T_1 and ECV.

Chapter 4 builds on these sex-related differences, bringing the discussion into the realm of heart failure. While there is considerable overlap within the spectra of disease, subtle differences in myocardial native T_1 and ECV are present between those with at risk for heart failure, those with heart failure and preserved ejection fraction, and those with heart failure and reduced ejection fraction. In particular, more similarities exist between men at-risk and those with preserved ejection fraction, while in women the two heart failure subtypes have more similar estimates of diffuse fibrosis. While the descriptive nature of these findings is important, the Chapter also

illustrates the prognostic impact of fibrosis, with significantly difference incidence of outcomes in those with abnormal myocardial T_1 or ECV values. Unsurprisingly, the loss of prognostic importance when including additional variables demonstrates the complexity within the pathophysiology of cardiac illness.

Chapter 5 begins to push the utility of these techniques into an often overlooked and challenging constituent of the heart: the right ventricle. Within, it is shown that the changes in the right ventricle, including reduced myocardial native T_1 , in patients with Anderson-Fabry disease appear to be similar to those in their left ventricle, and are more reflective of the same pathophysiological process of accumulation of intracellular sphingolipids. This contrasts with changes measured in patients with pulmonary hypertension, where increases in native T_1 are noted and presumed to be related to myocardial fibrosis due to increased afterload. However, an important limitation within the study was the necessity to study those with hypertrophied right ventricles, as the relative thinness of right ventricular myocardium limits the widespread application of T_1 -mapping techniques.

Finally, Chapter 6 attempts to overcome inherent limitations in existing T_1 -mapping sequences to present a novel pulse sequence and approach. The CLAIR method (Contrast Level Assessment using Intensity Ratios) showed excellent correlation with the more traditional method and provided around twice as many pixels across the interventricular septum due to a combination of improved spatial and temporal footprints, allowing for end-systolic imaging. Unfortunately, even with these improvements, robust analysis of the right ventricle was not feasible.

7.2 Limitations

7.2.1 Image Acquisition Strategies

As with much in the field of MRI, trade-offs exist with balancing image spatial resolution, temporal resolution, and acquisition time. This is a keystone principle in cardiac imaging, where negotiating cardiac and/or respiratory phase is of critical consideration.

The application of pulse sequences developed in adults to children is not always a linear translation. Many of the sacrifices made to acquire the T_1 -weighted images used in the T_1 -mapping sequences result in images with relatively low spatial resolution (larger voxel sizes) compared to other MRI images. These T_1 -weighted images may be of sufficient spatial resolution for an adult heart, over a sufficiently short imaging window for a typical adult heart rates, and the series of

images needed to calculate T_1 values can be obtained over a duration that a typical adult can maintain a stable diaphragm position over a manageable breath-hold. However, the relatively smaller hearts, higher heart rates, and limited breath-holding ability of children lead to a challenge in deciding the extent to push sequence parameters in attempts to minimize errors from partial volume artifacts, blurring from myocardial motion over the image acquisition, and bulk cardiac motion between images. Many changes aimed at improving spatial resolution and acquisition time will come at the expense of signal to noise. The exact impact of these changes is not well characterized, particularly in pediatrics where improved signal may be present due to closer proximity of the heart to surface receive coils, and thus further study is required to better understand the impact and any potential clinical significance.

Related concerns exist when considering applying T_1 -mapping to other thin walled structures in the heart, regardless of the individual's age. While T_1 measurements have been demonstrated in the right ventricle,(109, 181, 188, 205-207) it is significantly challenging in the non-hypertrophied ventricle, often required more complex approaches not readily available at most centres. Additionally, while studies have extended the use of T_1 -mapping into the atria,(208-210) histological validation has not been performed to confirm the findings.

7.2.2 Normative Data

For a biomarker to be useful for clinical or research purposes, there must be an understanding of expected, normal values to which those with suspected pathology can be compared. Portions of the work in this thesis were on the application of T_1 -mapping in healthy individuals, providing some early and important data in this regard. However, there are important considerations at various steps in the works.

Research in children has unique challenges that do not present themselves in most adults. In particular, the level of acceptable risk within research studies is much stricter in children, particularly when most data on known or potential risks are derived from studies completed in adults. As such, recruitment of healthy children to receive intravenous MRI contrast agents is not possible, and thus normative data must be constructed from data collected from those who would be expected to have the lowest predicted risk of pathology. Similarly, the loud MRI environment and long scan times, where individuals are expected to remain as still as possible and follow breath-holding commands, often necessitate general anesthesia in young children who are unable to comprehend the situation and processes. This introduces additional risks that once again would

not be acceptable to expose healthy children to. Therefore, obtaining normal values in the very young is extremely challenging.

Unfortunately, the cardiac MRI community is still varied in its practice, and a unified consensus on a reference standard T_1 -mapping technique has not been achieved. This introduces significant variability across the literature, makes amalgamation of data difficult, and limits the generalizability of results. This is of particular significance in the pediatric age range, where establishment of centre specific normal, or normative, data would be challenging due to low volumes of cases, particularly those with a low index of suspected pathology. Thus, reliance on published normative reference data is of vital importance, though needs to be viewed with consideration given to the potential differences that may occur between institutions, MRI scanners, software versions, etc.

7.2.3 Histological Correlation

Generally, the use of T_1 and ECV serve to act as a surrogate for changes occurring at the microscopic level, particularly using it to non-invasively explore what remodelling is taking place within the extracellular space. Importantly, however, while studies have shown correlation between T_1 and ECV with fibrosis,(76-78, 80-85, 211) data from the chapters within this thesis do not have invasive tissue correlates to provide confirmation of the MRI findings. The invasiveness of tissue acquisition is not insignificant,(1) and thus obtaining such information systematically and in healthy individuals is difficult, and would be next to, if not entirely, impossible in children.

Additionally, T_1 is known to vary with other factors beyond extracellular space alterations, such as changes noted with iron overload and Anderson-Fabry disease,(55, 69, 72-75) which should always cause the clinicians and researchers to give critical thought to application and results of these techniques in patient and disease populations with different pathophysiology to published reports. Our study examining the native T_1 changes in patients with either pulmonary hypertension or Anderson-Fabry disease did not have histological correlation to support findings; however, the findings are in line with T_1 changes reported in other studies in the left ventricle in those with Anderson-Fabry disease(73, 74) and the right ventricle of those with pulmonary hypertension.(181, 205) Thus, there is reasonable biological plausibility to the findings presented.

7.3 Future Directions

7.3.1 Longitudinal Data

While larger, possibly multicentre, studies to obtain more comprehensive normative data for all age ranges would be of significant value, serial measurements within individuals via a longitudinal cohort would provide a better understanding of the changes that occur through development and healthy aging than can be estimated via cross-sectional data. Though not practical from birth to death, specifically obtaining longitudinal data over specified critical developmentally and hormonally shifting time periods, such as puberty or menopause, may help better understand any developmental or age related changes, and provide for better understanding and interpretation of results in the context of the age strata.

7.3.2 Prognostic and Outcome Data

Within the works of the thesis, we explore some of the ways in which native T_1 and ECV can provide useful information. This can be within the diagnostic realm, such as aiding in the detection of a suspected condition (ex: low native T_1 in Anderson-Fabry disease) or understanding the pathophysiology of different disease states. Certainly, as more studies are performed with native T_1 and ECV, our knowledge about cardiac remodelling will only continue to expand. As noted in Chapter 4, native T_1 and ECV may additionally provide prognostic data, helping clinicians to provide more comprehensive counselling to our patients. The T_1 -mapping community is in its relative infancy in this sphere, and it can be expected that we will see much more information in short order, as follow up studies are completed and published. However, native T_1 and ECV may additionally provide important targets to follow response to treatment strategies, such as enzyme replacement therapy in patients with Anderson-Fabry disease, or anti-fibrotic therapies in patients with heart failure or Duchenne muscular dystrophy. These examples merely scratch the surface on an essentially unlimited clinical and research avenue.

7.3.3 Technical Advancements

While perhaps the most important advancement in the T_1 -mapping field came with the ability to acquire the data reliably within a single breath-hold, taking off after the introduction of the MOLLI sequence by Messroghli et al.(63) Since that time, many of the advances have been aimed at improving the accuracy or precision of the results, with some changes as simple as more optimal sampling schemes,(50, 87, 142, 212, 213) or others focused on alternative magnetization preparation schemes.(51, 214, 215) Additionally, sequences like CLAIR (Chapter 6) and

Accelerated and navigator-gated look-locker imaging for cardiac T_1 estimation (ANGIE)(188) attempt to address limitations in spatial resolution to aid in assessment of thinner walled structures. This is primarily done with a segmented imaging approach, either within a breath-hold (CLAIR) or navigated free breathing acquisition (ANGIE), both of which have advantages and disadvantages. Regardless of demographics, advances in rapid image acquisition, such as improvements in parallel imaging techniques and compressed sensing(216) will likely provide benefits that can be leveraged into improvements in overall acquisition time, temporal footprint, and/or spatial resolution. Many of these advances may potentially provide particular benefit in the pediatric age range, where smaller heart sizes, higher heart rates, and limited breath-holding abilities are prevalent. Sequences are being designed to be purposefully run free breathing, without the use of a navigator-based strategy, and may provide particularly useful in children.

It is important to put perspective to the works of the thesis. The T_1 -mapping technique utilized in Chapter 2 remains in use in the largest CMR program in Canada, as it continues to be the current clinical product MOLLI sequence. The data provided within the Chapter continues to represent one of the largest cohorts of pediatric aged participants. However, in addition to direct longitudinally acquired data alluded to above, perhaps the use of novel approaches to T_1 -mapping, such as free breathing acquisition strategies,(217, 218) may allow for non-sedated CMR studies to be performed more easily in children less than 8 years old, who may be cooperative enough to lie still for a study, but not able to adequately perform a breath-hold. Since the time of data collection for Chapters 3 through 6, the prototypical SASHA sequence used has seen technical improvements in spatial resolution, variable flip angle single-shot imaging, saturation pulse design, saturation recovery time sampling strategies, recovery curve fitting strategies, and free breathing acquisition.(200, 217, 219, 220) These improvements primarily aim the precision of the method, without significantly affecting its accuracy. Since the publication of Chapter 3, a study of healthy individuals was completed using the majority of these improvements.(221) In the study, the authors found a similar sex-related difference in both native T_1 and ECV as was found in our study (1120 ms and 22.6% in men vs. 1171 ms and 26.0% in women). The cohort also had MOLLI and ShMOLLI T_1 data, which showed similar sex-related differences, but characteristically different native T_1 and ECV values as compared to SASHA. In keeping with our study, there was an absence of age-related association with SASHA native T_1 and ECV values. Since the preparation of Chapter 4, or prior for that matter, there have not been any publications examining the differences

between heart failure groups or the association of outcomes utilizing the SASHA sequence, irrespective of its acquisition parameters. Since the time of the publication of Chapter 5, there have been few publications on T_1 -mapping in Anderson-Fabry disease, with one publication attempting T_1 analysis in the right ventricle.(222) Importantly, subjects were not selected based on a minimum wall thickness, and the study was performed at 3T using a MOLLI T_1 -mapping sequence. Over 25% of the participants were not able to have right ventricular measurements performed, likely related to an average maximum wall thickness of 3.7 mm. While lower right ventricular T_1 values were present between those with Anderson-Fabry compared to individuals with hypertrophic cardiomyopathy, they were statistically increased as compared to within other portions of the left ventricle. However, very poor reliability measures for the right ventricular measurements raise significant concerns of errors presumed to be related to partial volume artifacts. While additional studies have examined left ventricular T_1 values in subjects with pulmonary hypertension, only one further study not referenced in Chapter 5 specifically measured right ventricular T_1 .(205) However, as it was a contemporary publication to Chapter 5, it utilized the original MOLLI variant that most of the T_1 -mapping community has moved away from. Finally, the spirit of Chapter 6 is pervasive throughout the T_1 -mapping community, in attempts to improve the robustness and reliability no matter the region of the heart or the population of interest. Much of these improvements have been alluded to in previous references, and it would be unfeasible to detail all possible combinations and permutations of sequence variants that currently, or previously, exist. However, it would appear since the time Chapter 6 was prepared, few studies have focused on benefits of end-systolic T_1 -mapping. By reducing the readout duration to approximately 160 ms, on average a 209-255% increase in the full-width-at-half-maximum intensity profile was achieved, with native T_1 times at 3T of 1563 ms, comparable to SASHA 3T diastolic values.(223) However, it is important to note that simply applying the same diastolic imaging parameters to the systolic phase resulted in non-significant increased native T_1 values compared to both the systolic-optimized approach or imaging in the diastolic phase. Thus, appropriate use of T_1 mapping requires careful consideration of the multitude of patient and technical factors to ensure the most accurate and meaningful results.

Of course, as we have seen within the field, issues exist with fragmentation of the techniques used and therefore the variety of expected values. This unfortunately introduces potential trepidation in the acceptance and dissemination of novel techniques, as the breadth of

existing data may not be relatable to that which is newly acquired. Attempts at standardization are an important part of the field, and through work such as the T₁MES phantom,(132) may provide a means for establishing accurate relationships and/or conversions between methods.

7.4 Conclusions

The utility of cardiac MRI is nearly unrivaled by other modalities, and its ability in tissue characterization is a significant strength, particularly as alternatives are often invasive and carry non-significant risks. Myocardial fibrosis, be it focal or diffuse, is prevalent in many different conditions, and has been associated with adverse clinical status and outcomes. Importantly, however, while fibrosis may be the most common and ubiquitous pathological change affecting most hearts, there are other histopathological processes that may be non-invasively detected with cardiac MRI.

Notably, while initial uses relied on qualitative, relative signal differences for detection and diagnosis of pathology, the progress in the field to develop more robust, clinically practical, quantitative measures provides for opportunities not previously available, such as assessment of diffuse myocardial fibrosis. Important in the understanding of pathological processes is understanding the normal situation, with availability of reference values for comparisons. Related, appreciation of differences that may exist between sex and through aging aids in the contextual application of acquired data. Differences exist between females and males, and thus should be taken into consideration when interpreting subsequent results; meanwhile variation with aging does not appear to be present, which may aid in extrapolation of data from adults to the more challenging to study pediatric population.

Importantly, different diseases demonstrate diverse patterns in native T₁ and ECV. Mimicking findings on the left ventricle, when right ventricular hypertrophy is present in patients with Anderson-Fabry disease, a reduction in native T₁ is present, suggesting a different mechanism to the hypertrophy than noted in those with pulmonary hypertension. While heart failure may be a unifying constellation of symptoms, differing patterns of native T₁ and ECV in those at risk for heart failure, with preserved ejection fraction, or with reduced ejection fraction can be observed, particularly when considering sex-related patterns.

Technical developments have allowed for significant advancements in T₁-mapping, leading to a widespread adoption and utilization; however, challenges exist in the application in

areas of relatively thinner myocardium. Ongoing improvements in sequence design, and alternative strategies like CLAIR, strive to enable reliable assessments in these regions. Challenges continue to face the community, such as the challenge found in evaluating young children or the right ventricle, however enduring advances lead to optimism of inevitable success.

References

1. Cooper LT, Baughman KL, Feldman AM, Frustaci A, Jessup M, Kuhl U, et al. The role of endomyocardial biopsy in the management of cardiovascular disease: a scientific statement from the American Heart Association, the American College of Cardiology, and the European Society of Cardiology. Endorsed by the Heart Failure Society of America and the Heart Failure Association of the European Society of Cardiology. *J Am Coll Cardiol.* 2007;50(19):1914-31. doi: 10.1016/j.jacc.2007.09.008. PubMed PMID: 17980265.
2. Hunt SA, Baker DW, Chin MH, Cinquegrani MP, Feldman AM, Francis GS, et al. ACC/AHA guidelines for the evaluation and management of chronic heart failure in the adult: executive summary. A report of the American College of Cardiology/American Heart Association Task Force on Practice Guidelines (Committee to revise the 1995 Guidelines for the Evaluation and Management of Heart Failure). *J Am Coll Cardiol.* 2001;38(7):2101-13. doi: 10.1016/s0735-1097(01)01683-7. PubMed PMID: 11738322.
3. Yancy CW, Jessup M, Bozkurt B, Butler J, Casey DE, Drazner MH, et al. 2013 ACCF/AHA guideline for the management of heart failure: a report of the American College of Cardiology Foundation/American Heart Association Task Force on Practice Guidelines. *J Am Coll Cardiol.* 2013;62(16):e147-239. doi: 10.1016/j.jacc.2013.05.019. PubMed PMID: 23747642.
4. Yamada S, Komuro K. Integrated backscatter for the assessment of myocardial viability. *Curr Opin Cardiol.* 2006;21(5):433-7. doi: 10.1097/01.hco.0000240578.05053.f9. PubMed PMID: 16900004.
5. Scully PR, Bastarrika G, Moon JC, Treibel TA. Myocardial Extracellular Volume Quantification by Cardiovascular Magnetic Resonance and Computed Tomography. *Curr Cardiol Rep.* 2018;20(3):15. Epub 2018/03/06. doi: 10.1007/s11886-018-0961-3. PubMed PMID: 29511861; PubMed Central PMCID: PMC5840231.
6. Heart & Stroke Foundation: 2016 report on the health of Canadians: the burden of heart failure www.heartandstroke.ca [cited 2019 March].
7. Benjamin EJ, Virani SS, Callaway CW, Chamberlain AM, Chang AR, Cheng S, et al. Heart Disease and Stroke Statistics-2018 Update: A Report From the American Heart

- Association. *Circulation*. 2018;137(12):e67-e492. Epub 2018/01/31. doi: 10.1161/CIR.0000000000000558. PubMed PMID: 29386200.
8. Wang TJ, Evans JC, Benjamin EJ, Levy D, LeRoy EC, Vasani RS. Natural history of asymptomatic left ventricular systolic dysfunction in the community. *Circulation*. 2003;108(8):977-82. Epub 2003/08/11. doi: 10.1161/01.CIR.0000085166.44904.79. PubMed PMID: 12912813.
 9. Ezekowitz JA, O'Meara E, McDonald MA, Abrams H, Chan M, Ducharme A, et al. 2017 Comprehensive Update of the Canadian Cardiovascular Society Guidelines for the Management of Heart Failure. *Can J Cardiol*. 2017;33(11):1342-433. Epub 2017/09/06. doi: 10.1016/j.cjca.2017.08.022. PubMed PMID: 29111106.
 10. Vliegen HW, van der Laarse A, Cornelisse CJ, Eulderink F. Myocardial changes in pressure overload-induced left ventricular hypertrophy. A study on tissue composition, polyploidization and multinucleation. *Eur Heart J*. 1991;12(4):488-94. PubMed PMID: 1829680.
 11. Weber KT. Cardiac interstitium in health and disease: the fibrillar collagen network. *J Am Coll Cardiol*. 1989;13(7):1637-52. PubMed PMID: 2656824.
 12. Frank JS, Langer GA. The myocardial interstitium: its structure and its role in ionic exchange. *J Cell Biol*. 1974;60(3):586-601. PubMed PMID: 4824287; PubMed Central PMCID: PMC2109249.
 13. Mewton N, Liu CY, Croisille P, Bluemke D, Lima JA. Assessment of myocardial fibrosis with cardiovascular magnetic resonance. *J Am Coll Cardiol*. 2011;57(8):891-903. doi: 10.1016/j.jacc.2010.11.013. PubMed PMID: 21329834; PubMed Central PMCID: PMC3081658.
 14. Díez J, Querejeta R, López B, González A, Larman M, Martínez Ubago JL. Losartan-dependent regression of myocardial fibrosis is associated with reduction of left ventricular chamber stiffness in hypertensive patients. *Circulation*. 2002;105(21):2512-7. PubMed PMID: 12034658.
 15. López B, Querejeta R, González A, Sánchez E, Larman M, Díez J. Effects of loop diuretics on myocardial fibrosis and collagen type I turnover in chronic heart failure. *J Am Coll Cardiol*. 2004;43(11):2028-35. doi: 10.1016/j.jacc.2003.12.052. PubMed PMID: 15172408.
 16. López B, González A, Beaumont J, Querejeta R, Larman M, Díez J. Identification of a potential cardiac antifibrotic mechanism of torasemide in patients with chronic heart failure. *J*

- Am Coll Cardiol. 2007;50(9):859-67. doi: 10.1016/j.jacc.2007.04.080. PubMed PMID: 17719472.
17. Brilla CG, Funck RC, Rupp H. Lisinopril-mediated regression of myocardial fibrosis in patients with hypertensive heart disease. *Circulation*. 2000;102(12):1388-93. PubMed PMID: 10993857.
 18. Pitt B, Zannad F, Remme WJ, Cody R, Castaigne A, Perez A, et al. The effect of spironolactone on morbidity and mortality in patients with severe heart failure. Randomized Aldactone Evaluation Study Investigators. *N Engl J Med*. 1999;341(10):709-17. doi: 10.1056/NEJM199909023411001. PubMed PMID: 10471456.
 19. Zannad F, Alla F, Dousset B, Perez A, Pitt B. Limitation of excessive extracellular matrix turnover may contribute to survival benefit of spironolactone therapy in patients with congestive heart failure: insights from the randomized aldactone evaluation study (RALES). Rales Investigators. *Circulation*. 2000;102(22):2700-6. doi: 10.1161/01.cir.102.22.2700. PubMed PMID: 11094035.
 20. Sutton MG, Sharpe N. Left ventricular remodeling after myocardial infarction: pathophysiology and therapy. *Circulation*. 2000;101(25):2981-8. PubMed PMID: 10869273.
 21. Francone M, Chimenti C, Galea N, Scopelliti F, Verardo R, Galea R, et al. CMR sensitivity varies with clinical presentation and extent of cell necrosis in biopsy-proven acute myocarditis. *JACC Cardiovasc Imaging*. 2014;7(3):254-63. Epub 2014/02/19. doi: 10.1016/j.jcmg.2013.10.011. PubMed PMID: 24560214.
 22. Lagana SM, Parwani AV, Nichols LC. Cardiac sarcoidosis: a pathology-focused review. *Arch Pathol Lab Med*. 2010;134(7):1039-46. doi: 10.1043/2009-0274-RA.1. PubMed PMID: 20586635.
 23. Gertz MA, Lacy MQ, Dispenzieri A. Amyloidosis: recognition, confirmation, prognosis, and therapy. *Mayo Clin Proc*. 1999;74(5):490-4. doi: 10.4065/74.5.490. PubMed PMID: 10319082.
 24. Fast JH, Kubat K, van Haelst UJ, Schuurmans Stekhoven JH. The usefulness of an endomyocardial biopsy in heart disease of unknown etiology. *Int J Cardiol*. 1986;11(3):317-28. PubMed PMID: 3013787.
 25. Funabashi N, Toyozaki T, Matsumoto Y, Yonezawa M, Yanagawa N, Yoshida K, et al. Images in cardiovascular medicine. Myocardial fibrosis in fabry disease demonstrated by

- multislice computed tomography: comparison with biopsy findings. *Circulation*. 2003;107(19):2519-20. doi: 10.1161/01.CIR.0000062036.35852.01. PubMed PMID: 12756193.
26. Kass DA, Bronzwaer JG, Paulus WJ. What mechanisms underlie diastolic dysfunction in heart failure? *Circ Res*. 2004;94(12):1533-42. doi: 10.1161/01.RES.0000129254.25507.d6. PubMed PMID: 15217918.
27. Martos R, Baugh J, Ledwidge M, O'Loughlin C, Conlon C, Patle A, et al. Diastolic heart failure: evidence of increased myocardial collagen turnover linked to diastolic dysfunction. *Circulation*. 2007;115(7):888-95. Epub 2007/02/05. doi: 10.1161/CIRCULATIONAHA.106.638569. PubMed PMID: 17283265.
28. Yamamoto K, Masuyama T, Sakata Y, Nishikawa N, Mano T, Yoshida J, et al. Myocardial stiffness is determined by ventricular fibrosis, but not by compensatory or excessive hypertrophy in hypertensive heart. *Cardiovasc Res*. 2002;55(1):76-82. PubMed PMID: 12062710.
29. Nishikawa N, Masuyama T, Yamamoto K, Sakata Y, Mano T, Miwa T, et al. Long-term administration of amlodipine prevents decompensation to diastolic heart failure in hypertensive rats. *J Am Coll Cardiol*. 2001;38(5):1539-45. PubMed PMID: 11691537.
30. Norton GR, Tsotetsi J, Trifunovic B, Hartford C, Candy GP, Woodiwiss AJ. Myocardial stiffness is attributed to alterations in cross-linked collagen rather than total collagen or phenotypes in spontaneously hypertensive rats. *Circulation*. 1997;96(6):1991-8. PubMed PMID: 9323091.
31. López B, González A, Querejeta R, Larman M, Díez J. Alterations in the pattern of collagen deposition may contribute to the deterioration of systolic function in hypertensive patients with heart failure. *J Am Coll Cardiol*. 2006;48(1):89-96. doi: 10.1016/j.jacc.2006.01.077. PubMed PMID: 16814653.
32. van Heerebeek L, Borbély A, Niessen HW, Bronzwaer JG, van der Velden J, Stienen GJ, et al. Myocardial structure and function differ in systolic and diastolic heart failure. *Circulation*. 2006;113(16):1966-73. doi: 10.1161/CIRCULATIONAHA.105.587519. PubMed PMID: 16618817.
33. Montera MW, Drumond C, Takiya C, Mesquita CT, Dohmann HF, Mady C. Correlation of myocardial interstitial collagen in the right ventricular septum with ventricular function of

patients with ischemic cardiomyopathy. *Arq Bras Cardiol.* 2009;92(1):54-62. PubMed PMID: 19219265.

34. Wu TJ, Ong JJ, Hwang C, Lee JJ, Fishbein MC, Czer L, et al. Characteristics of wave fronts during ventricular fibrillation in human hearts with dilated cardiomyopathy: role of increased fibrosis in the generation of reentry. *J Am Coll Cardiol.* 1998;32(1):187-96. PubMed PMID: 9669269.

35. Kawara T, Derksen R, de Groot JR, Coronel R, Tasseron S, Linnenbank AC, et al. Activation delay after premature stimulation in chronically diseased human myocardium relates to the architecture of interstitial fibrosis. *Circulation.* 2001;104(25):3069-75. PubMed PMID: 11748102.

36. Anderson KP, Walker R, Urie P, Ershler PR, Lux RL, Karwande SV. Myocardial electrical propagation in patients with idiopathic dilated cardiomyopathy. *J Clin Invest.* 1993;92(1):122-40. doi: 10.1172/JCI116540. PubMed PMID: 8325977; PubMed Central PMCID: PMCPMC293548.

37. McLenachan JM, Dargie HJ. Ventricular arrhythmias in hypertensive left ventricular hypertrophy. Relationship to coronary artery disease, left ventricular dysfunction, and myocardial fibrosis. *Am J Hypertens.* 1990;3(10):735-40. PubMed PMID: 2145865.

38. Spach MS, Boineau JP. Microfibrosis produces electrical load variations due to loss of side-to-side cell connections: a major mechanism of structural heart disease arrhythmias. *Pacing Clin Electrophysiol.* 1997;20(2 Pt 2):397-413. PubMed PMID: 9058844.

39. Pogwizd SM, McKenzie JP, Cain ME. Mechanisms underlying spontaneous and induced ventricular arrhythmias in patients with idiopathic dilated cardiomyopathy. *Circulation.* 1998;98(22):2404-14. PubMed PMID: 9832485.

40. Gulati A, Jabbour A, Ismail TF, Guha K, Khwaja J, Raza S, et al. Association of fibrosis with mortality and sudden cardiac death in patients with nonischemic dilated cardiomyopathy. *JAMA.* 2013;309(9):896-908. doi: 10.1001/jama.2013.1363. PubMed PMID: 23462786.

41. Arteaga E, de Araújo AQ, Bernstein M, Ramires FJ, Ianni BM, Fernandes F, et al. Prognostic value of the collagen volume fraction in hypertrophic cardiomyopathy. *Arq Bras Cardiol.* 2009;92(3):210-4, 6-20. PubMed PMID: 19390710.

42. Neilan TG, Coelho-Filho OR, Danik SB, Shah RV, Dodson JA, Verdini DJ, et al. CMR quantification of myocardial scar provides additive prognostic information in nonischemic

cardiomyopathy. *JACC Cardiovasc Imaging*. 2013;6(9):944-54. doi:

10.1016/j.jcmg.2013.05.013. PubMed PMID: 23932642; PubMed Central PMCID:

PMC3952043.

43. Assomull RG, Prasad SK, Lyne J, Smith G, Burman ED, Khan M, et al. Cardiovascular magnetic resonance, fibrosis, and prognosis in dilated cardiomyopathy. *J Am Coll Cardiol*. 2006;48(10):1977-85. Epub 2006/10/31. doi: 10.1016/j.jacc.2006.07.049. PubMed PMID: 17112987.

44. Kwon DH, Halley CM, Popovic ZB, Carrigan TP, Zysek V, Setser R, et al. Gender differences in survival in patients with severe left ventricular dysfunction despite similar extent of myocardial scar measured on cardiac magnetic resonance. *Eur J Heart Fail*. 2009;11(10):937-44. doi: 10.1093/eurjhf/hfp118. PubMed PMID: 19789396.

45. Kwong RY, Chan AK, Brown KA, Chan CW, Reynolds HG, Tsang S, et al. Impact of unrecognized myocardial scar detected by cardiac magnetic resonance imaging on event-free survival in patients presenting with signs or symptoms of coronary artery disease. *Circulation*. 2006;113(23):2733-43. Epub 2006/06/05. doi: 10.1161/CIRCULATIONAHA.105.570648. PubMed PMID: 16754804.

46. Kwong RY, Sattar H, Wu H, Vorobiof G, Gandla V, Steel K, et al. Incidence and prognostic implication of unrecognized myocardial scar characterized by cardiac magnetic resonance in diabetic patients without clinical evidence of myocardial infarction. *Circulation*. 2008;118(10):1011-20. Epub 2008/08/25. doi: 10.1161/CIRCULATIONAHA.107.727826. PubMed PMID: 18725488; PubMed Central PMCID: PMC3952043.

47. Lauterbur PC. Image Formation by Induced Local Interactions: Examples Employing Nuclear Magnetic Resonance. *Nature*. 1973;242:190-1. doi: 10.1038/242190a0.

48. Brown RW, Cheng Y-CN, Haacke EM, Thompson MR, Venkatesan R. *Magnetic resonance imaging : physical principles and sequence design*. Second edition. ed. Hoboken, New Jersey: John Wiley & Sons, Inc.; 2014. xxxii, 944 pages p.

49. Bushberg JT. *The essential physics of medical imaging*. 3rd ed. Philadelphia: Wolters Kluwer Health/Lippincott Williams & Wilkins; 2012. xii, 1030 p. p.

50. Kellman P, Hansen MS. T1-mapping in the heart: accuracy and precision. *J Cardiovasc Magn Reson*. 2014;16:2. doi: 10.1186/1532-429X-16-2. PubMed PMID: 24387626; PubMed Central PMCID: PMC3927683.

51. Chow K, Flewitt JA, Green JD, Pagano JJ, Friedrich MG, Thompson RB. Saturation recovery single-shot acquisition (SASHA) for myocardial T(1) mapping. *Magn Reson Med*. 2014;71(6):2082-95. doi: 10.1002/mrm.24878. PubMed PMID: 23881866.
52. Weingärtner S, Meßner NM, Budjan J, Loßnitzer D, Mattler U, Papavassiliu T, et al. Myocardial T₁-mapping at 3T using saturation-recovery: reference values, precision and comparison with MOLLI. *J Cardiovasc Magn Reson*. 2016;18(1):84. Epub 2016/11/18. doi: 10.1186/s12968-016-0302-x. PubMed PMID: 27855705; PubMed Central PMCID: PMC5114738.
53. Baeßler B, Schaarschmidt F, Stehning C, Schnackenburg B, Maintz D, Bunck AC. A systematic evaluation of three different cardiac T₂-mapping sequences at 1.5 and 3T in healthy volunteers. *Eur J Radiol*. 2015;84(11):2161-70. Epub 2015/08/05. doi: 10.1016/j.ejrad.2015.08.002. PubMed PMID: 26276731.
54. Luetkens JA, Homsy R, Dabir D, Kuetting DL, Marx C, Doerner J, et al. Comprehensive Cardiac Magnetic Resonance for Short-Term Follow-Up in Acute Myocarditis. *J Am Heart Assoc*. 2016;5(7). Epub 2016/07/19. doi: 10.1161/JAHA.116.003603. PubMed PMID: 27436306; PubMed Central PMCID: PMC5015395.
55. Sado DM, Maestrini V, Piechnik SK, Banyersad SM, White SK, Flett AS, et al. Noncontrast myocardial T₁ mapping using cardiovascular magnetic resonance for iron overload. *J Magn Reson Imaging*. 2015;41(6):1505-11. doi: 10.1002/jmri.24727. PubMed PMID: 25104503.
56. Anderson LJ, Holden S, Davis B, Prescott E, Charrier CC, Bunce NH, et al. Cardiovascular T₂-star (T₂^{*}) magnetic resonance for the early diagnosis of myocardial iron overload. *Eur Heart J*. 2001;22(23):2171-9. doi: 10.1053/euhj.2001.2822. PubMed PMID: 11913479.
57. Kim RJ, Fieno DS, Parrish TB, Harris K, Chen EL, Simonetti O, et al. Relationship of MRI delayed contrast enhancement to irreversible injury, infarct age, and contractile function. *Circulation*. 1999;100(19):1992-2002. PubMed PMID: 10556226.
58. Been M, Smith MA, Ridgeway JP, Brydon JW, Douglas RH, Kean DM, et al. Characterisation of acute myocardial infarction by gated magnetic resonance imaging. *Lancet*. 1985;2(8451):348-50. doi: 10.1016/s0140-6736(85)92494-8. PubMed PMID: 2862512.

59. Flacke SJ, Fischer SE, Lorenz CH. Measurement of the gadopentetate dimeglumine partition coefficient in human myocardium in vivo: normal distribution and elevation in acute and chronic infarction. *Radiology*. 2001;218(3):703-10. doi: 10.1148/radiology.218.3.r01fe18703. PubMed PMID: 11230643.
60. Wacker CM, Bock M, Hartlep AW, Beck G, van Kaick G, Ertl G, et al. Changes in myocardial oxygenation and perfusion under pharmacological stress with dipyridamole: assessment using T*2 and T1 measurements. *Magn Reson Med*. 1999;41(4):686-95. PubMed PMID: 10332843.
61. Wacker CM, Fidler F, Dueren C, Hirn S, Jakob PM, Ertl G, et al. Quantitative assessment of myocardial perfusion with a spin-labeling technique: preliminary results in patients with coronary artery disease. *J Magn Reson Imaging*. 2003;18(5):555-60. doi: 10.1002/jmri.10386. PubMed PMID: 14579398.
62. Messroghli DR, Niendorf T, Schulz-Menger J, Dietz R, Friedrich MG. T1 mapping in patients with acute myocardial infarction. *J Cardiovasc Magn Reson*. 2003;5(2):353-9. doi: 10.1081/jcmr-120019418. PubMed PMID: 12765114.
63. Messroghli DR, Radjenovic A, Kozerke S, Higgins DM, Sivananthan MU, Ridgway JP. Modified Look-Locker inversion recovery (MOLLI) for high-resolution T1 mapping of the heart. *Magn Reson Med*. 2004;52(1):141-6. doi: 10.1002/mrm.20110. PubMed PMID: 15236377.
64. Robson MD, Piechnik SK, Tunnicliffe EM, Neubauer S. T1 measurements in the human myocardium: the effects of magnetization transfer on the SASHA and MOLLI sequences. *Magn Reson Med*. 2013;70(3):664-70. doi: 10.1002/mrm.24867. PubMed PMID: 23857710.
65. Piechnik SK, Ferreira VM, Lewandowski AJ, Ntusi NA, Banerjee R, Holloway C, et al. Normal variation of magnetic resonance T1 relaxation times in the human population at 1.5 T using ShMOLLI. *J Cardiovasc Magn Reson*. 2013;15:13. doi: 10.1186/1532-429X-15-13. PubMed PMID: 23331520; PubMed Central PMCID: PMC3610210.
66. Ferreira VM, Piechnik SK, Dall'Armellina E, Karamitsos TD, Francis JM, Ntusi N, et al. T(1) mapping for the diagnosis of acute myocarditis using CMR: comparison to T2-weighted and late gadolinium enhanced imaging. *JACC Cardiovasc Imaging*. 2013;6(10):1048-58. doi: 10.1016/j.jcmg.2013.03.008. PubMed PMID: 24011774.
67. Puntmann VO, Voigt T, Chen Z, Mayr M, Karim R, Rhode K, et al. Native T1 mapping in differentiation of normal myocardium from diffuse disease in hypertrophic and dilated

cardiomyopathy. *JACC Cardiovasc Imaging*. 2013;6(4):475-84. doi: 10.1016/j.jcmg.2012.08.019. PubMed PMID: 23498674.

68. Dass S, Suttie JJ, Piechnik SK, Ferreira VM, Holloway CJ, Banerjee R, et al. Myocardial tissue characterization using magnetic resonance noncontrast t1 mapping in hypertrophic and dilated cardiomyopathy. *Circ Cardiovasc Imaging*. 2012;5(6):726-33. Epub 2012/10/15. doi: 10.1161/CIRCIMAGING.112.976738. PubMed PMID: 23071146.

69. Liu JM, Liu A, Leal J, McMillan F, Francis J, Greiser A, et al. Measurement of myocardial native T1 in cardiovascular diseases and norm in 1291 subjects. *J Cardiovasc Magn Reson*. 2017;19(1):74. Epub 2017/09/28. doi: 10.1186/s12968-017-0386-y. PubMed PMID: 28954631; PubMed Central PMCID: PMC5618724.

70. Kali A, Choi EY, Sharif B, Kim YJ, Bi X, Spottiswoode B, et al. Native T1 Mapping by 3-T CMR Imaging for Characterization of Chronic Myocardial Infarctions. *JACC Cardiovasc Imaging*. 2015;8(9):1019-30. Epub 2015/08/19. doi: 10.1016/j.jcmg.2015.04.018. PubMed PMID: 26298071.

71. Hinojar R, Varma N, Child N, Goodman B, Jabbour A, Yu CY, et al. T1 Mapping in Discrimination of Hypertrophic Phenotypes: Hypertensive Heart Disease and Hypertrophic Cardiomyopathy: Findings From the International T1 Multicenter Cardiovascular Magnetic Resonance Study. *Circ Cardiovasc Imaging*. 2015;8(12). doi: 10.1161/CIRCIMAGING.115.003285. PubMed PMID: 26659373.

72. Fontana M, Banypersad SM, Treibel TA, Maestrini V, Sado DM, White SK, et al. Native T1 mapping in transthyretin amyloidosis. *JACC Cardiovasc Imaging*. 2014;7(2):157-65. Epub 2014/01/08. doi: 10.1016/j.jcmg.2013.10.008. PubMed PMID: 24412190.

73. Thompson RB, Chow K, Khan A, Chan A, Shanks M, Paterson I, et al. T₁ mapping with cardiovascular MRI is highly sensitive for Fabry disease independent of hypertrophy and sex. *Circ Cardiovasc Imaging*. 2013;6(5):637-45. doi: 10.1161/CIRCIMAGING.113.000482. PubMed PMID: 23922004.

74. Sado DM, White SK, Piechnik SK, Banypersad SM, Treibel T, Captur G, et al. Identification and assessment of Anderson-Fabry disease by cardiovascular magnetic resonance noncontrast myocardial T1 mapping. *Circ Cardiovasc Imaging*. 2013;6(3):392-8. doi: 10.1161/CIRCIMAGING.112.000070. PubMed PMID: 23564562.

75. Krittayaphong R, Zhang S, Saiviroonporn P, Viprakasit V, Tanapibunpon P, Komoltri C, et al. Detection of cardiac iron overload with native magnetic resonance T1 and T2 mapping in patients with thalassemia. *Int J Cardiol.* 2017;248:421-6. Epub 2017/06/29. doi: 10.1016/j.ijcard.2017.06.100. PubMed PMID: 28688717.
76. Mascherbauer J, Marzluf BA, Tufaro C, Pfaffenberger S, Graf A, Wexberg P, et al. Cardiac magnetic resonance postcontrast T1 time is associated with outcome in patients with heart failure and preserved ejection fraction. *Circ Cardiovasc Imaging.* 2013;6(6):1056-65. doi: 10.1161/CIRCIMAGING.113.000633. PubMed PMID: 24036385.
77. Iles LM, Ellims AH, Llewellyn H, Hare JL, Kaye DM, McLean CA, et al. Histological validation of cardiac magnetic resonance analysis of regional and diffuse interstitial myocardial fibrosis. *Eur Heart J Cardiovasc Imaging.* 2015;16(1):14-22. doi: 10.1093/ehjci/jeu182. PubMed PMID: 25354866.
78. Iles L, Pfluger H, Phrommintikul A, Cherayath J, Aksit P, Gupta SN, et al. Evaluation of diffuse myocardial fibrosis in heart failure with cardiac magnetic resonance contrast-enhanced T1 mapping. *J Am Coll Cardiol.* 2008;52(19):1574-80. doi: 10.1016/j.jacc.2008.06.049. PubMed PMID: 19007595.
79. Donahue KM, Weisskoff RM, Burstein D. Water diffusion and exchange as they influence contrast enhancement. *J Magn Reson Imaging.* 1997;7(1):102-10. PubMed PMID: 9039599.
80. Flett AS, Hayward MP, Ashworth MT, Hansen MS, Taylor AM, Elliott PM, et al. Equilibrium contrast cardiovascular magnetic resonance for the measurement of diffuse myocardial fibrosis: preliminary validation in humans. *Circulation.* 2010;122(2):138-44. doi: 10.1161/CIRCULATIONAHA.109.930636. PubMed PMID: 20585010.
81. Fontana M, White SK, Banypersad SM, Sado DM, Maestrini V, Flett AS, et al. Comparison of T1 mapping techniques for ECV quantification. Histological validation and reproducibility of ShMOLLI versus multibreath-hold T1 quantification equilibrium contrast CMR. *J Cardiovasc Magn Reson.* 2012;14:88. doi: 10.1186/1532-429X-14-88. PubMed PMID: 23272651; PubMed Central PMCID: PMC3552758.
82. White SK, Sado DM, Fontana M, Banypersad SM, Maestrini V, Flett AS, et al. T1 mapping for myocardial extracellular volume measurement by CMR: bolus only versus primed

- infusion technique. *JACC Cardiovasc Imaging*. 2013;6(9):955-62. doi: 10.1016/j.jcmg.2013.01.011. PubMed PMID: 23582361.
83. Miller CA, Naish JH, Bishop P, Coutts G, Clark D, Zhao S, et al. Comprehensive validation of cardiovascular magnetic resonance techniques for the assessment of myocardial extracellular volume. *Circ Cardiovasc Imaging*. 2013;6(3):373-83. Epub 2013/04/03. doi: 10.1161/CIRCIMAGING.112.000192. PubMed PMID: 23553570.
84. aus dem Siepen F, Buss SJ, Messroghli D, Andre F, Lossnitzer D, Seitz S, et al. T1 mapping in dilated cardiomyopathy with cardiac magnetic resonance: quantification of diffuse myocardial fibrosis and comparison with endomyocardial biopsy. *Eur Heart J Cardiovasc Imaging*. 2015;16(2):210-6. Epub 2014/09/22. doi: 10.1093/ehjci/jeu183. PubMed PMID: 25246502.
85. Kammerlander AA, Marzluft BA, Zotter-Tufaro C, Aschauer S, Duca F, Bachmann A, et al. T1 Mapping by CMR Imaging: From Histological Validation to Clinical Implication. *JACC Cardiovasc Imaging*. 2016;9(1):14-23. doi: 10.1016/j.jcmg.2015.11.002. PubMed PMID: 26684970.
86. Sado DM, Flett AS, Banyersad SM, White SK, Maestrini V, Quarta G, et al. Cardiovascular magnetic resonance measurement of myocardial extracellular volume in health and disease. *Heart*. 2012;98(19):1436-41. doi: 10.1136/heartjnl-2012-302346. PubMed PMID: 22936681.
87. Ugander M, Oki AJ, Hsu LY, Kellman P, Greiser A, Aletras AH, et al. Extracellular volume imaging by magnetic resonance imaging provides insights into overt and sub-clinical myocardial pathology. *Eur Heart J*. 2012;33(10):1268-78. doi: 10.1093/eurheartj/ehr481. PubMed PMID: 22279111; PubMed Central PMCID: PMC3350985.
88. Radunski UK, Lund GK, Stehning C, Schnackenburg B, Bohnen S, Adam G, et al. CMR in patients with severe myocarditis: diagnostic value of quantitative tissue markers including extracellular volume imaging. *JACC Cardiovasc Imaging*. 2014;7(7):667-75. Epub 2014/06/18. doi: 10.1016/j.jcmg.2014.02.005. PubMed PMID: 24954462.
89. Su MY, Lin LY, Tseng YH, Chang CC, Wu CK, Lin JL, et al. CMR-verified diffuse myocardial fibrosis is associated with diastolic dysfunction in HFpEF. *JACC Cardiovasc Imaging*. 2014;7(10):991-7. Epub 2014/09/17. doi: 10.1016/j.jcmg.2014.04.022. PubMed PMID: 25240451.

90. Banypersad SM, Sado DM, Flett AS, Gibbs SD, Pinney JH, Maestrini V, et al. Quantification of myocardial extracellular volume fraction in systemic AL amyloidosis: an equilibrium contrast cardiovascular magnetic resonance study. *Circ Cardiovasc Imaging*. 2013;6(1):34-9. Epub 2012/11/28. doi: 10.1161/CIRCIMAGING.112.978627. PubMed PMID: 23192846.
91. Chen CA, Dusenbery SM, Valente AM, Powell AJ, Geva T. Myocardial ECV Fraction Assessed by CMR Is Associated With Type of Hemodynamic Load and Arrhythmia in Repaired Tetralogy of Fallot. *JACC Cardiovasc Imaging*. 2016;9(1):1-10. Epub 2015/12/09. doi: 10.1016/j.jcmg.2015.09.011. PubMed PMID: 26684969.
92. Dusenbery SM, Jerosch-Herold M, Rickers C, Colan SD, Geva T, Newburger JW, et al. Myocardial extracellular remodeling is associated with ventricular diastolic dysfunction in children and young adults with congenital aortic stenosis. *J Am Coll Cardiol*. 2014;63(17):1778-85. Epub 2014/03/13. doi: 10.1016/j.jacc.2013.11.066. PubMed PMID: 24632273.
93. Kato A, Riesenkampff E, Yim D, Yoo SJ, Seed M, Grosse-Wortmann L. Pediatric Fontan patients are at risk for myocardial fibrotic remodeling and dysfunction. *Int J Cardiol*. 2017;240:172-7. Epub 2017/04/22. doi: 10.1016/j.ijcard.2017.04.073. PubMed PMID: 28461021.
94. Broberg CS, Chugh SS, Conklin C, Sahn DJ, Jerosch-Herold M. Quantification of diffuse myocardial fibrosis and its association with myocardial dysfunction in congenital heart disease. *Circ Cardiovasc Imaging*. 2010;3(6):727-34. Epub 2010/09/20. doi: 10.1161/CIRCIMAGING.108.842096. PubMed PMID: 20855860; PubMed Central PMCID: PMC3048790.
95. Ide S, Riesenkampff E, Chiasson DA, Dipchand AI, Kantor PF, Chaturvedi RR, et al. Histological validation of cardiovascular magnetic resonance T1 mapping markers of myocardial fibrosis in paediatric heart transplant recipients. *J Cardiovasc Magn Reson*. 2017;19(1):10. Epub 2017/02/01. doi: 10.1186/s12968-017-0326-x. PubMed PMID: 28143545; PubMed Central PMCID: PMC5286863.
96. Puntmann VO, Carr-White G, Jabbour A, Yu CY, Gebker R, Kelle S, et al. T1-Mapping and Outcome in Nonischemic Cardiomyopathy: All-Cause Mortality and Heart Failure. *JACC Cardiovasc Imaging*. 2016;9(1):40-50. doi: 10.1016/j.jcmg.2015.12.001. PubMed PMID: 26762873.

97. Schelbert EB, Piehler KM, Zareba KM, Moon JC, Ugander M, Messroghli DR, et al. Myocardial Fibrosis Quantified by Extracellular Volume Is Associated With Subsequent Hospitalization for Heart Failure, Death, or Both Across the Spectrum of Ejection Fraction and Heart Failure Stage. *J Am Heart Assoc.* 2015;4(12). Epub 2015/12/18. doi: 10.1161/JAHA.115.002613. PubMed PMID: 26683218; PubMed Central PMCID: PMC4845263.
98. Schelbert EB, Fridman Y, Wong TC, Abu Daya H, Piehler KM, Kadakkal A, et al. Temporal Relation Between Myocardial Fibrosis and Heart Failure With Preserved Ejection Fraction: Association With Baseline Disease Severity and Subsequent Outcome. *JAMA Cardiol.* 2017;2(9):995-1006. doi: 10.1001/jamacardio.2017.2511. PubMed PMID: 28768311; PubMed Central PMCID: PMC5710176.
99. Wong TC, Piehler K, Meier CG, Testa SM, Klock AM, Aneizi AA, et al. Association between extracellular matrix expansion quantified by cardiovascular magnetic resonance and short-term mortality. *Circulation.* 2012;126(10):1206-16. Epub 2012/07/31. doi: 10.1161/CIRCULATIONAHA.111.089409. PubMed PMID: 22851543; PubMed Central PMCID: PMC3464491.
100. Wong TC, Piehler KM, Kang IA, Kadakkal A, Kellman P, Schwartzman DS, et al. Myocardial extracellular volume fraction quantified by cardiovascular magnetic resonance is increased in diabetes and associated with mortality and incident heart failure admission. *Eur Heart J.* 2014;35(10):657-64. Epub 2013/06/11. doi: 10.1093/eurheartj/ehf193. PubMed PMID: 23756336; PubMed Central PMCID: PMC3945798.
101. Duca F, Kammerlander AA, Zotter-Tufaro C, Aschauer S, Schwaiger ML, Marzluft BA, et al. Interstitial Fibrosis, Functional Status, and Outcomes in Heart Failure With Preserved Ejection Fraction: Insights From a Prospective Cardiac Magnetic Resonance Imaging Study. *Circ Cardiovasc Imaging.* 2016;9(12). doi: 10.1161/CIRCIMAGING.116.005277. PubMed PMID: 27974408.
102. Duca F, Zotter-Tufaro C, Kammerlander AA, Panzenböck A, Aschauer S, Dalos D, et al. Cardiac extracellular matrix is associated with adverse outcome in patients with chronic heart failure. *Eur J Heart Fail.* 2017;19(4):502-11. Epub 2016/11/27. doi: 10.1002/ejhf.680. PubMed PMID: 27891745.

103. Roy C, Slimani A, de Meester C, Amzulescu M, Pasquet A, Vancraeynest D, et al. Associations and prognostic significance of diffuse myocardial fibrosis by cardiovascular magnetic resonance in heart failure with preserved ejection fraction. *J Cardiovasc Magn Reson.* 2018;20(1):55. Epub 2018/08/08. doi: 10.1186/s12968-018-0477-4. PubMed PMID: 30086783; PubMed Central PMCID: PMC6081897.
104. Ugander M, Bagi PS, Booker OJ, Hsu L-Y, Oki AJ, Greiser A, et al. Edema by T2-weighted imaging in salvaged myocardium is extracellular, not intracellular. 2011;13 (Suppl 1):P70. doi: <https://doi.org/10.1186/1532-429X-13-S1-P70>.
105. Ferreira VM, Piechnik SK, Dall'Armellina E, Karamitsos TD, Francis JM, Choudhury RP, et al. Non-contrast T1-mapping detects acute myocardial edema with high diagnostic accuracy: a comparison to T2-weighted cardiovascular magnetic resonance. *J Cardiovasc Magn Reson.* 2012;14:42. Epub 2012/06/21. doi: 10.1186/1532-429X-14-42. PubMed PMID: 22720998; PubMed Central PMCID: PMC3424120.
106. Ugander M, Bagi PS, Oki AJ, Chen B, Hsu LY, Aletras AH, et al. Myocardial edema as detected by pre-contrast T1 and T2 CMR delineates area at risk associated with acute myocardial infarction. *JACC Cardiovasc Imaging.* 2012;5(6):596-603. doi: 10.1016/j.jcmg.2012.01.016. PubMed PMID: 22698528; PubMed Central PMCID: PMC3769169.
107. Babu-Narayan SV, Kilner PJ, Li W, Moon JC, Goktekin O, Davlouros PA, et al. Ventricular fibrosis suggested by cardiovascular magnetic resonance in adults with repaired tetralogy of fallot and its relationship to adverse markers of clinical outcome. *Circulation.* 2006;113(3):405-13. doi: 10.1161/CIRCULATIONAHA.105.548727. PubMed PMID: 16432072.
108. Plymen CM, Sado DM, Taylor AM, Bolger AP, Lambiase PD, Hughes M, et al. Diffuse myocardial fibrosis in the systemic right ventricle of patients late after Mustard or Senning surgery: an equilibrium contrast cardiovascular magnetic resonance study. *Eur Heart J Cardiovasc Imaging.* 2013;14(10):963-8. Epub 2013/02/06. doi: 10.1093/ehjci/jet014. PubMed PMID: 23389732.
109. Yim D, Riesenkampff E, Caro-Dominguez P, Yoo SJ, Seed M, Grosse-Wortmann L. Assessment of Diffuse Ventricular Myocardial Fibrosis Using Native T1 in Children With Repaired Tetralogy of Fallot. *Circ Cardiovasc Imaging.* 2017;10(3). doi: 10.1161/CIRCIMAGING.116.005695. PubMed PMID: 28292861.

110. Olivieri LJ, Kellman P, McCarter RJ, Cross RR, Hansen MS, Spurney CF. Native T1 values identify myocardial changes and stratify disease severity in patients with Duchenne muscular dystrophy. *J Cardiovasc Magn Reson*. 2016;18(1):72. Epub 2016/10/28. doi: 10.1186/s12968-016-0292-8. PubMed PMID: 27788681; PubMed Central PMCID: PMC5084339.
111. Messroghli DR, Moon JC, Ferreira VM, Grosse-Wortmann L, He T, Kellman P, et al. Clinical recommendations for cardiovascular magnetic resonance mapping of T1, T2, T2* and extracellular volume: A consensus statement by the Society for Cardiovascular Magnetic Resonance (SCMR) endorsed by the European Association for Cardiovascular Imaging (EACVI). *J Cardiovasc Magn Reson*. 2017;19(1):75. Epub 2017/10/09. doi: 10.1186/s12968-017-0389-8. PubMed PMID: 28992817; PubMed Central PMCID: PMC5633041.
112. Buechel EV, Kaiser T, Jackson C, Schmitz A, Kellenberger CJ. Normal right- and left ventricular volumes and myocardial mass in children measured by steady state free precession cardiovascular magnetic resonance. *J Cardiovasc Magn Reson*. 2009;11:19. Epub 2009/06/21. doi: 10.1186/1532-429X-11-19. PubMed PMID: 19545393; PubMed Central PMCID: PMC2718870.
113. Kellman P, Herzka DA, Hansen MS. Adiabatic inversion pulses for myocardial T1 mapping. *Magn Reson Med*. 2014;71(4):1428-34. doi: 10.1002/mrm.24793. PubMed PMID: 23722695; PubMed Central PMCID: PMC3775900.
114. Muthusami P, Luining W, McCrindle B, van der Geest R, Riesenkampff E, Yoo SJ, et al. Myocardial Perfusion, Fibrosis, and Contractility in Children With Kawasaki Disease. *JACC Cardiovasc Imaging*. 2018. Epub 2018/08/06. doi: 10.1016/j.jcmg.2018.06.009. PubMed PMID: 30121268.
115. Riesenkampff E, Chen CK, Kantor PF, Greenway S, Chaturvedi RR, Yoo SJ, et al. Diffuse Myocardial Fibrosis in Children After Heart Transplantations: A Magnetic Resonance T1 Mapping Study. *Transplantation*. 2015;99(12):2656-62. doi: 10.1097/TP.0000000000000769. PubMed PMID: 26102614.
116. Tham EB, Haykowsky MJ, Chow K, Spavor M, Kaneko S, Khoo NS, et al. Diffuse myocardial fibrosis by T1-mapping in children with subclinical anthracycline cardiotoxicity: relationship to exercise capacity, cumulative dose and remodeling. *J Cardiovasc Magn Reson*.

- 2013;15:48. Epub 2013/06/10. doi: 10.1186/1532-429X-15-48. PubMed PMID: 23758789; PubMed Central PMCID: PMC3688348.
117. Soslow JH, Damon SM, Crum K, Lawson MA, Slaughter JC, Xu M, et al. Increased myocardial native T1 and extracellular volume in patients with Duchenne muscular dystrophy. *J Cardiovasc Magn Reson*. 2016;18:5. Epub 2016/01/21. doi: 10.1186/s12968-016-0224-7. PubMed PMID: 26795569; PubMed Central PMCID: PMC4722665.
118. Parekh K, Markl M, Deng J, de Freitas RA, Rigsby CK. T1 mapping in children and young adults with hypertrophic cardiomyopathy. *Int J Cardiovasc Imaging*. 2017;33(1):109-17. Epub 2016/09/22. doi: 10.1007/s10554-016-0979-9. PubMed PMID: 27659477; PubMed Central PMCID: PMC5250557.
119. Bulluck H, Bryant JA, Tan JZ, Go YY, Le TT, Tan RS, et al. Gender Differences in Native Myocardial T1 in a Healthy Chinese Volunteer Cohort. *Cardiovasc Imaging Asia*. 2017;1(2):110-5.
120. Messroghli DR, Plein S, Higgins DM, Walters K, Jones TR, Ridgway JP, et al. Human myocardium: single-breath-hold MR T1 mapping with high spatial resolution--reproducibility study. *Radiology*. 2006;238(3):1004-12. Epub 2006/01/19. doi: 10.1148/radiol.2382041903. PubMed PMID: 16424239.
121. Liu CY, Liu YC, Wu C, Armstrong A, Volpe GJ, van der Geest RJ, et al. Evaluation of age-related interstitial myocardial fibrosis with cardiac magnetic resonance contrast-enhanced T1 mapping: MESA (Multi-Ethnic Study of Atherosclerosis). *J Am Coll Cardiol*. 2013;62(14):1280-7. doi: 10.1016/j.jacc.2013.05.078. PubMed PMID: 23871886; PubMed Central PMCID: PMC3807823.
122. Dabir D, Child N, Kalra A, Rogers T, Gebker R, Jabbour A, et al. Reference values for healthy human myocardium using a T1 mapping methodology: results from the International T1 Multicenter cardiovascular magnetic resonance study. *J Cardiovasc Magn Reson*. 2014;16:69. doi: 10.1186/s12968-014-0069-x. PubMed PMID: 25384607; PubMed Central PMCID: PMC4203908.
123. McDiarmid AK, Broadbent DA, Higgins DM, Swoboda PP, Kidambi A, Ripley DP, et al. The effect of changes to MOLLI scheme on T1 mapping and extra cellular volume calculation in healthy volunteers with 3 tesla cardiovascular magnetic resonance imaging. *Quant Imaging Med*

- Surg. 2015;5(4):503-10. doi: 10.3978/j.issn.2223-4292.2015.04.07. PubMed PMID: 26435913; PubMed Central PMCID: PMCPMC4559984.
124. Burkhardt BEU, Menghini C, Rücker B, Kellenberger CJ, Valsangiacomo Buechel ER. Normal myocardial native T. *J Magn Reson Imaging*. 2020;51(3):897-903. Epub 2019/09/11. doi: 10.1002/jmri.26910. PubMed PMID: 31507010.
125. Neilan TG, Coelho-Filho OR, Shah RV, Abbasi SA, Heydari B, Watanabe E, et al. Myocardial extracellular volume fraction from T1 measurements in healthy volunteers and mice: relationship to aging and cardiac dimensions. *JACC Cardiovasc Imaging*. 2013;6(6):672-83. doi: 10.1016/j.jcmg.2012.09.020. PubMed PMID: 23643283; PubMed Central PMCID: PMCPMC3683385.
126. Liu CY, Lai S, Kawel-Boehm N, Chahal H, Ambale-Venkatesh B, Lima JAC, et al. Healthy aging of the left ventricle in relationship to cardiovascular risk factors: The Multi-Ethnic Study of Atherosclerosis (MESA). *PLoS One*. 2017;12(6):e0179947. Epub 2017/06/22. doi: 10.1371/journal.pone.0179947. PubMed PMID: 28640873.
127. Barczuk-Fałęcka M, Małek Ł, Werys K, Roik D, Adamus K, Brzewski M. Normal values of native T. *J Magn Reson Imaging*. 2020;51(3):912-8. Epub 2019/07/30. doi: 10.1002/jmri.26886. PubMed PMID: 31361078.
128. Piro M, Della Bona R, Abbate A, Biasucci LM, Crea F. Sex-related differences in myocardial remodeling. *J Am Coll Cardiol*. 2010;55(11):1057-65. doi: 10.1016/j.jacc.2009.09.065. PubMed PMID: 20223363.
129. Olivetti G, Giordano G, Corradi D, Melissari M, Lagrasta C, Gambert SR, et al. Gender differences and aging: effects on the human heart. *J Am Coll Cardiol*. 1995;26(4):1068-79. doi: 10.1016/0735-1097(95)00282-8. PubMed PMID: 7560601.
130. Robbers-Visser D, Boersma E, Helbing WA. Normal biventricular function, volumes, and mass in children aged 8 to 17 years. *J Magn Reson Imaging*. 2009;29(3):552-9. doi: 10.1002/jmri.21662. PubMed PMID: 19243036.
131. Kawel N, Nacif M, Zavodni A, Jones J, Liu S, Sibley CT, et al. T1 mapping of the myocardium: intra-individual assessment of post-contrast T1 time evolution and extracellular volume fraction at 3T for Gd-DTPA and Gd-BOPTA. *J Cardiovasc Magn Reson*. 2012;14:26. Epub 2012/04/28. doi: 10.1186/1532-429X-14-26. PubMed PMID: 22540153; PubMed Central PMCID: PMCPMC3405486.

132. Captur G, Gatehouse P, Keenan KE, Heslinga FG, Bruehl R, Prothmann M, et al. A medical device-grade T1 and ECV phantom for global T1 mapping quality assurance-the T. *J Cardiovasc Magn Reson*. 2016;18(1):58. Epub 2016/09/22. doi: 10.1186/s12968-016-0280-z. PubMed PMID: 27660042; PubMed Central PMCID: PMC5034411.
133. Eng J, McClelland RL, Gomes AS, Hundley WG, Cheng S, Wu CO, et al. Adverse Left Ventricular Remodeling and Age Assessed with Cardiac MR Imaging: The Multi-Ethnic Study of Atherosclerosis. *Radiology*. 2016;278(3):714-22. doi: 10.1148/radiol.2015150982. PubMed PMID: 26485617; PubMed Central PMCID: PMC5034411.
134. Carrick-Ranson G, Hastings JL, Bhella PS, Shibata S, Fujimoto N, Palmer MD, et al. Effect of healthy aging on left ventricular relaxation and diastolic suction. *Am J Physiol Heart Circ Physiol*. 2012;303(3):H315-22. doi: 10.1152/ajpheart.00142.2012. PubMed PMID: 22661507; PubMed Central PMCID: PMC3423165.
135. Gazoti Debessa CR, Mesiano Maifrino LB, Rodrigues de Souza R. Age related changes of the collagen network of the human heart. *Mech Ageing Dev*. 2001;122(10):1049-58. PubMed PMID: 11389923.
136. Dworatzek E, Baczko I, Kararigas G. Effects of aging on cardiac extracellular matrix in men and women. *Proteomics Clin Appl*. 2016;10(1):84-91. doi: 10.1002/prca.201500031. PubMed PMID: 26280680.
137. Cheng S, Xanthakis V, Sullivan LM, Lieb W, Massaro J, Aragam J, et al. Correlates of echocardiographic indices of cardiac remodeling over the adult life course: longitudinal observations from the Framingham Heart Study. *Circulation*. 2010;122(6):570-8. doi: 10.1161/CIRCULATIONAHA.110.937821. PubMed PMID: 20660804; PubMed Central PMCID: PMC2942081.
138. Rossi MA. Pathologic fibrosis and connective tissue matrix in left ventricular hypertrophy due to chronic arterial hypertension in humans. *J Hypertens*. 1998;16(7):1031-41. PubMed PMID: 9794745.
139. Asbun J, Villarreal FJ. The pathogenesis of myocardial fibrosis in the setting of diabetic cardiomyopathy. *J Am Coll Cardiol*. 2006;47(4):693-700. doi: 10.1016/j.jacc.2005.09.050. PubMed PMID: 16487830.
140. Haaf P, Garg P, Messroghli DR, Broadbent DA, Greenwood JP, Plein S. Cardiac T1 Mapping and Extracellular Volume (ECV) in clinical practice: a comprehensive review. *J*

- Cardiovasc Magn Reson. 2016;18(1):89. Epub 2016/11/30. doi: 10.1186/s12968-016-0308-4. PubMed PMID: 27899132; PubMed Central PMCID: PMC5129251.
141. de Meester de Ravenstein C, Bouzin C, Lazam S, Boulif J, Amzulescu M, Melchior J, et al. Histological Validation of measurement of diffuse interstitial myocardial fibrosis by myocardial extravascular volume fraction from Modified Look-Locker imaging (MOLLI) T1 mapping at 3 T. *J Cardiovasc Magn Reson.* 2015;17:48. doi: 10.1186/s12968-015-0150-0. PubMed PMID: 26062931; PubMed Central PMCID: PMC4464705.
142. Piechnik SK, Ferreira VM, Dall'Armellina E, Cochlin LE, Greiser A, Neubauer S, et al. Shortened Modified Look-Locker Inversion recovery (ShMOLLI) for clinical myocardial T1-mapping at 1.5 and 3 T within a 9 heartbeat breathhold. *J Cardiovasc Magn Reson.* 2010;12:69. doi: 10.1186/1532-429X-12-69. PubMed PMID: 21092095; PubMed Central PMCID: PMC3001433.
143. Ezekowitz JA, Becher H, Belenkie I, Clark AM, Duff HJ, Friedrich MG, et al. The Alberta Heart Failure Etiology and Analysis Research Team (HEART) study. *BMC Cardiovasc Disord.* 2014;14:91. doi: 10.1186/1471-2261-14-91. PubMed PMID: 25063541; PubMed Central PMCID: PMC4222863.
144. Robinson JD, Lupkiewicz SM, Palenik L, Lopez LM, Ariet M. Determination of ideal body weight for drug dosage calculations. *Am J Hosp Pharm.* 1983;40(6):1016-9. PubMed PMID: 6869387.
145. Arheden H, Saeed M, Higgins CB, Gao DW, Bremerich J, Wyttenbach R, et al. Measurement of the distribution volume of gadopentetate dimeglumine at echo-planar MR imaging to quantify myocardial infarction: comparison with ^{99m}Tc-DTPA autoradiography in rats. *Radiology.* 1999;211(3):698-708. doi: 10.1148/radiology.211.3.r99jn41698. PubMed PMID: 10352594.
146. Roujol S, Weingärtner S, Foppa M, Chow K, Kawaji K, Ngo LH, et al. Accuracy, precision, and reproducibility of four T1 mapping sequences: a head-to-head comparison of MOLLI, ShMOLLI, SASHA, and SAPHIRE. *Radiology.* 2014;272(3):683-9. doi: 10.1148/radiol.14140296. PubMed PMID: 24702727.
147. Messroghli DR, Greiser A, Fröhlich M, Dietz R, Schulz-Menger J. Optimization and validation of a fully-integrated pulse sequence for modified look-locker inversion-recovery

- (MOLLI) T1 mapping of the heart. *J Magn Reson Imaging*. 2007;26(4):1081-6. doi: 10.1002/jmri.21119. PubMed PMID: 17896383.
148. Bönner F, Janzarik N, Jacoby C, Spieker M, Schnackenburg B, Range F, et al. Myocardial T2 mapping reveals age- and sex-related differences in volunteers. *J Cardiovasc Magn Reson*. 2015;17(1):9. Epub 2015/02/06. doi: 10.1186/s12968-015-0118-0. PubMed PMID: 25656484; PubMed Central PMCID: PMC4318191.
149. Rauhalampi SM, Mangion K, Barrientos PH, Carrick DJ, Clerfond G, McClure J, et al. Native myocardial longitudinal (T1) relaxation time: Regional, age, and sex associations in the healthy adult heart. *J Magn Reson Imaging*. 2016;44(3):541-8. Epub 2016/03/04. doi: 10.1002/jmri.25217. PubMed PMID: 26946323; PubMed Central PMCID: PMC45025725.
150. Kuruvilla S, Janardhanan R, Antkowiak P, Keeley EC, Adenaw N, Brooks J, et al. Increased extracellular volume and altered mechanics are associated with LVH in hypertensive heart disease, not hypertension alone. *JACC Cardiovasc Imaging*. 2015;8(2):172-80. doi: 10.1016/j.jcmg.2014.09.020. PubMed PMID: 25577446; PubMed Central PMCID: PMC4418794.
151. Rodrigues JC, Amadu AM, Dastidar AG, Szantho GV, Lyen SM, Godsave C, et al. Comprehensive characterisation of hypertensive heart disease left ventricular phenotypes. *Heart*. 2016;102(20):1671-9. doi: 10.1136/heartjnl-2016-309576. PubMed PMID: 27260191.
152. Moon JC, Messroghli DR, Kellman P, Piechnik SK, Robson MD, Ugander M, et al. Myocardial T1 mapping and extracellular volume quantification: a Society for Cardiovascular Magnetic Resonance (SCMR) and CMR Working Group of the European Society of Cardiology consensus statement. *J Cardiovasc Magn Reson*. 2013;15:92. doi: 10.1186/1532-429X-15-92. PubMed PMID: 24124732; PubMed Central PMCID: PMC3854458.
153. Savarese G, Lund LH. Global Public Health Burden of Heart Failure. *Card Fail Rev*. 2017;3(1):7-11. doi: 10.15420/cfr.2016:25:2. PubMed PMID: 28785469; PubMed Central PMCID: PMC5494150.
154. Curtis JP, Sokol SI, Wang Y, Rathore SS, Ko DT, Jadbabaie F, et al. The association of left ventricular ejection fraction, mortality, and cause of death in stable outpatients with heart failure. *J Am Coll Cardiol*. 2003;42(4):736-42. doi: 10.1016/s0735-1097(03)00789-7. PubMed PMID: 12932612.

155. Kanagala P, Cheng ASH, Singh A, Khan JN, Gulsin GS, Patel P, et al. Relationship Between Focal and Diffuse Fibrosis Assessed by CMR and Clinical Outcomes in Heart Failure With Preserved Ejection Fraction. *JACC Cardiovasc Imaging*. 2019. Epub 2019/02/11. doi: 10.1016/j.jcmg.2018.11.031. PubMed PMID: 30772227.
156. Collins J, Sommerville C, Magrath P, Spottiswoode B, Freed BH, Benzuly KH, et al. Extracellular volume fraction is more closely associated with altered regional left ventricular velocities than left ventricular ejection fraction in nonischemic cardiomyopathy. *Circ Cardiovasc Imaging*. 2015;8(1). Epub 2014/12/31. doi: 10.1161/CIRCIMAGING.114.001998. PubMed PMID: 25552491; PubMed Central PMCID: PMC4283574.
157. Rommel KP, von Roeder M, Latuscynski K, Oberueck C, Blazek S, Fengler K, et al. Extracellular Volume Fraction for Characterization of Patients With Heart Failure and Preserved Ejection Fraction. *J Am Coll Cardiol*. 2016;67(15):1815-25. doi: 10.1016/j.jacc.2016.02.018. PubMed PMID: 27081022.
158. Pagano JJ, Chow K, Paterson DI, Mikami Y, Schmidt A, Howarth A, et al. Effects of age, gender, and risk-factors for heart failure on native myocardial T1. *J Magn Reson Imaging*. 2018;48(5):1307-17. Epub 2018/06/13. doi: 10.1002/jmri.26160. PubMed PMID: 29897656.
159. Duca F, Zotter-Tufaro C, Kammerlander AA, Aschauer S, Binder C, Mascherbauer J, et al. Gender-related differences in heart failure with preserved ejection fraction. *Sci Rep*. 2018;8(1):1080. Epub 2018/01/18. doi: 10.1038/s41598-018-19507-7. PubMed PMID: 29348420; PubMed Central PMCID: PMC5773700.
160. Lam CS, Carson PE, Anand IS, Rector TS, Kuskowski M, Komajda M, et al. Sex differences in clinical characteristics and outcomes in elderly patients with heart failure and preserved ejection fraction: the Irbesartan in Heart Failure with Preserved Ejection Fraction (I-PRESERVE) trial. *Circ Heart Fail*. 2012;5(5):571-8. Epub 2012/08/10. doi: 10.1161/CIRCHEARTFAILURE.112.970061. PubMed PMID: 22887722; PubMed Central PMCID: PMC4768740.
161. Dewan P, Rørth R, Jhund PS, Shen L, Raparelli V, Petrie MC, et al. Differential Impact of Heart Failure With Reduced Ejection Fraction on Men and Women. *J Am Coll Cardiol*. 2019;73(1):29-40. doi: 10.1016/j.jacc.2018.09.081. PubMed PMID: 30621948.
162. Meyer P, Desai RV, Mujib M, Feller MA, Adamopoulos C, Banach M, et al. Right ventricular ejection fraction <20% is an independent predictor of mortality but not of

- hospitalization in older systolic heart failure patients. *Int J Cardiol.* 2012;155(1):120-5. Epub 2011/06/12. doi: 10.1016/j.ijcard.2011.05.046. PubMed PMID: 21664707; PubMed Central PMCID: PMC3640328.
163. Costa AF, van der Pol CB, Maralani PJ, McInnes MDF, Shewchuk JR, Verma R, et al. Gadolinium Deposition in the Brain: A Systematic Review of Existing Guidelines and Policy Statement Issued by the Canadian Association of Radiologists. *Can Assoc Radiol J.* 2018;69(4):373-82. Epub 2018/09/22. doi: 10.1016/j.carj.2018.04.002. PubMed PMID: 30249408.
164. Clarke JT. Narrative review: Fabry disease. *Ann Intern Med.* 2007;146(6):425-33. PubMed PMID: 17371887.
165. Putko BN, Wen K, Thompson RB, Mullen J, Shanks M, Yogasundaram H, et al. Anderson-Fabry cardiomyopathy: prevalence, pathophysiology, diagnosis and treatment. *Heart Fail Rev.* 2015;20(2):179-91. doi: 10.1007/s10741-014-9452-9. PubMed PMID: 25030479.
166. Nair V, Butany J. Heart transplant biopsies: interpretation and significance. *J Clin Pathol.* 2010;63(1):12-20. doi: 10.1136/jcp.2009.072462. PubMed PMID: 19858528.
167. Yousef Z, Elliott PM, Cecchi F, Escoubet B, Linhart A, Monserrat L, et al. Left ventricular hypertrophy in Fabry disease: a practical approach to diagnosis. *Eur Heart J.* 2013;34(11):802-8. doi: 10.1093/eurheartj/ehs166. PubMed PMID: 22736678; PubMed Central PMCID: PMC3596758.
168. Madonna R, Cevik C, Cocco N. Multimodality imaging for pre-clinical assessment of Fabry's cardiomyopathy. *Eur Heart J Cardiovasc Imaging.* 2014;15(10):1094-100. doi: 10.1093/ehjci/jeu080. PubMed PMID: 24904036.
169. Hughes DA, Elliott PM, Shah J, Zuckerman J, Coghlan G, Brookes J, et al. Effects of enzyme replacement therapy on the cardiomyopathy of Anderson-Fabry disease: a randomised, double-blind, placebo-controlled clinical trial of agalsidase alfa. *Heart.* 2008;94(2):153-8. doi: 10.1136/hrt.2006.104026. PubMed PMID: 17483124.
170. Putko BN, Yogasundaram H, Chow K, Pagano J, Khan A, Paterson DI, et al. Normal left-atrial structure and function despite concentric left-ventricular remodelling in a cohort of patients with Anderson-Fabry disease. *Eur Heart J Cardiovasc Imaging.* 2015. Epub 2015 Mar 6. Epub 2015 Mar 6. doi: 10.1093/ehjci/jev057. PubMed PMID: 25750198.

171. Shanks M, Thompson RB, Paterson DI, Putko B, Khan A, Chan A, et al. Systolic and diastolic function assessment in fabry disease patients using speckle-tracking imaging and comparison with conventional echocardiographic measurements. *J Am Soc Echocardiogr.* 2013;26(12):1407-14. doi: 10.1016/j.echo.2013.09.005. PubMed PMID: 24125876.
172. Cheng-Baron J, Chow K, Pagano JJ, Punithakumar K, Paterson DI, Oudit GY, et al. Quantification of circumferential, longitudinal, and radial global fractional shortening using steady-state free precession cines: A comparison with tissue-tracking strain and application in fabry disease. *Magn Reson Med.* 2014;73(2):586-96. Epub 2014 Mar 13. doi: 10.1002/mrm.25166. PubMed PMID: 24634139.
173. Morris DA, Blaschke D, Canaan-Kühl S, Krebs A, Knobloch G, Walter TC, et al. Global cardiac alterations detected by speckle-tracking echocardiography in Fabry disease: left ventricular, right ventricular, and left atrial dysfunction are common and linked to worse symptomatic status. *Int J Cardiovasc Imaging.* 2015;31(2):301-13. Epub 2014 Oct 15. doi: 10.1007/s10554-014-0551-4. PubMed PMID: 25315709.
174. Pica S, Sado DM, Maestrini V, Fontana M, White SK, Treibel T, et al. Reproducibility of native myocardial T1 mapping in the assessment of Fabry disease and its role in early detection of cardiac involvement by cardiovascular magnetic resonance. *J Cardiovasc Magn Reson.* 2014;16:99. doi: 10.1186/s12968-014-0099-4. PubMed PMID: 25475749; PubMed Central PMCID: PMC4256727.
175. Dall'Armellina E, Piechnik SK, Ferreira VM, Si QL, Robson MD, Francis JM, et al. Cardiovascular magnetic resonance by non contrast T1-mapping allows assessment of severity of injury in acute myocardial infarction. *J Cardiovasc Magn Reson.* 2012;14:15. doi: 10.1186/1532-429X-14-15. PubMed PMID: 22309452; PubMed Central PMCID: PMC3312869.
176. Kampmann C, Baehner FA, Whybra C, Bajbouj M, Baron K, Knuf M, et al. The right ventricle in Fabry disease. *Acta Paediatr Suppl.* 2005;94(447):15-8; discussion 9-0. PubMed PMID: 15895706.
177. Palecek T, Dostalova G, Kuchynka P, Karetova D, Bultas J, Elleder M, et al. Right ventricular involvement in Fabry disease. *J Am Soc Echocardiogr.* 2008;21(11):1265-8. doi: 10.1016/j.echo.2008.09.002. PubMed PMID: 18835697.

178. Niemann M, Breunig F, Beer M, Herrmann S, Strotmann J, Hu K, et al. The right ventricle in Fabry disease: natural history and impact of enzyme replacement therapy. *Heart*. 2010;96(23):1915-9. doi: 10.1136/hrt.2010.204586. PubMed PMID: 20965976.
179. Wuest W, Machann W, Breunig F, Weidemann F, Koestler H, Hahn D, et al. Right ventricular involvement in patients with Fabry's disease and the effect of enzyme replacement therapy. *Rofo*. 2011;183(11):1037-42. doi: 10.1055/s-0031-1281744. PubMed PMID: 21959886.
180. Sheppard MN, Cane P, Florio R, Kavantzias N, Close L, Shah J, et al. A detailed pathologic examination of heart tissue from three older patients with Anderson-Fabry disease on enzyme replacement therapy. *Cardiovasc Pathol*. 2010;19(5):293-301. doi: 10.1016/j.carpath.2009.05.003. PubMed PMID: 19631563.
181. Mehta BB, Auger DA, Gonzalez JA, Workman V, Chen X, Chow K, et al. Detection of elevated right ventricular extracellular volume in pulmonary hypertension using Accelerated and Navigator-Gated Look-Locker Imaging for Cardiac T1 Estimation (ANGIE) cardiovascular magnetic resonance. *J Cardiovasc Magn Reson*. 2015;17(1):110. doi: 10.1186/s12968-015-0209-y. PubMed PMID: 26692265; PubMed Central PMCID: PMC4687111.
182. Klein S, Staring M, Murphy K, Viergever MA, Pluim JP. elastix: a toolbox for intensity-based medical image registration. *IEEE Trans Med Imaging*. 2010;29(1):196-205. doi: 10.1109/TMI.2009.2035616. PubMed PMID: 19923044.
183. Sanz J, Dellegrottaglie S, Kariisa M, Sulica R, Poon M, O'Donnell TP, et al. Prevalence and correlates of septal delayed contrast enhancement in patients with pulmonary hypertension. *Am J Cardiol*. 2007;100(4):731-5. doi: 10.1016/j.amjcard.2007.03.094. PubMed PMID: 17697838.
184. Petritsch B, Köstler H, Machann W, Horn M, Weng AM, Goltz JP, et al. Non-invasive determination of myocardial lipid content in Fabry disease by ¹H-MR spectroscopy. *Rofo*. 2012;184(11):1020-5. doi: 10.1055/s-0032-1313059. PubMed PMID: 22893488.
185. García-Álvarez A, García-Lunar I, Pereda D, Fernández-Jimenez R, Sánchez-González J, Mirelis JG, et al. Association of Myocardial T1-Mapping CMR With Hemodynamics and RV Performance in Pulmonary Hypertension. *JACC Cardiovasc Imaging*. 2015;8(1):76-82. doi: 10.1016/j.jcmg.2014.08.012. PubMed PMID: 25592698.

186. Foale R, Nihoyannopoulos P, McKenna W, Kleinebenne A, Nadazdin A, Rowland E, et al. Echocardiographic measurement of the normal adult right ventricle. *Br Heart J*. 1986;56(1):33-44. PubMed PMID: 3730205; PubMed Central PMCID: PMCPMC1277383.
187. Lang RM, Badano LP, Mor-Avi V, Afilalo J, Armstrong A, Ernande L, et al. Recommendations for cardiac chamber quantification by echocardiography in adults: an update from the American Society of Echocardiography and the European Association of Cardiovascular Imaging. *Eur Heart J Cardiovasc Imaging*. 2015;16(3):233-70. doi: 10.1093/ehjci/jev014. PubMed PMID: 25712077.
188. Mehta BB, Chen X, Bilchick KC, Salerno M, Epstein FH. Accelerated and navigator-gated look-locker imaging for cardiac t1 estimation (ANGIE): Development and application to T1 mapping of the right ventricle. *Magn Reson Med*. 2015;73(1):150-60. doi: 10.1002/mrm.25100. PubMed PMID: 24515952; PubMed Central PMCID: PMCPMC4128906.
189. Moon JC, Sachdev B, Elkington AG, McKenna WJ, Mehta A, Pennell DJ, et al. Gadolinium enhanced cardiovascular magnetic resonance in Anderson-Fabry disease. Evidence for a disease specific abnormality of the myocardial interstitium. *Eur Heart J*. 2003;24(23):2151-5. PubMed PMID: 14643276.
190. De Cobelli F, Esposito A, Belloni E, Pieroni M, Perseghin G, Chimenti C, et al. Delayed-enhanced cardiac MRI for differentiation of Fabry's disease from symmetric hypertrophic cardiomyopathy. *AJR Am J Roentgenol*. 2009;192(3):W97-102. doi: 10.2214/AJR.08.1201. PubMed PMID: 19234246.
191. Niemann M, Herrmann S, Hu K, Breunig F, Strotmann J, Beer M, et al. Differences in Fabry cardiomyopathy between female and male patients: consequences for diagnostic assessment. *JACC Cardiovasc Imaging*. 2011;4(6):592-601. doi: 10.1016/j.jcmg.2011.01.020. PubMed PMID: 21679893.
192. Jerosch-Herold M, Sheridan DC, Kushner JD, Nauman D, Burgess D, Dutton D, et al. Cardiac magnetic resonance imaging of myocardial contrast uptake and blood flow in patients affected with idiopathic or familial dilated cardiomyopathy. *Am J Physiol Heart Circ Physiol*. 2008;295(3):H1234-H42. doi: 10.1152/ajpheart.00429.2008. PubMed PMID: 18660445; PubMed Central PMCID: PMCPMC2544489.
193. Kawel N, Turkbey EB, Carr JJ, Eng J, Gomes AS, Hundley WG, et al. Normal left ventricular myocardial thickness for middle-aged and older subjects with steady-state free

- precession cardiac magnetic resonance: the multi-ethnic study of atherosclerosis. *Circ Cardiovasc Imaging*. 2012;5(4):500-8. doi: 10.1161/CIRCIMAGING.112.973560. PubMed PMID: 22705587; PubMed Central PMCID: PMC3412148.
194. Kawel N, Nacif M, Zavodni A, Jones J, Liu S, Sibley CT, et al. T1 mapping of the myocardium: intra-individual assessment of the effect of field strength, cardiac cycle and variation by myocardial region. *J Cardiovasc Magn Reson*. 2012;14:27. doi: 10.1186/1532-429X-14-27. PubMed PMID: 22548832; PubMed Central PMCID: PMC3424109.
195. Reiter U, Reiter G, Dorr K, Greiser A, Maderthaner R, Fuchsjäger M. Normal diastolic and systolic myocardial T1 values at 1.5-T MR imaging: correlations and blood normalization. *Radiology*. 2014;271(2):365-72. doi: 10.1148/radiol.13131225. PubMed PMID: 24475837.
196. Ferreira VM, Wijesurendra RS, Liu A, Greiser A, Casadei B, Robson MD, et al. Systolic ShMOLLI myocardial T1-mapping for improved robustness to partial-volume effects and applications in tachyarrhythmias. *J Cardiovasc Magn Reson*. 2015;17:77. doi: 10.1186/s12968-015-0182-5. PubMed PMID: 26315682; PubMed Central PMCID: PMC4552368.
197. Detsky JS, Stainsby JA, Vijayaraghavan R, Graham JJ, Dick AJ, Wright GA. Inversion-recovery-prepared SSFP for cardiac-phase-resolved delayed-enhancement MRI. *Magn Reson Med*. 2007;58(2):365-72. doi: 10.1002/mrm.21291. PubMed PMID: 17654582.
198. Connelly KA, Detsky JS, Graham JJ, Paul G, Vijayaragavan R, Dick AJ, et al. Multicontrast late gadolinium enhancement imaging enables viability and wall motion assessment in a single acquisition with reduced scan times. *J Magn Reson Imaging*. 2009;30(4):771-7. doi: 10.1002/jmri.21907. PubMed PMID: 19787723.
199. Scheffler K, Hennig J. T(1) quantification with inversion recovery TrueFISP. *Magn Reson Med*. 2001;45(4):720-3. PubMed PMID: 11284003.
200. Chow K, Kellman P, Spottiswoode BS, Nielles-Vallespin S, Arai AE, Salerno M, et al. Saturation pulse design for quantitative myocardial T1 mapping. *J Cardiovasc Magn Reson*. 2015;17:84. Epub 2015/10/01. doi: 10.1186/s12968-015-0187-0. PubMed PMID: 26428468; PubMed Central PMCID: PMC4589956.
201. Stanisiz GJ, Henkelman RM. Gd-DTPA relaxivity depends on macromolecular content. *Magn Reson Med*. 2000;44(5):665-7. PubMed PMID: 11064398.

202. Rohrer M, Bauer H, Mintorovitch J, Requardt M, Weinmann HJ. Comparison of magnetic properties of MRI contrast media solutions at different magnetic field strengths. *Invest Radiol.* 2005;40(11):715-24. PubMed PMID: 16230904.
203. Kramer CM, Barkhausen J, Flamm SD, Kim RJ, Nagel E, Protocols SfcMRBoTTFoS. Standardized cardiovascular magnetic resonance (CMR) protocols 2013 update. *J Cardiovasc Magn Reson.* 2013;15:91. doi: 10.1186/1532-429X-15-91. PubMed PMID: 24103764; PubMed Central PMCID: PMC3851953.
204. Fontana M, Banypersad SM, Treibel TA, Abdel-Gadir A, Maestrini V, Lane T, et al. Differential Myocyte Responses in Patients with Cardiac Transthyretin Amyloidosis and Light-Chain Amyloidosis: A Cardiac MR Imaging Study. *Radiology.* 2015;277(2):388-97. doi: 10.1148/radiol.2015141744. PubMed PMID: 25997029.
205. Spruijt OA, Vissers L, Bogaard HJ, Hofman MB, Vonk-Noordegraaf A, Marcus JT. Increased native T1-values at the interventricular insertion regions in precapillary pulmonary hypertension. *Int J Cardiovasc Imaging.* 2016;32(3):451-9. Epub 2015/10/16. doi: 10.1007/s10554-015-0787-7. PubMed PMID: 26472581; PubMed Central PMCID: PMC4751160.
206. Kawel-Boehm N, Dellas Buser T, Greiser A, Bieri O, Bremerich J, Santini F. In-vivo assessment of normal T1 values of the right-ventricular myocardium by cardiac MRI. *Int J Cardiovasc Imaging.* 2014;30(2):323-8. doi: 10.1007/s10554-013-0326-3. PubMed PMID: 24221905.
207. Kozak MF, Redington A, Yoo SJ, Seed M, Greiser A, Grosse-Wortmann L. Diffuse myocardial fibrosis following tetralogy of Fallot repair: a T1 mapping cardiac magnetic resonance study. *Pediatr Radiol.* 2014;44(4):403-9. doi: 10.1007/s00247-013-2840-9. PubMed PMID: 24419492.
208. Beinart R, Khurram IM, Liu S, Yarmohammadi H, Halperin HR, Bluemke DA, et al. Cardiac magnetic resonance T1 mapping of left atrial myocardium. *Heart Rhythm.* 2013;10(9):1325-31. Epub 2013/05/02. doi: 10.1016/j.hrthm.2013.05.003. PubMed PMID: 23643513; PubMed Central PMCID: PMC3757110.
209. Ling LH, McLellan AJ, Taylor AJ, Iles LM, Ellims AH, Kumar S, et al. Magnetic resonance post-contrast T1 mapping in the human atrium: validation and impact on clinical

outcome after catheter ablation for atrial fibrillation. *Heart Rhythm*. 2014;11(9):1551-9. Epub 2014/06/12. doi: 10.1016/j.hrthm.2014.06.012. PubMed PMID: 24931636.

210. Luetkens JA, Wolpers AC, Beiert T, Kuetting D, Dabir D, Homsy R, et al. Cardiac magnetic resonance using late gadolinium enhancement and atrial T1 mapping predicts poor outcome in patients with atrial fibrillation after catheter ablation therapy. *Sci Rep*. 2018;8(1):13618. Epub 2018/09/11. doi: 10.1038/s41598-018-31916-2. PubMed PMID: 30206274; PubMed Central PMCID: PMC6134059.

211. Bull S, White SK, Piechnik SK, Flett AS, Ferreira VM, Loudon M, et al. Human non-contrast T1 values and correlation with histology in diffuse fibrosis. *Heart*. 2013;99(13):932-7. doi: 10.1136/heartjnl-2012-303052. PubMed PMID: 23349348; PubMed Central PMCID: PMC3686317.

212. Schelbert EB, Testa SM, Meier CG, Ceyrolles WJ, Levenson JE, Blair AJ, et al. Myocardial extravascular extracellular volume fraction measurement by gadolinium cardiovascular magnetic resonance in humans: slow infusion versus bolus. *J Cardiovasc Magn Reson*. 2011;13:16. Epub 2011/03/04. doi: 10.1186/1532-429X-13-16. PubMed PMID: 21375743; PubMed Central PMCID: PMC3059279.

213. Salerno M, Janardhanan R, Jiji RS, Brooks J, Adenaw N, Mehta B, et al. Comparison of methods for determining the partition coefficient of gadolinium in the myocardium using T1 mapping. *J Magn Reson Imaging*. 2013;38(1):217-24. Epub 2012/11/29. doi: 10.1002/jmri.23875. PubMed PMID: 23197434; PubMed Central PMCID: PMC3899916.

214. Higgins DM, Ridgway JP, Radjenovic A, Sivananthan UM, Smith MA. T1 measurement using a short acquisition period for quantitative cardiac applications. *Med Phys*. 2005;32(6):1738-46. doi: 10.1118/1.1921668. PubMed PMID: 16013731.

215. Weingärtner S, Akçakaya M, Basha T, Kissinger KV, Goddu B, Berg S, et al. Combined saturation/inversion recovery sequences for improved evaluation of scar and diffuse fibrosis in patients with arrhythmia or heart rate variability. *Magn Reson Med*. 2014;71(3):1024-34. doi: 10.1002/mrm.24761. PubMed PMID: 23650078.

216. Lustig M, Donoho D, Pauly JM. Sparse MRI: The application of compressed sensing for rapid MR imaging. *Magn Reson Med*. 2007;58(6):1182-95. doi: 10.1002/mrm.21391. PubMed PMID: 17969013.

217. Chow K, Yang Y, Shaw P, Kramer CM, Salerno M. Robust free-breathing SASHA T1 mapping with high-contrast image registration. *J Cardiovasc Magn Reson*. 2016;18(1):47. Epub 2016/08/17. doi: 10.1186/s12968-016-0267-9. PubMed PMID: 27535744; PubMed Central PMCID: PMC4989502.
218. Shaw JL, Yang Q, Zhou Z, Deng Z, Nguyen C, Li D, et al. Free-breathing, non-ECG, continuous myocardial T. *Magn Reson Med*. 2019;81(4):2450-63. Epub 2018/11/19. doi: 10.1002/mrm.27574. PubMed PMID: 30450749; PubMed Central PMCID: PMC6372325.
219. Chow K, Spottiswoode B, Pagano JJ, Thompson RB. Improved precision in SASHA T1 mapping with a variable flip angle readout. *J Cardiovasc Magn Reson* 2014.
220. Kellman P, Xue H, Chow K, Spottiswoode BS, Arai AE, Thompson RB. Optimized saturation recovery protocols for T1-mapping in the heart: influence of sampling strategies on precision. *J Cardiovasc Magn Reson*. 2014;16:55. Epub 2014/09/04. doi: 10.1186/s12968-014-0055-3. PubMed PMID: 25190004; PubMed Central PMCID: PMC4244052.
221. Rosmini S, Bulluck H, Captur G, Treibel TA, Abdel-Gadir A, Bhuva AN, et al. Myocardial native T1 and extracellular volume with healthy ageing and gender. *Eur Heart J Cardiovasc Imaging*. 2018;19(6):615-21. doi: 10.1093/ehjci/jev034. PubMed PMID: 29617988; PubMed Central PMCID: PMC5963299.
222. Karur GR, Robison S, Iwanochko RM, Morel CF, Crean AM, Thavendiranathan P, et al. Use of Myocardial T1 Mapping at 3.0 T to Differentiate Anderson-Fabry Disease from Hypertrophic Cardiomyopathy. *Radiology*. 2018;288(2):398-406. Epub 2018/04/24. doi: 10.1148/radiol.2018172613. PubMed PMID: 29688154.
223. Meßner NM, Budjan J, Loßnitzer D, Papavassiliu T, Schad LR, Weingärtner S, et al. Saturation-Recovery Myocardial T1-Mapping during Systole: Accurate and Robust Quantification in the Presence of Arrhythmia. *Sci Rep*. 2018;8(1):5251. Epub 2018/03/27. doi: 10.1038/s41598-018-23506-z. PubMed PMID: 29588504; PubMed Central PMCID: PMC5869699.